DEVELOPMENT AND CHARACTERIZATION OF PRINT PARTICLES AS DRUG DELIVERY VEHICLES IN THE LUNG

Tammy Shen

A dissertation submitted to the faculty of the University of North Carolina at Chapel Hill in partial fulfillment of the requirements for the degree of Doctor of Philosophy in the Division of Molecular Pharmaceutics in the UNC Eshelman School of Pharmacy

Chapel Hill
2014

Approved by:

Joseph DeSimone

Samuel Lai

James Bear

William Bennett

William Zamboni

ABSTRACT

Tammy W. Shen: Development and Characterization of PRINT® Particles as Drug Delivery Vehicles in the Lung
(Under the direction of Joseph M. DeSimone)

The aim of this dissertation is to develop and investigate the utility of the Particle Replication in Non-wetting Templates (PRINT®) technology as a toolbox to generate precisely defined particles in shape, matrix, and surface functionality to further the understanding of particulate drug delivery to the lung. The pulmonary route of administration is of particular interest in analyzing the effects of particles due to the vast exposure of our lungs to a wide array of airborne particulates. From pollen to bacteria to diesel exhaust, the fate and physiological impacts of these particulates cause a multitude of disease states in the human body. Understanding, and even harnessing, the specific characteristics which make these airborne invaders so potent at evading or wreaking havoc on the body's defense systems will hopefully lead to the development of more safe and efficient drug delivery vehicles.

Particles of varying geometries were fabricated and shape effects on macrophage internalization *in vitro* were investigated to explore physical particle characteristics that may impart the ability to tailor alveolar macrophage uptake for use in pulmonary therapeutics. PEG particles ranging from 80x320 nm to 6 μm in diameter were instilled into the lungs of mice and cellular uptake, residence time, and inflammatory responses in the lung were analyzed. Being able to precisely tune individual particle parameters allowed for the

determination of specific characteristics that could target or de-target specific cell populations in the lung. These PRINT particles were also shown to reside in the lung out to twenty-eight days without inducing an inflammatory response which demonstrates the potential of these particles as immunologically inert drug carriers to the lung.

ACKNOWLEDGEMENTS

I would like to thank my advisor Joseph DeSimone for giving me the opportunity to be part of his lab. He has continually challenged me to become a better scientist and I appreciate his guidance and advice during my graduate career. I would also like to thank Chris Luft and Mary Napier for their support and advice throughout the years. Vicki Haithcock and Crista Farrell helped make my life so much easier in lab and I appreciate their friendship. My committee members James Bear, William Bennett, Samuel Lai, and William Zamboni have helped me tremendously with experimental advice as they are all experts in their respective fields and I am thankful for their time and guidance. I would also like to thank Leaf Huang for his support throughout these past five years. Thanks to the MOPH faculty and staff who have taught me much and have helped me through graduate school.

I would like to acknowledge the great core facilities at UNC which were essential for my research. CHANL – Amar Kumbhar, Carrie Donley, Wallace Ambrose. MSL – Bob Bagnell and Victoria Madden, Flow Cytometry Core, LCCC Animal Histopathology core, Histology Research Core, and the Animal Studies Core Facility.

Thanks to all of my lab mates and classmates who made lab and life outside of lab more enjoyable – Kevin, Stu, Whit, Mel, James, Detter, Reid, Tojan, Ashley, Reuter, Sarah, Dom, and a multitude of others! Donald, Reggie and Erica, we've had some good laughs. I would like to especially acknowledge my partners in crime, Cathy and Marc, whose help and friendship has been invaluable. Finally, I would like to thank my family for their support and, who, when asked by others what I do, respond proudly with, "she does drugs."

TABLE OF CONTENTS

LIST OF TABLES

LIST OF FIGURES

LIST OF ABBREVIATIONS AND SYMBOLS

ACI	Anderson Cascade Impactor
AEM	2-aminoetheyl methacrylate hydrochloride
AM	Alveolar Macrophage
ANOVA	Analysis of Variance
APC	Antigen Presenting Cell
BALF	Bronchoalveolar Lavage Fluid
BSA	Bovine Serum Albumin
CF	Cystic Fibrosis
CFTR	Cystic Fibrosis Transmembrane Conductance
COPD	Chronic Obstructive Pulmonary Disease
CPD	Critical Point Drying
D_a	Aerodynamic Diameter
DC	Dendritic Cell
DMEM	Dulbecco's Modified Eagle Medium
DMF	Dimethylformamide
DNA	Deoxyribonucleic Acid
DPBS	Dulbecco's Phosphate Buffered Saline
DPI	Dry Powder Inhaler
DPPC	Dipalmitoylphosphatidylcholine
ELISA	Enzyme-linked immunosorbent assay
FBS	Fetal Bovine Serum

FcR	Fc Receptor
H&E	Hematoxylin and eosin
HP_4A	Hydroxy-tetraethylene glycol monoacrylate
HPMC	Hydroxypropyl methyl-cellulose
IL-1β	Interleukin 1β
IL-6	Interleukin 6
LABA	Long Acting $Beta_2$-adrenoceptor Agonist
LPS	Lipopolysaccharide
MFI	Median Fluorescence Intensity
MMAD	Mass Median Aerodynamic Diameter
NSCLS	Non-small Cell Lung Cancer
PAMP	Pathogen associated molecular pattern
PBS	Phosphate Buffered Saline
PDI	Polydispersity index
PEG	Poly(ethylene glycol)
PET	Poly(ethylene terephthalate)
PFA	Paraformaldehyde
PFPE	Perfluoropolyether
PHT	Pulmonary Hypertension
PLGA	Poly(lactic-co-glycolic acid)
pMDI	pressurized Metered Dose Inhalers
PRINT	Particle Replication in Non-wetting Templates
PVOH	Polyvinyl alcohol

PVP	Polyvinylpyrrolidone
RBC	Red Blood Cell
RNA	Ribonucleic Acid
ROS	Reactive Oxygen Species
RSV	Respiratory Syncytial Virus
SABA	Short Acting $Beta_2$-adrenoceptor Agonist
SCLC	Small Cell Lung Cancer
SD	Shape Diameter
SEM	Scanning Electron Microscope
TB	Tuberculosis
TEA	Triethanolamine
TGA	Thermogravimetric analysis
TNF- α	Tumor necrosis factor alpha
TPO	Diphenyl (2,4,6-trimethylbenzoyl)phosphine oxide
UV	Ultraviolet
WHO	World Health Organization
Ω	Contact Angle

CHAPTER 1

INTRODUCTION

The pulmonary route is an attractive option for therapeutic delivery due to its ease of access, non-invasive nature, large absorptive surface area, rapid onset of therapeutic action, localized drug delivery, and clinical relevance to diseases of the lung. It is preferred over oral drug delivery for many disease states due to its decreased susceptibility to first pass metabolism, faster onset of action, higher localized drug concentration, and decreased systemic toxicities [1]. Pulmonary drug delivery also has advantages over intravenous drug delivery in avoiding invasive dosing methods, such as needles, and, similar to the benefits over oral delivery, decreased systemic toxicities and increased local lung concentrations of the therapeutic [2].

The study of particles in the lung spans several different fields of research. Research in environmental health science studies the effects of environmental particulates, such as diesel exhaust particles and TiO_2 particles, on lung injury, inflammatory responses and cellular clearance mechanisms in the lung [3-8]. In pharmaceutical particle engineering, the technology of formulating and characterizing aerodynamically relevant particles for drug delivery to the lung is an area of high interest in both administration (i.e. dry powder inhalers and nebulizers) and therapeutic efficacy [9-11]. In medicine and physiology, the pharmacodynamics and pharmacokinetic effects of the drug molecule itself as well as how the disease states affect particle deposition and drug release are investigated [1, 12].

Combining the methodology and knowledge from these various particle research areas will allow for a more integrated approach to exploring the specific design parameters important for drug carriers to the lung.

1.1 Diseases of the Lung

According to the World Health Organization (WHO), of the top ten leading causes of death in the world in 2012, three of the top five were related to diseases of the lung: #3 chronic obstructive pulmonary disease (COPD), #4 lower respiratory infections and #5 lung cancer. COPD killed 3.1 million people worldwide with smoking as a primary cause of the disease. Smoking was also implicated in 80-90% of patients with lung cancer and led to 1.6 million deaths in 2012. It is projected that there will be 1.6 billion smokers worldwide by 2025 and thus the projected deaths for COPD and lung cancer are expected to increase significantly. Tuberculosis (TB), just out of the top ten leading causes of death, was second only to HIV/AIDS as a leading cause of death due to a single infectious agent; 1.3 million people died from TB infection in 2012 [13]. On a smaller scale, cystic fibrosis (CF) affects 70,000 people worldwide, but there is currently no cure for this deadly disease and the median age of survival is only 40 years [14]. In addition, asthma, although not a significant cause of death, affects over 235 million people worldwide and 25 million in the United States alone [15]. Pulmonary diseases account for a large economic burden in both healthcare costs and in productivity loss due to the symptoms and care needed for patients. Thus, there is a significant and urgent need to continue the development of more effective therapies to prevent and combat these pulmonary diseases.

1.1.1 Chronic Obstructive Pulmonary Disorder

COPD is characterized by persistent airflow limitation and has been associated with an enhanced chronic inflammatory response, often leading to the destruction of parenchymal tissue and small airway fibrosis [16]. Smoking is the primary cause of COPD but, in some countries, may also stem from exposure to high levels of outdoor and indoor air pollution [17]. In addition to symptoms disrupting workplace and home productivity, COPD has a significant economic health care burden estimated at $50 billion in the United States alone [18].

Cessation of smoking is the most significant intervention to diminish the progression of COPD. Because the disease symptoms and progression vary from patient to patient, personal tailored combinations of medicines are administered. $Beta_2$-agonists, anticholinergics, and inhaled corticosteroids are most often prescribed to COPD patients.

1.1.2 Lower respiratory infections

Lower respiratory infections can be categorized into either viral or bacterial causes. Ninety percent of lower respiratory infections are caused by viruses such as respiratory syncytial virus (RSV), influenza, adenovirus, coronavirus, and rhinovirus [19]. While there is no cure for viral infection, immunizations are recommended in order to arm the immune system and prevent infection. Bacterial infection is often caused by *Streptococcus pneumonia*, *Mycoplasma pneumonia* or *Bordetella pertussis* [19, 20]. Antibiotics are administered for bacterial infections, but with the increase of antibiotic administration there is an increasing incidence of antibiotic resistance among bacteria. Thus, there is a need to

better understand both the pathogenic and the host defense mechanisms to more effectively treat these bacterial infections.

1.1.3 Lung Cancer

Lung cancer has been the most prevalent type of cancer in the world for the past several decades. It is also the most common cause of death from cancer worldwide, accounting for one in five of cancer related deaths (19.4% of total cancer deaths) [21]. There are two main types of lung cancer, non-small cell lung cancer (NSCLS), accounting for 85% of lung cancers, and small cell lung cancer (SCLC). General lung cancer staging is based on the location and spread of the cancer and five-year survival rates are shown in **Table 1.1**. Early stage cancers are often difficult to detect: common symptoms such as coughing and fatigue are often attributed to other causes. Because of this, most lung cancer patients are not diagnosed until the cancer has spread to regional lymph nodes or has metastasized to other organs.

Table 1.1 5-Year Relative Survival of Lung Cancer Patients in the U.S. [22]

Stage	Cancer Locale	5-Year Relative Survival (%)
Localized	Cancer cells are localized to the lung	54.0
Regional	Cancer has spread to regional lymph nodes	26.5
Distant	Cancer has metastasized	4.0
Unknown	Unstaged	7.4

The usual course of treatment, depending on the cancer stage and other patient related factors, involves surgery, radiation therapy, chemotherapy, and targeted therapies (i.e. monoclonal antibodies, proteins). The chemotherapeutic drugs docetaxel, cisplatin, and paclitaxel are often used to treat lung cancer, but emerging immunotherapy drugs that

harness the immune system to fight cancer have shown great promise such as Merck's pembrolizumab, a PD-1 inhibitor, which was just recently approved by the FDA. Due to the ease of access to the lung and the ability for localized delivery, the inhaled route continues to be attractive for therapies targeting lung cancer treatment [23-28].

1.1.4 Tuberculosis

Tuberculosis is a lethal infectious disease, infecting over eight million people and causing 1.3 million deaths in 2012 [13]. The TB infection is caused by the *Mycobacterium tuberculosis* bacterium. Over two billion people in the world are estimated to be infected, and of those, 5-10% will develop the clinical disease [29]. Although TB is not exclusive to infections of the lung, its primary deposition and resulting pathology occurs in the lung. It is characterized by the formation of granulomas, which arise from aggregates of macrophages responding to persistent inflammatory stimuli [30, 31]. As these granulomas grow, they become surrounded by giant foam cells and epithelioid cells while other immune cells such as B and T cells, neutrophils, and dendritic cells are often seen within and surrounding the granuloma **(Figure 1.1)**. The granulomas harbor the bacteria, which continue to multiply slowly. And as macrophages at the necrotic core of the mass begin to die they send signals to recruit more macrophages to the site. The recruited macrophages phagocytose the apoptotic cells and bacteria facilitating the formation of secondary granulomas. Further progression of the disease may cause tissue damage by liquefying infected regions of the lung and ultimately spreading the infection to other parts of the body [32].

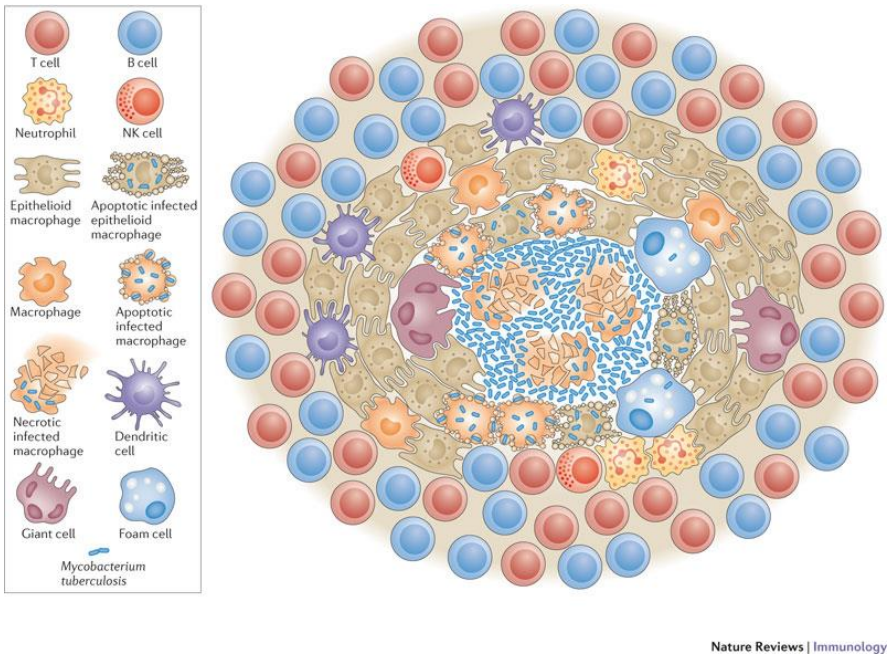

Figure 1.1 Schematic of the tuberculous granuloma
Figure reproduced from Ramakrishnan [31] with permission from Nature Publishing Group.

Treatment of TB involves the administration of a combination of first line antibiotics (isoniazid, rifampicin, pyrazinamide, and ethambutol) over a six month period [33]. The length of treatment, multiple drug dosages, and potential toxic side effects often result in a reduction in patient compliance leading to relapses of infection and increased probability of drug resistance. Second and even third line drugs have been developed to combat multi-drug resistant instances of TB. Inhaled antibiotic delivery has been investigated to mitigate some of the severe side effects of these potent TB drugs with promising results in animal studies [34]. Inhaled bacterial vaccines are also being developed [35].

1.1.5 Cystic Fibrosis

Cystic fibrosis is a genetic disease in which a mutation occurs within the cystic fibrosis transmembrane conductance regulator (CFTR) gene. CFTR regulates the chloride channel in epithelial cell membranes and primarily affects the lungs, pancreas, gastrointestinal tract, and sweat glands. In CF patients, this mutation leads to thick mucus which can block the airways and provide an environment conducive to bacterial growth. Repeat infections over time can lead to sever lung damage.

In addition to physical therapy, medicines such as antibiotics, mucolytics, and bronchodilators are given to decrease bacterial burden in the lung, loosen thick mucus buildup, and open up airways, respectively. Gene delivery to the lungs has been explored by in many animal models, but has yet to be translated for human therapy [36]. Others have explored nanoparticle delivery of DNA for gene therapy applications in CF patients [37].

1.1.6 Asthma

Asthma is a chronic inflammatory disease characterized by bronchospasms that tighten the muscles around the airway thus restricting airflow. For acute symptoms, asthma is often treated using short acting $beta_2$-adrenoceptor agonists (SABA) such as salbutamol. The delivery target for SABA treatment is the airway smooth muscle cells [38]. For long-term control of asthma, corticosteroids such as fluticasone and budesonide are administered for their anti-inflammatory effects. Long acting $beta_2$-agonists (LABAs) such as salmeterol and formoterol have a slower onset of action compared with SABAs, but have a longer duration of action of about 12 hours compared to 4-6 hours for SABAs. Combination

therapies combining a corticosteroid with a LABA are often prescribed to prevent inflammation and widen the airways.

Although asthma is manageable with current treatments, it still requires constant vigilance in one's symptoms and often involves a dosing regimen of many drugs multiple times per day. Thus, there is a need for the development of sustained-release therapies to decrease both the amount of different medications as well as the number of doses needed to control asthma symptoms while increasing patient compliance.

1.2 Lung Physiology

A fundamental understanding of lung physiology is needed in order to develop and deliver effective pulmonary drug delivery vehicles. The lung can be separated into three main regions; the extrathoracic region which includes the nasal and oral airways, the conducting zone, and the respiratory zone **(Figure 1.2)** [39]. The airways in the lung consist of twenty-three generations of asymmetrical branching networks, with each subsequent branch decreasing in diameter [40]. The conducting zone covers the region from the trachea (G0) to the terminal bronchioles (G16) and is characterized bya layer ofmucus-producing cells and ciliated cells with a surface area of 2-3 m^2. The respiratory zone, where gas exchange takes place, begins from the respiratory bronchioles (G17) ends at the alveolus (G23) and is characterized by minimal surfactant coverage and a surface area of 102 m^2 [41].

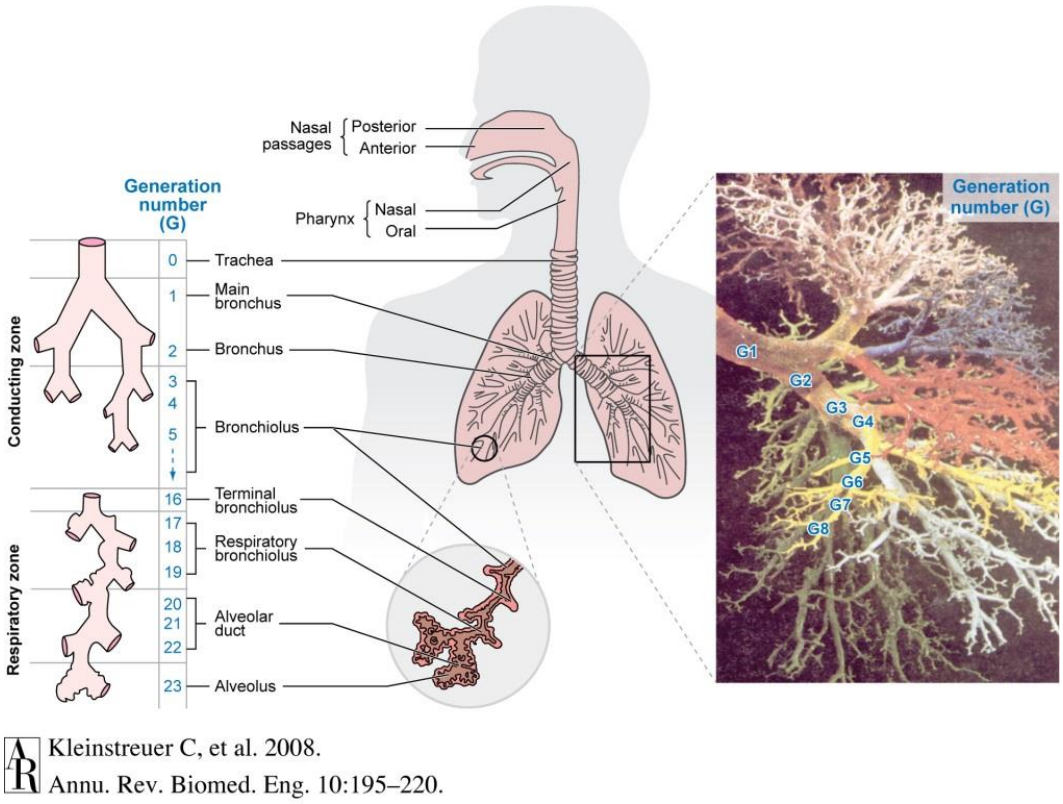

Figure 1.2 Schematics of the human respiratory system.
Figure taken from Kleinstreuer (2008) [39]

The cellular makeup of the lung epithelium between the conducting zone and the respiratory zone is significantly different and of noted importance for drug delivery applications. In the conducting airways, the epithelium consists of mucus and ciliated cells (~ 58 μm tall) that form the mucociliary escalator. There is a liquid layer on top of the epithelium which is approximately 8 μm in thickness in the upper airways. The thickness of the cells and the mucus layer decreases progressively through each generation. In the alveolar region, there is a less than 0.2 μm barrier between the airway and bloodstream **(Figure 1.3)**.

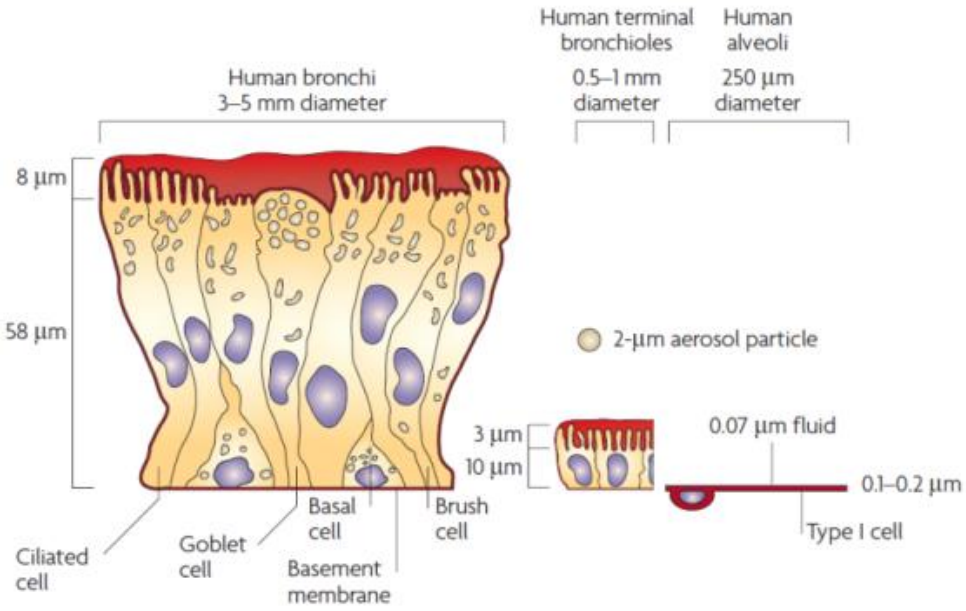

Figure 1.3 Comparison of the lung epithelium at different sites within the lungs.
Figure reproduced from Byron and Patton (2007) [1] with permission from Nature Publishing Group.

Inhaled particulates that deposit in the conducting zone may be caught in the mucus layer and are swept out of the lungs via the mucociliary elevator. Macrophages in the pericillary environment scavenge particles as well and aid in clearance. Particles which land in the alveolar region are rapidly engulfed by one of the 12-14 alveolar macrophages (AM) patrolling each of the 500 million alveoli in the human lung [42]. Neutrophils are quickly recruited to the lung in response to microbes where they phagocytose and kill the invading pathogen through the production of proteases, reactive oxygen species (ROS) and reactive nitrogen species (RNS) [43]. They can also enhance further neutrophil recruitment with the release of cytokines (IL-6, TNFα, IL-1) as well as other chemical signals. Dendritic cells (DCs), key regulators of adaptive immunity, act as sentinels in the lung by recognizing and internalizing foreign antigens then transporting them into the draining mediastinal lymph nodes where the antigens are presented to naïve T cells [44].

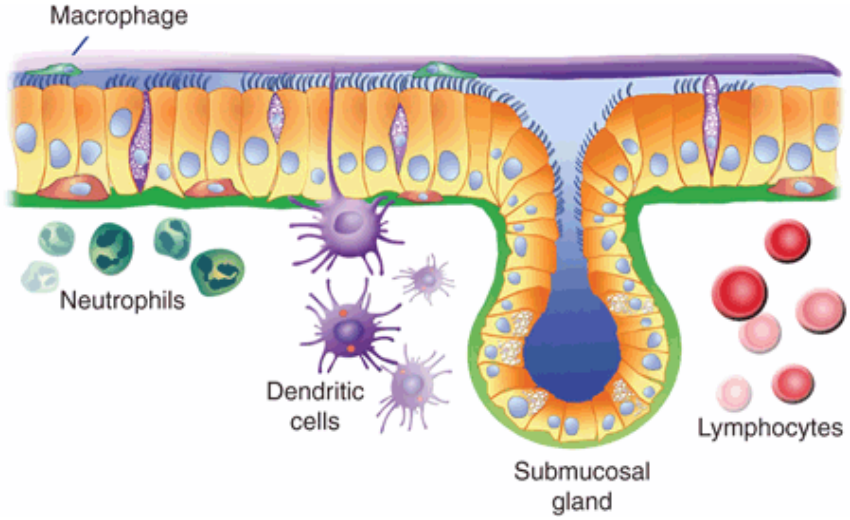

Figure 1.4 Schematic representation of airway mucus layer and component cells. Ciliated and nonciliated epithelia (yellow) line the conducting airway surface with their basolateral surfaces interacting with the basal lamina (green). Basal cells (orange) are an important progenitor cell type. Submucosal glands are a major source of secreted liquid, host defense factors, and mucins. The mucus (gel) layer (purple) covers the periciliary fluid (sol) layer (blue) in which cilia are submerged. Figure and caption reproduced from Oakland (2012) [45] with permission from Nature Publishing Group.

1.3 Physiological Barriers to Efficient Drug Delivery to the Lung

The average human adult takes over 20,000 breaths a day, breathing in a considerable number of foreign particulates. Because of this, the lung has developed highly efficient particle clearance mechanisms such as macrophage phagocytosis, mucociliary clearance, and metabolic degradation. A schematic of the factors that can affect drug deposition and clearance in the lung is shown in **Figure 1.5**. The physiological clearance mechanisms, unfortunately, are non-discriminatory of enemy invaders intent on wreaking havoc in the body or of allied reinforcements looking to fortify the body's defense system. Thus, it is necessary to better understand the physiologic lung-particle interactions in order to design drug carriers that can overcome, or even utilize, the body's defense mechanisms.

Macrophage clearance and mucociliary clearance are the primary focus of this work and will be described in more detail.

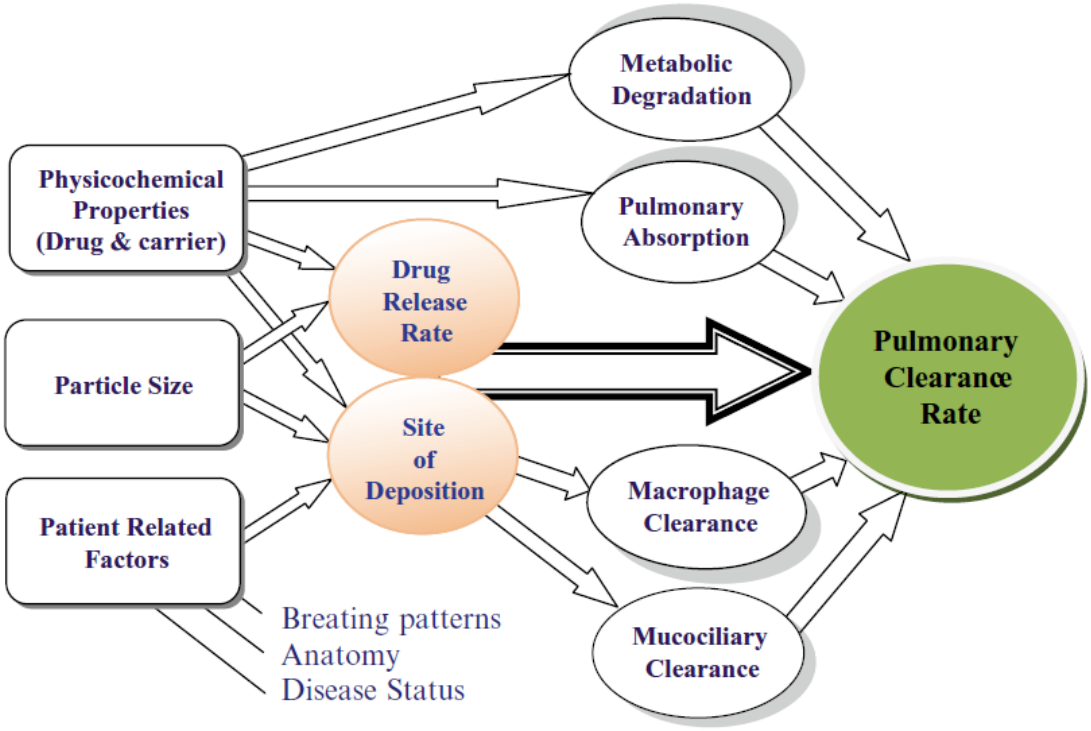

Figure 1.5 Factors affecting drug deposition and clearance in the lung.
Figure reproduced from El-Sherbiny (2011) [46] with permission from Springer Publishing.

1.3.1 Mucociliary Clearance

Mucus in the lung serves to trap inhaled particulates such as allergens, pollutants, and pathogens. Goblet cells are the mucus-producing cells of the lung and work in tandem with the ciliated cells to sweep the mucus upwards towards the trachea and out of the lung. The primary components of mucus are the entangled and cross-linked mucin glycoproteins secreted by goblet cells and the seromucinous glands [47]. The regulation and production of these fibers along with the other components of mucus (salts, DNA, lipids, cells, proteins and water) is highly complex and the alteration of the balance of these components due to disease

states leads to rheological properties that may contribute to patient mortality and reduced therapeutic effect of inhaled drugs [48, 49].

Mucociliary clearance can be avoided by targeting the site of deposition of a particulate delivery vehicle away from the mucociliary escalator. This is accomplished by generating particles with aerodynamic diameters (d_a) between 1-5 μm which have been shown to deposit deep in the alveolar airspaces where there is minimal mucus coverage compared to the upper airways [50, 51]. Some approaches attempt to harness the highly adhesive properties of mucus by formulating their drug and/or carrier with mucoadhesives, such as chitosan and hydroxypropyl methyl-cellulose (HPMC) to increase absorption of a drug by increasing the residence time of the formulation at the site of absorption [52, 53]. Others have developed particles with modified surface chemistries in order to reduce particle immobilization in mucus and allow further penetration of the particles through the mucus layer [54, 55].

1.3.2 Macrophage Clearance

Upon delivery to the pulmonary region, particles of 1-5 μm in diameter are phagocytosed by alveolar macrophages [56, 57]. The importance and efficiency of alveolar macrophage clearance is supported by the half a billion AMs found in the human lung [1] making this one of the major obstacles to efficient drug delivery to the lung. Avoidance of macrophage uptake may be preferred for aerosolized therapeutics targeted to the alveoli and associated epithelial cells as well as for systemic delivery [58]. This was shown in studies in which depletion of AMs by clodronate resulted in an increased pulmonary bioavailability of larger inhaled proteins such as IgG and human chorionic gonadotropin [56]. Because

particles with geometric diameters of 1-5 microns have been shown to be preferentially taken up by AMs [58, 59], large, porous particles [58] and swellable microparticles [60] were developed to deposit in the alveolar airspace while avoiding macrophage uptake due to their large (> 5 μm) geometric size. On the other hand, the sequestration of bacteria in macrophages for diseases such as tuberculosis and pneumonia may make AMs prime targets for antibacterial delivery [61]. Targeted apoptosis of AMs has also been shown to lead to increased protection from *M. tuberculosis* infection and an enhanced Th1-mediated immune response [62].

Modifying the surface chemistry of proteins and particulate drug carriers through PEGylation has been shown to increase steric stability and impart stealth properties [63]. Adding PEG chains to the particle surface create a barrier that mitigates the adhesion of opsonins onto the particle and reduces recognition and phagocytosis by macrophages. These benefits have been demonstrated with multiple particle systems *in vitro* and *in vivo* [64-66]. PEGylation of PLGA particles dosed *in vitro* to J774 murine alveolar macrophages showed a significant decrease in uptake compared to the unPEGylated particles [67]. Other coatings such as 1,2-dipalmitoylphophatidylcholine (DPPC), a major component of lung surfactant, on the surface of PLGA particles have also been shown to reduce uptake in alveolar macrophages *in vitro* [68]. Surendrakumar, *et al.* have shown that co-spray drying insulin and hyaluronic acid (HA) can extend the mean residence time of the insulin in the canine lung compared to spray dried insulin alone [69].

In addition to particle size and surface properties, particle shape has also been shown to influence macrophage uptake kinetics. The local particle shape at the point of attachment has been observed to influence the kinetics of particle uptake [70]. This is unsurprising as

phagocytosis is actin-dependent, and thus an energy-dependent, process. The more actin remodeling that the cell must undergo in order to engulf a particle, the slower the rate of internalization. A dimensionless parameter, Ω, has been developed to denote the local contact angle the cell membrane makes with the particle at the initial point of contact [70, 71]. A local particle contact angle of $\Omega < 45°$ indicates that phagocytosis will be initiated while at $\Omega > 45°$ the macrophage will not initiate phagocytosis and may instead spread over the particle without engulfing it [70] (**Figure 1.6**).

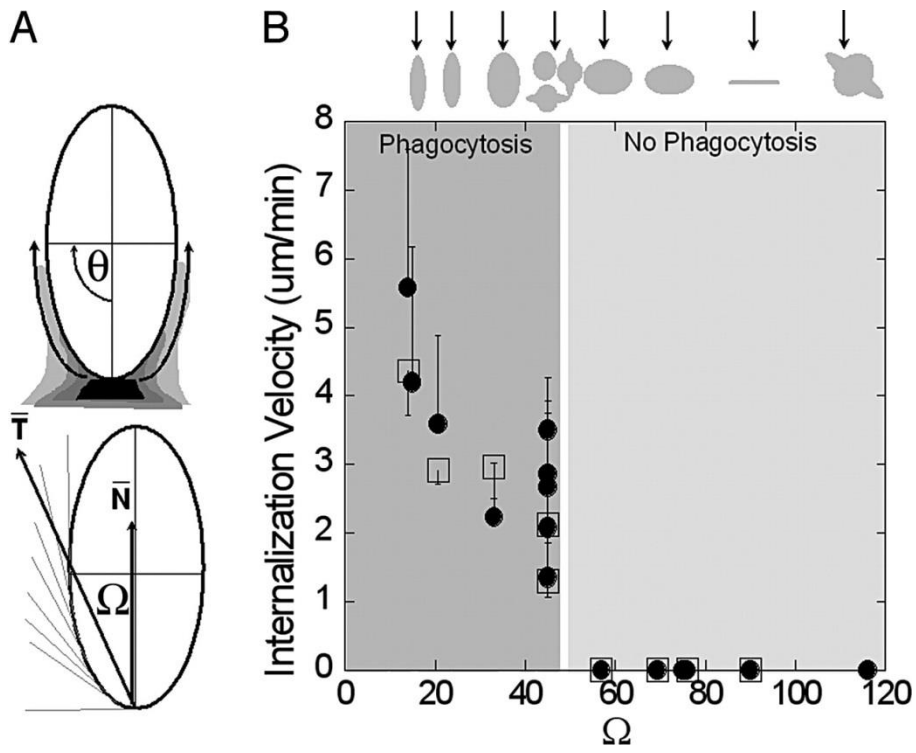

Figure 1.6 Schematic diagram of particle contact angle (Ω) influence on phagocytosis. T represents the average of tangential angles from $\theta = 0$ to $\theta = \pi/2$. Ω is the angle between T and cell membrane at the site of attachment, N. Figure reproduced from Champion (2006) [71] and copyright © by the National Academy of Sciences.

Interestingly, Hutter *et al*. have shown that nanoparticle geometry can influence the type of cytokines released when taken up by microglial cells, the resident macrophages in the brain (**Figure 1.7**) [72].

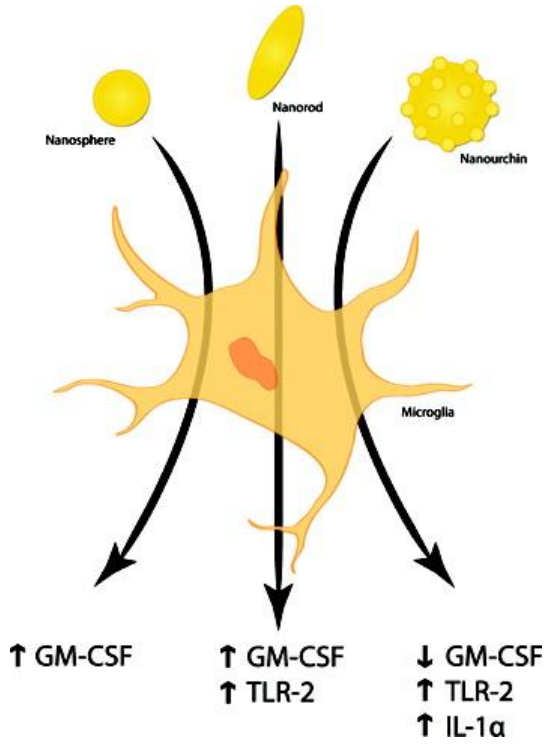

Figure 1.7 Differential release of chemical mediators in response to nanoparticle geometry.
Reprinted with permission from Albanese, A., E.A. Sykes, and W.C.W. Chan, Rough around the Edges: The Inflammatory Response of Microglial Cells to Spiky Nanoparticles. ACS Nano, 2010. 4(5): p. 2490-2493. Copyright 2010 American Chemical Society. [73]

Research has shown that the aspect ratio of a particle may also affect uptake. Work investigating the uptake of gold nanoparticles has shown that higher aspect ratio nanorods (1:3 and 1:5) are internalized less than spherical particles [74, 75]. However, Gratton *et al*. has shown that polymeric nanoparticles with a higher aspect ratio (1:3) are in fact internalized more quickly than nanoparticles of a similar volume but with an aspect ratio of 1:1 [76]. These reports demonstrate the variability of findings that may depend on the

particle matrix, cell type, particle size, and particle shape, thus reinforcing the need for further elucidation of these complex particle-biological interactions. With the various particle characteristics, such as size, shape and surface chemistry, being explored for inhaled therapeutics, can we systematically "build" a particle to test each of these characteristics and their effects on cellular uptake and residence time in the lung?

1.4 Generation of Aerosols for Inhaled Drug Delivery

1.4.1 Delivery Methods of Inhaled Aerosols

The development of inhaled therapies has been documented as far back as 1554 BC when the Egyptians vaporized the leaves of black henbane to treat those who had trouble breathing [77]. Since then, methods of delivering drugs to the lung have evolved from the inhalation of burning plant material over a fire to the development of complex devices with internals consisting of reservoirs for the active pharmaceutical ingredient (API) and multi-stage aerosolization systems. Current inhaler devices are categorized into three major systems: nebulizers, propellant driven pressurized metered-dose inhalers (pMDIs), and dry powder inhalers (DPIs). It has been shown that current asthma drug inhalers only achieve dose-delivery efficiencies of 10-30% in adults and 3-15% in children [39]. As such, there is a critical need to develop inhalers with increased dose efficiency.

Nebulizers generate aerosolized mists by directing compressed air or ultrasonic atomization mechanisms at a reservoir of liquid drug generating dispersed liquid droplets [78]. The aerosolized mist is generated and inhaled for 10-20 minutes. Due to the extended inhalation time of the aerosolized drug, higher doses are achieved with a nebulizer than with pMDIs or DPIs. However, an external energy source is needed to aerosolize the liquid drug;

thus, nebulizers are often heavy, bulky, and power intensive. Because of this, nebulizers are more commonly used in hospital and in-home settings.

A pMDI device is more patient friendly as it is more portable than a nebulizer and each dose is administered in less than a minute. The pMDI formulation consists of a liquid formulation of the API, a high vapor pressure propellant, and surfactants and other excipients that decrease drug-aerosol aggregates and lubricate the metering valves of the device. It releases a metered dose of liquid drug at high pressure, emitting the drug in the form of heterogeneous droplets from the actuator mouthpiece. Coordinated breathing and actuation of the drug by the patient is essential for achieving optimal dose-delivery to the lung.

While nebulizers and pMDIs employ a liquid drug form, DPIs utilize solid drug particles in dry powder form. DPIs are propellant free and breath-actuated which reduces the breathing and actuation coordination often needed with pMDIs. The three major components of a DPI are the dry powder formulation of the API, an aerosolization mechanism, and a metering system. The dry powder formulation for a DPI often consists of micronized drug and carrier excipients which are used to enhance drug aerosolization and increase the bulk volume of the powder for more uniform capsule filling. Because a DPI is breath-actuated, it is not recommended for those with low levels of lung function and young children. Dry powders are also sensitive to moisture which may affect the stability of the emitted drug aerosol, but new manufacturing and packaging technologies have increased the storage and reproducibility of DPIs.

1.4.2 Characterization of Inhaled Aerosols

Particle size is an important parameter in the determination of dose deposition in the lung. Aerosol particles (greater than 0.5 μm in geometric diameter)are characterized by their aerodynamic diameter, D_a, which is defined as the diameter of a sphere (density 1 g/cm^3) with the same settling velocity as a non-spherical particle. Particles with a D_a of 10 μm or larger will primarily deposit in the mouth, pharynx, and trachea. Particles of 5-10 μm in size typically deposit in the large conducting airways of the lung. Particles between 1-5 μm can deposit in the respiratory zone consisting of the smaller, lower bronchi and alveolar regions. Generating aerosols with an appropriate D_a is essential for optimal therapeutic efficacy in the lung.

Characterization of the aerodynamic diameter is analyzed using an Andersen cascade impactor (ACI), the current gold standard in industry for inhaler aerosol testing [79, 80]. The ACI sizes particles based on inertial momentum through an eight-stage impactor. Particles are dispersed into the ACI and pulled through a series of stages with decreasing nozzle diameters with a vacuum. Particle of certain cut-off diameters will impact on the collection plates of a stage while particles of smaller diameter will continue to follow the air flow around the collection plate and enter the subsequent stage through the nozzles (**Figure 1.8**). Aerosol particles are also characterized using an Aerodynamic Particle Sizer spectrometer (APS). The APS sizes particles by utilizing a time-of-flight technique that measures the residence time of the particles in flow through a nozzle with two parallel lasers. The APS counts individual particles as they pass through the measurement zone where their aerodynamic diameter is determined.

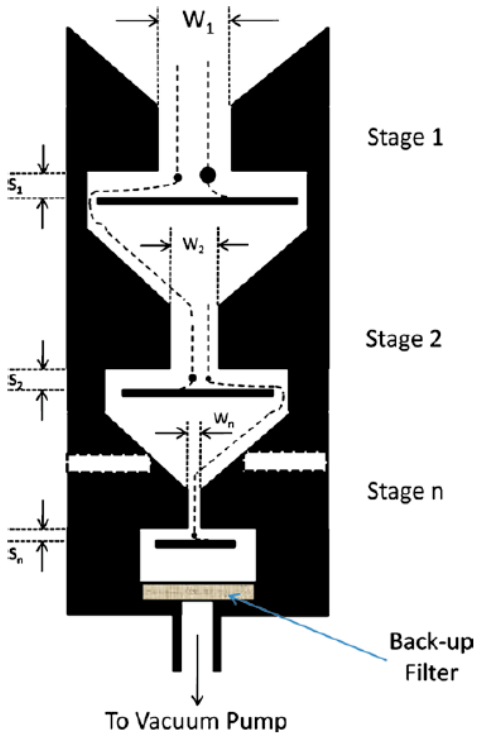

Figure 1.8 Schematic of a cascade impactor.
Figure reproduced from Son (2011) [80] with permission from Springer Publishing.

1.4.3 Particle Fabrication Techniques for Inhaled Drugs

Particle fabrication can be divided into two main categories, bottom-up and top-down. Bottom-up approaches to particle fabrication allow for the precursor particle components to increase in size via methods such as self-assembly, chemical synthesis, or colloidal aggregation. Examples of bottom-up fabrication methods of particles investigated for pulmonary drug delivery and/or toxicology include carbon nanotubes [81, 82], gold nanoparticles [83], micelles [84], liposomes [85, 86], silica nanoparticles [87], polyplexes [88], and spray-dried particles [11]. Top-down fabrication approaches start with a bulk material and break it down into smaller particle sizes. Common top-down particle fabrication methods include milling [89] and soft lithography [90]. Dry powder formulations

generated from conventional manufacturing techniques for pharmaceutical aerosols such as spray-drying (bottom-up) or milling (top-down) are shown in **Figure 1.9** [91].

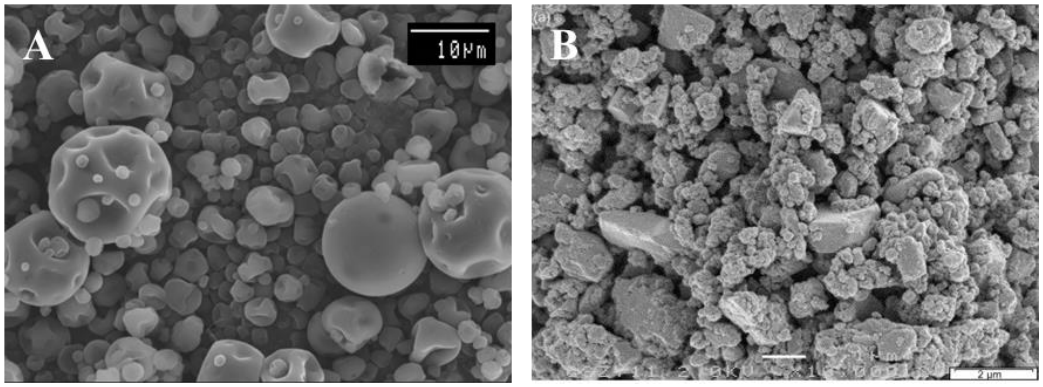

Figure 1.9 SEM images of spray-dried particles (A) and milled particles (B).
Images adapted from Senatore (2010) [92] and Zijlstra (2004) [93] and reprinted with permission.

As seen in the figure, these powders exhibit a large polydisperse aerosol population and lack control over the resulting particle shape. Thus, there remains a lack of understanding of the influence of particle shape and size on aerosol delivery to the lung. Top-down lithographic particle fabrication techniques can reproducibly generate monodisperse particle populations of many different sizes and shapes and is an emerging technique to better understand the effects of specific particle parameters in drug delivery.

1.5 Particle Replication in Non-wetting Templates (PRINT)

Particle Replication in Non-wetting Templates (PRINT) is a top-down nanofabrication technique which was inspired by the microelectronics industry and utilizes soft-lithography to produce calibration quality, monodisperse nano- and micro-particles with precise control over particle size, shape, composition, modulus, and surface chemistry [94-97].

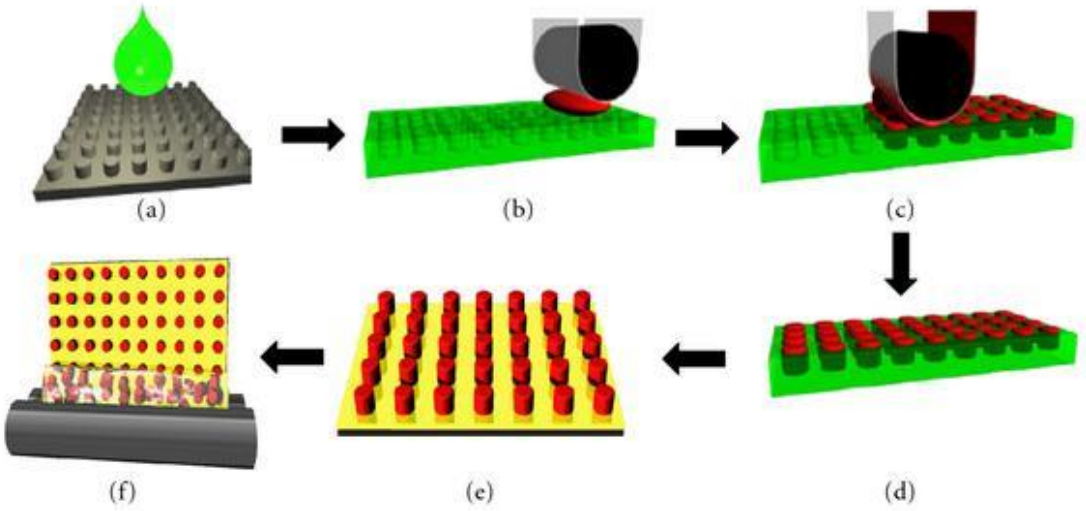

Figure 1.10 Schematic illustration of the PRINT process.
(a) Features on a hard silicon master template are replicated with high fidelity (b) to obtain a soft, polymeric mold with micro- and nanocavities that can then be (c) filled with relevant particle matrix and (d) extracted out of the mold and onto a harvest array for (e) particle collection and purification. Figure and caption reproduced from Garcia (2012) [83].

Particle fabrication via PRINT is illustrated in **Figure 1.10**. It is a multi-step process beginning with physically etching a silicon wafer with the intended shaped-pattern. Perfluoropolyether (PFPE) molds are generated by replication of the silicon master template resulting in a mold with precisely shaped cavities. PFPE was used due to its very low surface energy, flexibility, UV transparency, nonswelling properties, and its ability to be photochemically cured [98]. Particle solutions are then contacted with the mold and spontaneously fill the cavities via capillary forces without wetting the area around the cavities preventing the interconnected "flash" layer from forming. The material in the filled mold can then be solidified through a wide range of methods such as photochemical cross-linking, evaporation, or crystallization. The solidified particles are then transferred to harvest layer which can then be dissolved using appropriate solvents. This results in a solution of

free particles that can then be lyophilized for storage or chemically modified as needed. Depending on the particle composition used, fluorescent dye may be incorporated into the particle matrix in order to track particles *in vitro* and *in vivo*. Special monomers can be incorporated into the particle as well to provide function handles for the addition of targeting ligands and/or a PEG stealthing layer to tailor uptake by specific cell populations.

Because of its mild processing conditions, aerosols consisting of a variety of small molecule drugs and sensitive biologics (siRNA, BSA, DNAse) can be fabricated into precise shapes with monodisperse particle populations (**Figure 1.11**). Utilizing the plug-and-play characteristics of PRINT, applications in red blood cell mimics [99, 100], chemotherapeutic delivery [101, 102], and microneedle drug delivery [103] have also been explored.

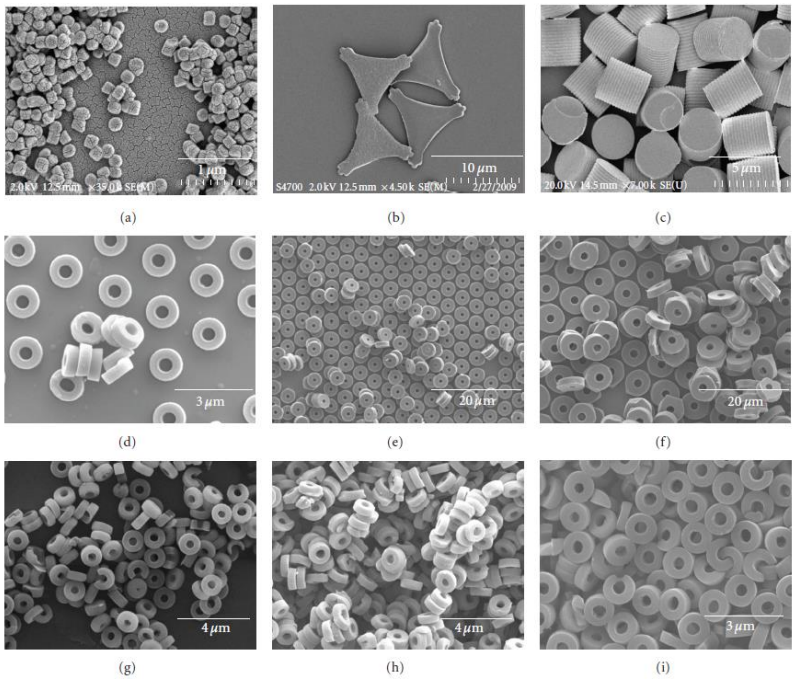

Figure 1.11 SEM micrographs of diverse PRINT aerosols.
(a) BSA/Lactose 200 × 200nm cylinders; (b) IgG/Lactose10 μm pollen; (c) 30k PLGA 3 μm cylinders; (d) itraconazole 1.5 μm torus; (e) itraconazole 3 μm torus; (f) itraconazole 6 μm torus; (g) zanamivir 1.5 μm torus; (h) DNAse 1.5 μm torus; (i) siRNA 1.5 μm torus. Figure and caption reproduced from Garcia (2012) [90].

1.6 Thesis Overview

The goal of this thesis is to examine the influence of different particle parameters of potential drug carriers on physiological responses in the lung. Utilizing PRINT technology, nano- and micron-sized particles were fabricated with precise shapes, sizes, compositions, and surface chemistries. The versatility of PRINT allowed for the systematic tuning of particle characteristics in order to investigate the impact of these parameters on cell uptake and lung distribution. Further, differential uptake was explored for potential implications in therapeutic applications.

In Chapter 2, cross-linked hydrogels of different aerodynamically relevant non-spherical shapes were fabricated and characterized. PRINT allowed for the generation of interesting particle shapes such as pollen-mimicking geometries and ball-and-stick geometries with varying number of arms and purposeful asymmetry, none of which are accessible via common particle fabrication methods. Because alveolar macrophages play a significant role in particle clearance, *in vitro* experiments investigating the effect of particle shape and size on macrophage uptake were performed.

In Chapter 3, the effect of particles on the innate immune system was investigated. For use as drug delivery vehicles, particles dosed to the lung should not cause unintended inflammatory responses. PLGA (poly(lactic-*co*-glycolic acid)) and PEG (poly(ethylene glycol)) PRINT particles were instilled into the lungs of mice and immunological outcomes were measured. Particle residence time and cellular uptake in lung cells were also observed for both nano- and micro-particles.

In Chapter 4, particle distribution and cellular uptake in the lung was explored with an additional emphasis on the effect of surface chemistry. In these experiments, a more in

depth analysis of the physiological response to instilled particles was pursued to investigate both inflammatory effects as well as particle clearance by specific cell populations in the lung.

In Chapter 5, a summary of the findings and future directions of this work is presented.

CHAPTER 2

EFFECTS OF PARTICLE SHAPE AND SIZE ON ALVEOLAR MACROPHAGE UPTAKE

2.1 Overview

There is a significant unmet need in the delivery of respiratory drugs to target or de-target macrophages depending on the desired site of action of various therapeutics. Alveolar macrophages often present a significant barrier to efficient pulmonary drug delivery applications because of i) their rapid and undesirable clearance of certain deposited drugs in the lung whose site of action involves non-macrophage targets, like aerosolized therapeutics targeted to the alveoli and epithelial cells; or ii) by their protection and harboring of disease targets, such as infectious bacteria like tuberculosis, which makes it difficult to treat effectively. There has been widespread interest in designing particles for use in dry powder inhalers that have the ability to target or de-target alveolar macrophages in order to increase their therapeutic index. Using PRINT®, a top-down nano- and micro-molding particle fabrication technique based on soft lithography, we were able to generate unique micron-sized particle geometries with aerodynamic diameters between 1-5 μm but with volumes that ranged between 5 – 45 μm^3 which was achieved by controlling particle shapes. Over two-fold reduction in particle uptake by alveolar macrophages with selected shapes was observed indicating the potential for tailored avoidance of macrophage clearance in the lung. Cell interactions with these shape-specific particles were further investigated using microscopy

techniques to gain a better understanding of how particle shape affects the kinetics of phagocytosis. Integrating drug delivery design with particle geometry engineering in order to modulate phagocytic tendencies may lead to novel therapeutic and diagnostic paradigms for a wide range of diseases.

2.2 Introduction

Common particle fabrication techniques for pulmonary delivery, like self-assembled and spray dried methods, favor the formation of spherical particles which minimize surface energy and yield significant dispersions in particle sizes and shapes [9]. Indeed, the study of aerosols is complicated because of the heterogeneous nature of traditional particle fabrication technologies. With the advent of PRINT (Particle Replication in Non-wetting Templates) technology and other lithographic particle fabrication methods, an added dimension of shape can be explored for both deposition and cell targeting properties of particle-based therapies. Additionally, PRINT allows for the precise control over many particle characteristics such as size, composition, porosity, modulus, and surface functionality [104, 105]. The ability to screen particles by altering one variable at a time may provide insights into the underlying fundamental mechanisms of drug delivery to the lung, potentially leading to the development of more efficient and effective drug delivery vehicles.

The ease of access, large absorptive surface area, and reduced enzymatic activity of the lung make it an attractive target for both local and systemic drug delivery. Inhaled aerosol treatments for local lung diseases such as chronic obstructive pulmonary disease

(COPD), pulmonary hypertension (PHT), asthma, cystic fibrosis (CF), and tuberculosis (TB) have been widely investigated [61, 106-108]. However, current aerosolized drugs often underperform therapeutically, owing to a variety of issues such as a polydisperse population of particle sizes, inefficient control of deposition in the lung, and a lack of efficient mechanisms for controlled release of the therapeutic. In addition, drug particles must circumvent the lung's highly efficient particle clearance mechanisms such as mucociliary transport, phagocytosis by macrophages [109], and rapid absorption of drug molecules into the systemic circulation [110].

Mucociliary clearance can be reduced by delivering particles less than 5 μm in aerodynamic diameter, thereby avoiding particle deposition in the mucociliary escalator of the tracheobronchial region [51]. Upon delivery to the pulmonary region, particles are rapidly taken up by alveolar macrophages (AM) [56]. Avoidance of macrophage uptake may be preferred for aerosolized therapeutics targeted to the alveoli and epithelial cells as well as for systemic delivery [58]. This was shown in studies in which depletion of AMs by clodronate resulted in an increased pulmonary bioavailability of larger inhaled proteins such as IgG and human chorionic gonadotropin [56]. Because particles with geometric diameters of 1-5 microns have been shown to be preferentially taken up by AMs [58, 59], large, porous particles [58] and swellable microparticles [60] were developed to deposit in the alveolar airspace successfully avoiding macrophage uptake due to their large (> 5 μm) geometric size. However, the sequestering of bacteria in macrophages for diseases such as tuberculosis (TB) and pneumonia may make AMs prime targets for antibacterial delivery [61]. Targeted apoptosis of AMs has also been shown to lead to increased protection from *M. tuberculosis* infection and an enhanced Th1-mediated immune response [62].

Recent research concerning cellular internalization of particles has investigated the influence of geometry on cellular internalization and trafficking [70, 111, 112]. *In vitro* investigations into shape effects of polystyrene particles on macrophage phagocytosis have found that the local contact angle between the particle and the cell may play a role in the initiation of phagocytosis [70, 113]. Utilizing PRINT, we were able to synthesize unique geometric shapes with varying numbers of appendages and bearing distinct terminal shapes and sizes to further explore the role of shape on macrophage phagocytosis. Due to the versatility of chemical composition enabled by the PRINT technology, particles composed of various polymers, chemotherapeutics, and sensitive biologics could be produced allowing defined therapeutic effects to be tuned for particular applications [100, 114, 115]. PRINT enables the synthesis of bio-inspired shapes such as pollen and bacteria, thereby allowing us to mimic the diversity of inhaled particles in order to screen characteristics relevant to overcoming the barriers to efficient drug delivery to the lung.

Herein, we show that the geometry of distinctly shaped particles with similar aerodynamic diameters can influence the extent of alveolar macrophage phagocytosis. This ability to target or de-target pulmonary macrophages upon administration of aerosolized drug particles may be used as a novel strategy for the design of efficient inhaled drug delivery systems.

2.3 Materials and Methods

PRINT Particle Fabrication

Master templates of all the shapes tested were prepared using photolithography. Fluorocur PRINT molds were generated from silicon master templates of the particles

(Liquidia Technologies). PRINT particles were composed of 96 wt. % poly(ethylene glycol) diacrylate (MW: 700), 2 wt. % fluorescein-O-acrylate, and 2 wt. % 2,2,-diethoxyacetophenone. This polymer mixture was drop-cast onto PRINT molds. A polyvinylpyrrolidone (PVP)-coated poly(ethylene terephthalate) (PET) cover sheet was laminated on top of the mold to aid in homogenous spreading of the monomer solution across the mold. The PVP cover sheet was then peeled away from the filled mold at the nip of a laminator, removing residual monomer and a filled mold with no connecting flash later. The mold was then placed in a UV curing chamber, purged with nitrogen, and cured (λ=365 nm, power >20 mW/cm^2) for 4 minutes in order to polymerize the monomer solution. Cured particles were transferred out of the mold onto a polyvinyl alcohol (PVOH) – coated PET harvesting sheet by laminating the mold and harvesting sheet together and running them through a heated laminator nip. The mold was then peeled off leaving free particles on the harvesting sheet. Particles were collected from the harvesting sheet by bead harvesting with water. After washing the particles 5 times with water, the particles were pelleted by centrifugation, the supernatant removed, and the pellet was resuspended in tert-butanol and flash frozen with liquid nitrogen. The particles were lyophilized overnight to generate a dry powder.

Zeta Potential Measurements

The zeta potential of PRINT particles was measured in 30% (w/w) sucrose solution using a nano ZS Zetasizer (Malvern Instruments).

Aerodynamic Diameter Calculation

Mass median aerodynamic diameters (MMADs) were calculated for each particle geometry using computational software developed in house. Aerosol geometries, surface and volume meshes were defined using Gmsh software and discretized into appropriate triangles and tetrahedra. Particle trajectories were then computed for aerosols settling based on a Stokes flow assumption by solving equations of motion using fourth order Runge-Kutta integration in time. From these computations, a dynamic shape factor (χ) was calculated, and subsequently, MMADs could be determined from the following equation:

$$MMAD = \sqrt[3]{\left(\frac{6V_p}{\pi}\right)}\sqrt{\left(\frac{\rho_p}{\chi\rho_0}\right)}$$

where V_p is the particle volume, ρ_p is the density of the particle and ρ_0 is a reference density.

Uptake Experiments

MH-S (ATCC) and RAW264.7 (ATCC) cell lines were used for the particle uptake experiments. Cells were plated at 2 x 10^4 cells/well in a 24-well plate 48 hours before dosing. Particles were re-suspended in water and particle number counted with a hemacytometer. Cells were dosed at a constant particle number (10 particles / cell) in media consisting of high glucose Dulbecco's Modified Eagle Medium (DMEM) (Gibco) and 10% fetal bovine serum (FBS) and were incubated together from 0.5 to 24 hr (37°C, 5% CO_2). After incubation, cells were washed with Dulbecco's Phosphate Buffer Saline (PBS) solution and detached with trypsin (MH-S) or cell-scraped (RAW264.7). The cells were then re-suspended in an 0.2% trypan blue (Sigma) solution in PBS to quench extracellular

fluorescence. The samples were analyzed by flow cytometry (CyAn ADP, Dako). 5,000 cells were measured for each sample. Two different particle batches were tested for all shapes and time points.

Live Cell Imaging

MH-S cells were plated at $4x10^4$ cells/well in a 0.17 mm Delta T dish (Fisher) 48 hours before dosing. Cells were then dosed at a particle concentration of 50 µg/mL in DMEM with 10% FBS and imaging was begun within 10 minutes of dosing. An Olympus FlowView 500 confocal microscope was used to collect fluorescent and bright-field images every 5 minutes for one hour. Consecutive 1-hour videos were made totaling 4 hours for one field of view. The image files were then condensed into a video using Imaris (Bitplane) image processing software.

Confocal Laser Scanning Microscopy

MH-S cells were plated at 5×10^5 cells on cover slips in 6-well dishes and grown for 24 hours before dosing. Cells were treated with particles for 0.5 to 12 hours. Cells were then washed with phosphate- buffered saline, pH 7.4(PBS) and fixed with 4% Para formaldehyde in PBS for 10 min at room temperature. Cells were permeablized with 0.1% Triton –X100 in PBS for 3min and incubated in phalloidin (Alexa-555) (Molecular Probes) for one hour at room temperature in the dark. Coverslips were washed three times with PBS and mounted with FluorSave reagent (Calbiochem). Samples were then analyzed by confocal microscopy.

Confocal images were acquired using a Zeiss 710 laser scanning confocal imaging system (Zeiss) fluorescence microscope fitted with a PlanApo 60× oil objective (Zeiss).

Scanning Electron Microscopy

MH-S cells were seeded at 20k cells/well on glass slides placed in each well of 24-well plates and allowed to adhere overnight. The cells were dosed at a particle number of 8 particles/cell and were incubated for time points between 0.5 and 4 hours. After incubation, cells were fixed with 4% paraformaldehyde (PFA) at room temperature and dehydrated with washes of increasing ethanol concentration. Cells were then run under critical point drying (CPD) conditions. After drying, cells were sputter-coated with gold-palladium for SEM imaging.

Modulus Testing

The modulus of the cross-linked PEG_{700}-DA hydrogels was measured using polymerized macroscopic "dog-bone"-shaped bulk samples. The samples were tested on an Instron 5566 Universal Testing Machine (Instron) with a strain rate of 10 mm/min.

2.4 Results and Discussion

PRINT provides the opportunity to produce geometrically diverse particles that have similar aerodynamic diameters, but result in very different macrophage uptake kinetics.

Screening geometric characteristics of particles that influence macrophage uptake can be done rapidly using PRINT because the same fabrication method can be used to generate all of the shapes studied with consistent particle composition and other physical properties. By adding aerodynamic shape characteristics, such as fenestrations, to the particle, we were able to generate particles of larger volume with the same mass median aerodynamic diameters (MMAD) as particles with smaller volumes.

2.4.1 Fabrication of PRINT Particles

A collection of non-spherical shapes was fabricated using PRINT to create near monodisperse and geometrically precise populations of particles. Aerodynamically inspired shapes, such as pollen, were designed to investigate aerosolization efficacy, pulmonary deposition and cellular internalization properties. These hydrogel micro-particles were primarily composed of cross-linked poly(ethylene glycol) and have calculated aerodynamic diameters between 1-5 μm, the ideal size for pulmonary deposition. Four particle characteristics were used to describe the shapes examined: (1) the shape diameter (SD), which is the minimum diameter of a circumscribed circle around the particle (and is the number that precedes the shape name throughout the manuscript to differentiate different sizes of the same geometry); (2) the minimum feature size (MFS), which is the diameter of the smallest distinct geometry of the shape; (3) the particle volume; and (4) the aerodynamic diameter (MMAD) of the particle. Three distinct families of shapes were examined: (1) a toroid (donut)-shaped series (SDs = 3 μm, and 6 μm; **Figure 2.1 A,B**); (2) a pollen shape (SD=11.68 μm, MFS=10 μm; **Figure 2.1 C**); and (3) a ball-and-stick series [7.77 μm lollipop, SD=7.77 μm, MFS=4 μm (**Figure 2.1 D**); 10.24 μm helicopter, SD=10.24 μm,

MFS=1.6 µm, (Fig 1E); 9.54 µm l-dumbbell, SD=9.54 , MFS=2.5 µm (**Figure 2.1 F**); 12.3 µm v-boomerang, SD=12.3 µm, MFS= 2.25 µm (**Figure 2.1 G**)]. Scanning electron microscopy was used to confirm the dimensions of the particles. The measured zeta potential of all particle geometries was approximately -20 mV.

Table 2.1 Volumes, dimensions, and Mass Median Aerodynamic Diameter (MMAD) of shaped particles

Shape	Total Volume (μm^3)	Min. Feature Size (µm)	Calc. MMAD (µm)
3 µm Donut	5.03	3	1.73
10.24 µm Helicopter	6.91	1.6	1.68
12.3 µm V-Boomerang	7.75	2.25	1.75
9.54 µm L-dumbbell	9.22	2.5	1.95
7.77 µm Lollipop	12.30	1	2.25
11.68 µm Pollen	35.60	10	2.74
6 µm Donut	40.67	6	3.26

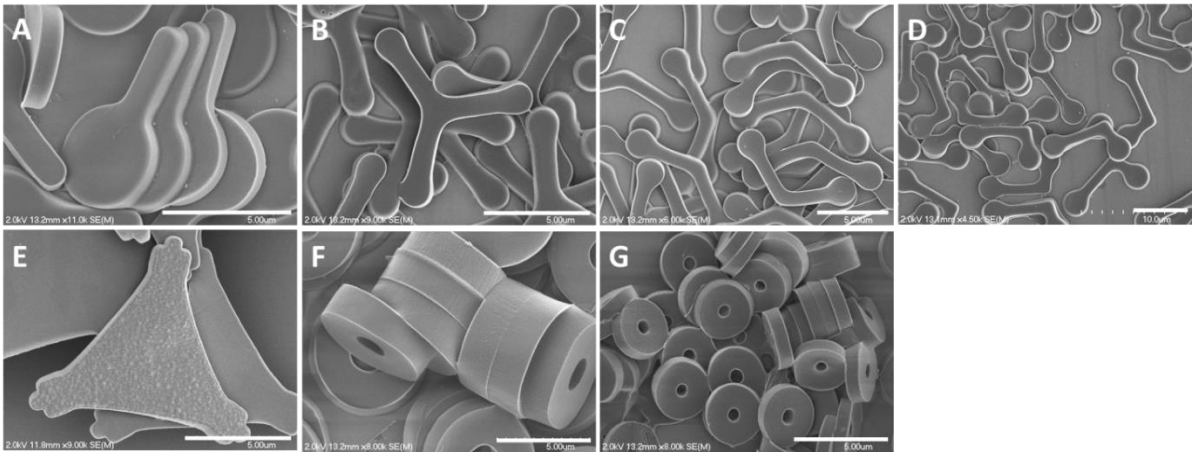

Figure 2.1 Scanning electron micrographs of PRINT particles.
(A) 7.77 µmm Lollipop. (B) 10.24 µm Helicopter. (C) 12.3 µm V-Boomerang. (D) 9.54 µm L-dumbbell. (E) 11.68 µm Pollen. (F) 6 µm Donut. (G) 3 µm Donut. (**Scale bar:** 5 µm)

2.4.2 Kinetics of Particle Uptake as a Function of Shape and Size

Flow cytometry was used to investigate effects of particle geometry on macrophage internalization. MH-S murine alveolar macrophages were dosed with a constant particle number (10 particles/ cell) and uptake was measured from 0.5 to 24 hours at five time points. Kinetics of cellular internalization was analyzed using a flow cytometry method in which membrane-bound and internalized particles were differentiated using fluorescence quenching with trypan blue [116]. For particle shapes that were internalized efficiently, a rapid increase in particle-positive cells was observed within the first eight hours after which intracellular particle concentration remained constant **(Figure 2.2 A)**. The internalization percentage of particles that were less efficiently internalized also leveled out after eight hours, but the initial internalization kinetics were significantly slower. By utilizing knowledge from previous studies on macrophage internalization based on size and volume [58, 59, 112], we were able to generate rationally designed geometric shapes that encompassed certain characteristics to either increase or decrease macrophage phagocytosis. It was observed that different shapes with aerodynamic diameters of 2.6 ± 0.7 μm could be tailored to have over two-fold difference in macrophage internalization **(Figure 2.2 B)**. Phagocytosis of these PRINT particles was predominantly influenced by volume, as shapes of similar volume had similar internalization patterns. After 24 hours, MH-S cells with internalized particles of all of the ball-and-stick series of shapes with volumes of 7-12 μm^3 was approximately 40% while the internalization of 6 μm donut and 11.68 μm pollen geometries, which have volumes greater than 35 μm^3, leveled out at 20%. This significant reduction in macrophage uptake is promising for pulmonary therapies which would benefit from enhanced residence time and minimal drug clearance from the lung. The same trends

were also seen when RAW264.7 murine leukaemic macrophages were dosed similarly (**Figure 2.3)** indicating that the findings from this work may potentially be utilized in applications targeting or de-targeting macrophages in other parts of the body. These results demonstrate the influence of particle geometry on macrophage uptake and the ability of PRINT to generate particles of similar aerodynamic diameter but vastly different geometric dimensions.

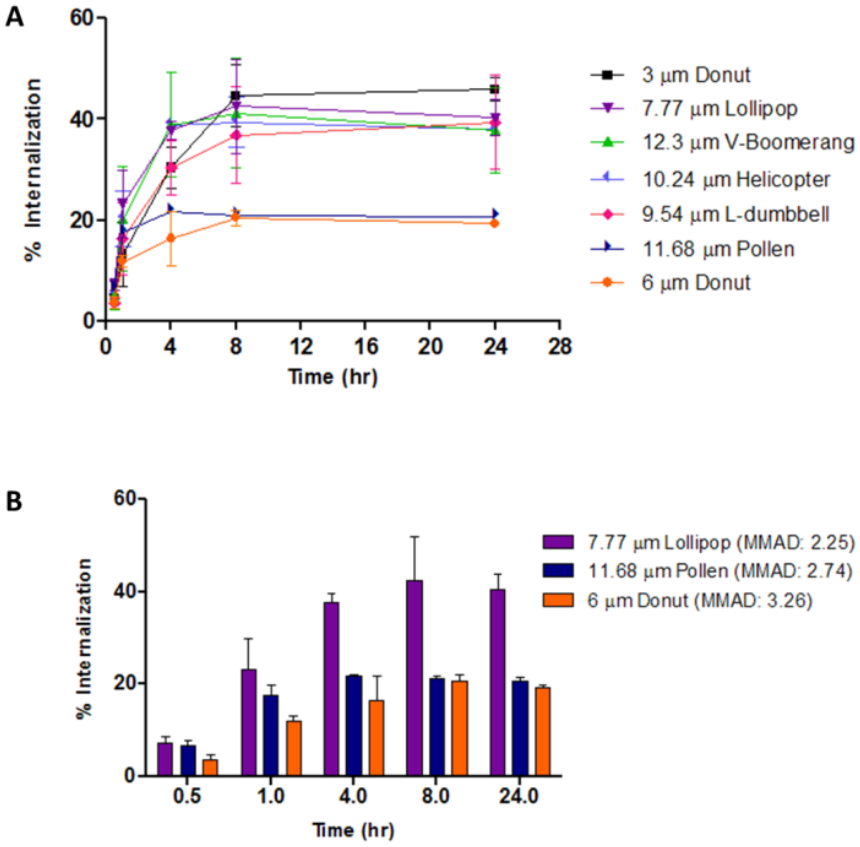

Figure 2.2 Internalization profile of particles in MH-S cells (24 hrs)
(A) Particle uptake timecourse of all PRINT shapes dosed. (B) Comparison of particle uptake between shapes with similar aerodynamic diameters (2.6 ± 0.7 µm).

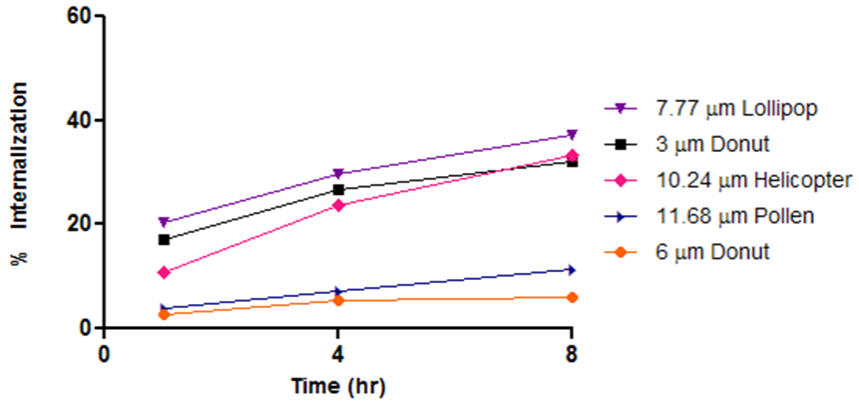

Figure 2.3 Internalization profile of particles in RAW264.7 cells (8 hrs)

2.4.3 Particle Orientation/Geometric Effects in Macrophage Phagocytosis

Macrophages in the lung constantly survey a numerous and diverse population of particulates. Research into how the cell acts on these particles has been limited by the lack of fabrication methods for generating non-spherically shaped particles. Budding yeast has been extensively used to investigate the proteins and cellular mechanisms involved in phagocytosis [117]. Champion, et al. stretched polystyrene particles to understand how local particle shape may influence the initiation of phagocytosis [118]. The unique shapes of these PRINT particles allow us to examine how additional geometric features such as asymmetry, appendages, angles, fenestrations, and size affect particle internalization by macrophages.

Previous literature has shown that particles with maximal diameters of 2 µm had the highest percentage of particles internalized from initial particle number dosed [59]. Thus, it is interesting to note that, regardless of volume, all of the shapes with distinct minimum feature sizes less than or equal to 3 µm showed similar macrophage uptake from the flow cytometry data. The ball-and-stick series of shapes included geometries with variable

number of arms, angle lengths, and end terminal diameter in order to investigate how certain geometric features may influence macrophage uptake.

To more clearly examine geometric influences on macrophage uptake, fluorescent microscopy and scanning electron microscopy (SEM) techniques were utilized to capture cell-particle interactions at early time points **(Figure 2.4)**. The local particle shape at the point of attachment has been observed to influence the kinetics of particle uptake [70]. This is unsurprising as phagocytosis is actin-dependent, and thus an energy-dependent, process. The more actin remodeling that the cell must undergo in order to engulf a particle will slow the rate of internalization. A dimensionless parameter, Ω , has been developed to denote the local contact angle the cell membrane makes with the particle at the initial point of contact [70, 71]. When one cell is associated with two or more particles, the particle in which the local particle contact angle ($\Omega < 45°$) is more favorable towards phagocytosis is observed to be further engulfed **(Figure 2.4 A, D)** [70]. However, since these micrographs are of fixed cells, the order and timeline of cell attachment to the particle cannot be definitively determined.

Interestingly, we observed active phagocytosis of these PEG particles when Ω was larger than 45° **(Figure 2.4 B, E)**. Previous studies have shown that both IgG-opsonized and non-opsonized particles with $\Omega > 45°$ induced spreading of the cell membrane but did not induce phagocytosis [70]. The two most studied pathways of macrophage particle internalization are Fc receptor (FcR)- and complement-mediated phagocytosis; however, since these particles were not opsonized the exact mechanism by which they are phagocytosed is not defined. Complement-mediated phagocytosis involves particles "sinking" into the membrane [119, 120] while FcR-mediated phagocytosis, on the other

hand, extends the phagocytic cup around the particle before drawing the engulfed particle into the body of the cell [121, 122]. Since complement-mediated phagocytosis involves allowing the particle to sink into the membrane rather than totally enclosing it with actin filaments, the strict dependence on local contact angle as a determinant for internalization should be loosened. It was observed that a majority of particles associated with cells were raised above the plane of the surface as the cell drew it into the membrane **(Figure 2.4 C, F)**. This may allow the cell to "wrap" around the particle and initiate phagocytosis rather than just spreading along the flat side of the particle. However, it may be noted that most particles observed in the process of being internalized did have $\Omega < 45°$ which is more favorable for phagocytosis.

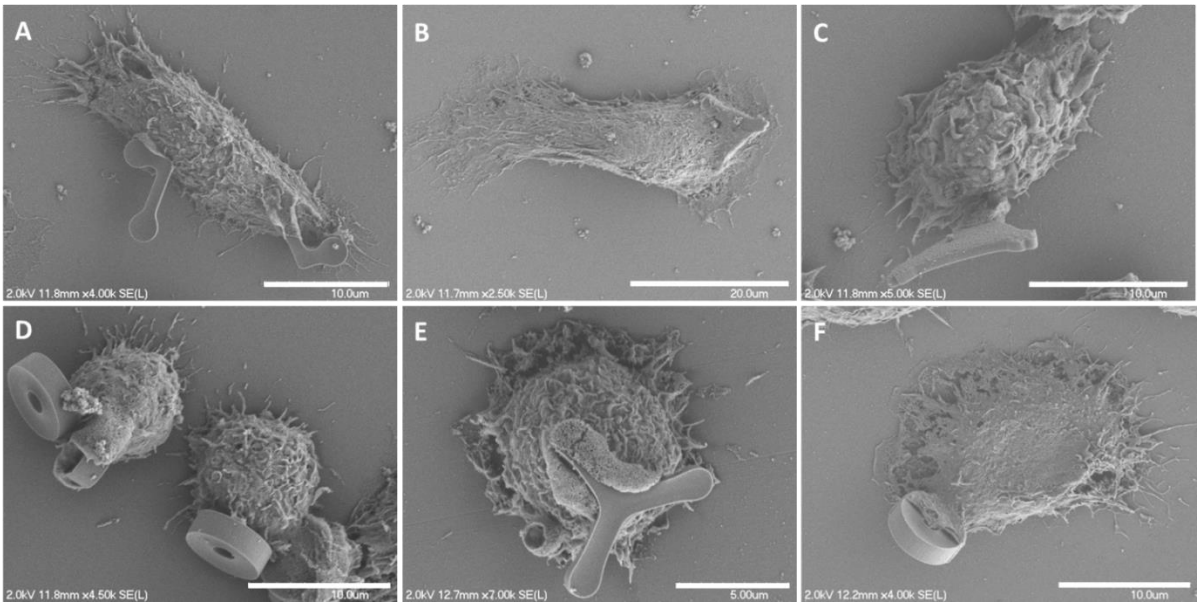

Figure 2.4 Micrographs of MH-S cells
Cell association with shaped PEG particles depicting local particle angle effects on phagocytosis (1 hour timepoint). (A) 9.54 µm L-dumbbells, (D, F) 6 µm donuts, (B, C) 11.68 µm pollen, (E) 10.24 µm helicopter. **Scale bar**: 10 µm (A, C, D, F), 20 µm (B), 5 µm (E)

To extend these observations, we were interested in identifying any trends in particle internalization characteristics when a macrophage is faced with two different geometries on the same particle. With the "ball" end having a diameter of 4 μm and the "stick" end having a diameter of 1 μm, the lollipop shape offered a unique test of how particle geometry may dictate the cellular mechanisms of phagocytosis. From the flow cytometry data, the lollipops had similar internalization kinetics to the rest of the ball-and-stick series indicating that having one end significantly larger than another may not affect overall kinetics in macrophage internalization. However, from fluorescent microscopy analysis it was observed that at early time points the macrophages had a preference for the narrow end of the lollipop particles during initiation of particle internalization (**Figure 2.5**). Because the cells are washed with PBS before fixation, unattached or loosely held particles are cleared away. This data suggests that the cell may have a better grip on the 1 μm "stick" end of the lollipops because it initiates phagocytosis (actin remodeling) faster than if it first took hold of the 4 μm "ball" end which requires more time for actin polymerization around the particle although it is not known whether the cell will manipulate the particle as it is drawing it into the cell membrane. This data may be useful in designing particles that de-target macrophages by incorporating larger feature sizes.

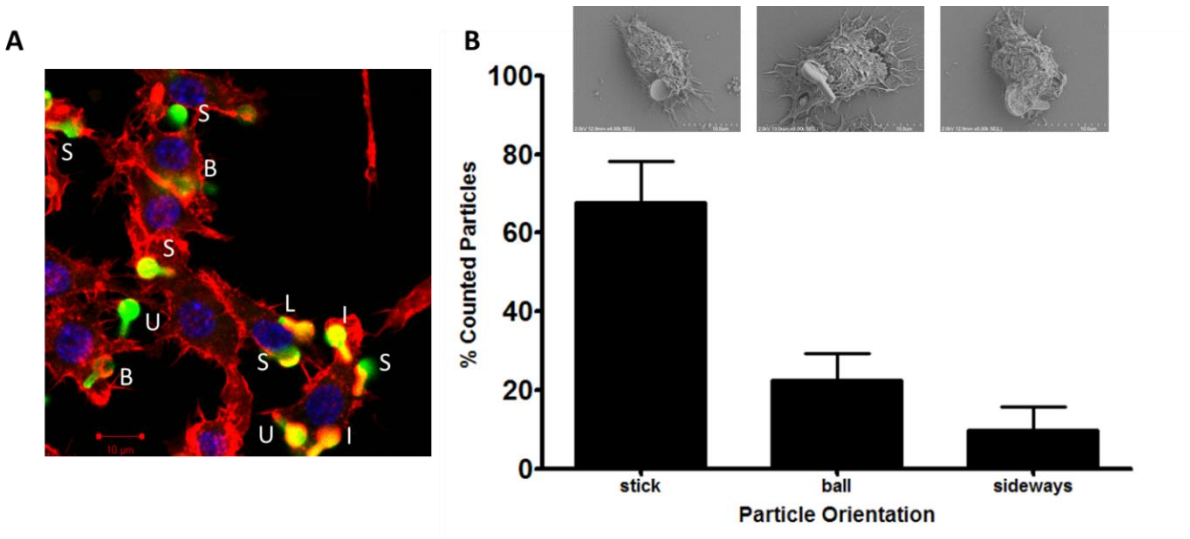

Figure 2.5 Particle orientation at early time points of phagocytosis
(A) Determination of particle internalization orientation using fluorescent microscopy (Orientation labels – S: stick, B: ball, L: sideways, I: fully internalized, U: Undetermined). (B) Graph of lollipop particle internalization orientation at 0.5 hours in MH-S macrophages (n=3 groups; 100 particles/group). Corresponding SEM images of particle orientation also shown.

The effect of angled geometries on cell interactions with the particle was visualized using live cell imaging. We hypothesized that the internalization kinetics of a particle would decrease when phagocytosis is initiated at the vertex versus at the terminal end of an appendage. Initial studies with live video microscopy of 9.54 µm L-dumbbells interactions with macrophages demonstrated that there may be a difference in uptake kinetics dependent on where the cell first contacts the particle (**Figure 2.6**). Notice that the particle first contacted by the cell on the "ball" section (labeled A) is fully internalized while the particle contacted in the middle of the particle at theangled "stick" section (labeled B) is still mostly external to the cell membrane and may be a result of the increased contact angle at that point.

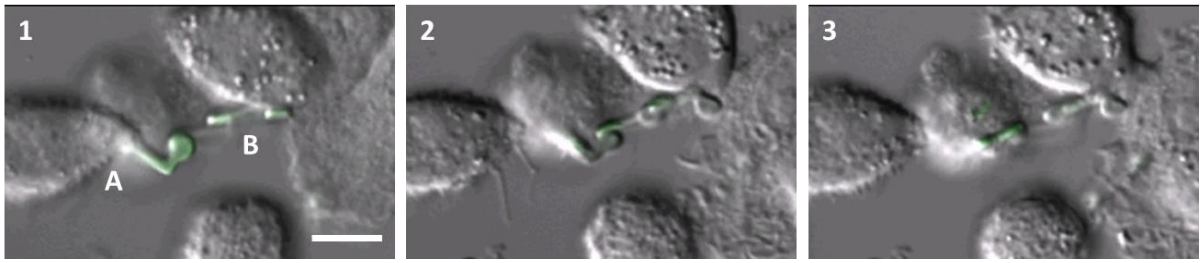

Figure 2.6 Time-lapse of particle internalization by macrophages
Notice that the particle first contacted by the cell on "ball" section is fully internalized while the particle contacted at the angled "stick" section is still attached to the outside of the cell membrane. (**Scale bar:** 10 μm)

Phagocytosis of curved budding yeast has been studied with *Dictyostelium* cells in which it was found that the cells scan for concave or convex regions and can switch between actin polymerization and depolymerization to fully engulf, release, or cleave the particle [123]. From these observations, it was hypothesized that the 10.24 μm helicopters would have slightly slower internalization kinetics than the other ball-and-stick shapes due to the 120° angle between each arm. Most of the helicopters had phagocytosis initialized at the terminal end of one of the arms, thus, as the cell membrane approaches the "Y" of the shape it encounters a wide angle (240°) which would require more actin polymerization to fully engulf the particle **(Figure 2.7)**. The flow cytometry data, however, does not show a difference in cellular internalization among the ball-and-stick family of shapes indicating that the arm angle of the 10.24 μm helicopter may not affect phagocytosis kinetics as significantly as overall particle volume or minimum feature size.

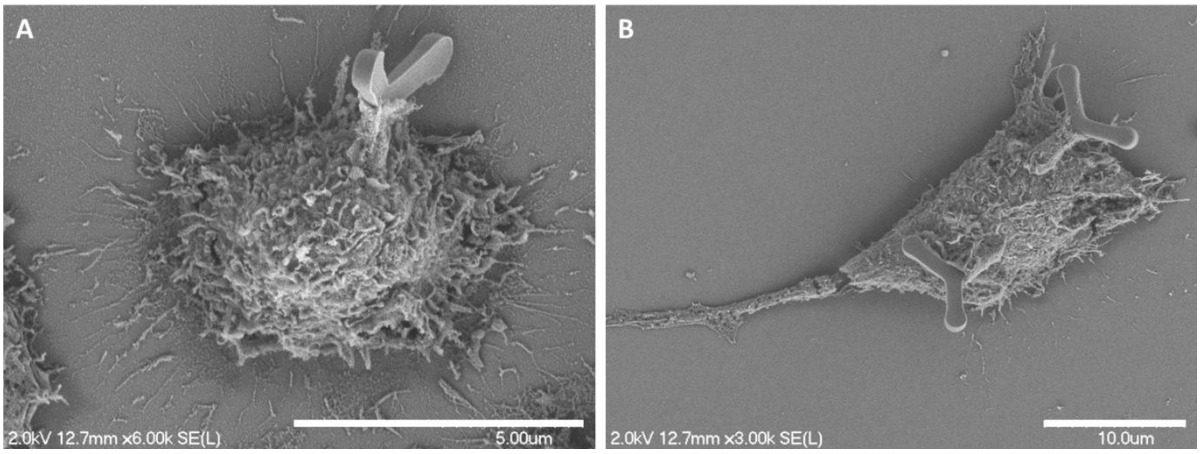

Figure 2.7 Illustration of particle angles encountered by macrophages
The actin cup must expand as it reaches the "Y" angle of the helicopter shape in order to complete phagocytosis. (**Scale bar:** 10 μm)

It is interesting to note that the cells exerted enough force to visibly stretch and bend these PRINT particles **(Figure 2.8)** which have a modulus measured around 6 MPa. Previous literature has shown that more rigid particles are preferentially phagocytosed over softer particles [124], and flexible, worm-like particles both *in vitro* and *in vivo* have been observed to reduce macrophage uptake [125, 126]**.** Recently, low-modulus (7.8 kPa) red blood cell (RBC) mimics fabricated using the PRINT technique have demonstrated extended circulation times *in vivo* likely due to their ability to circumvent the body's physical filtration barriers [100]. Reduced macrophage uptake of these RBC-like particles may also explain the increased time of circulation, thus, by decreasing the modulus of these aerodynamically-shaped particles one may be able to further reduce macrophage uptake.

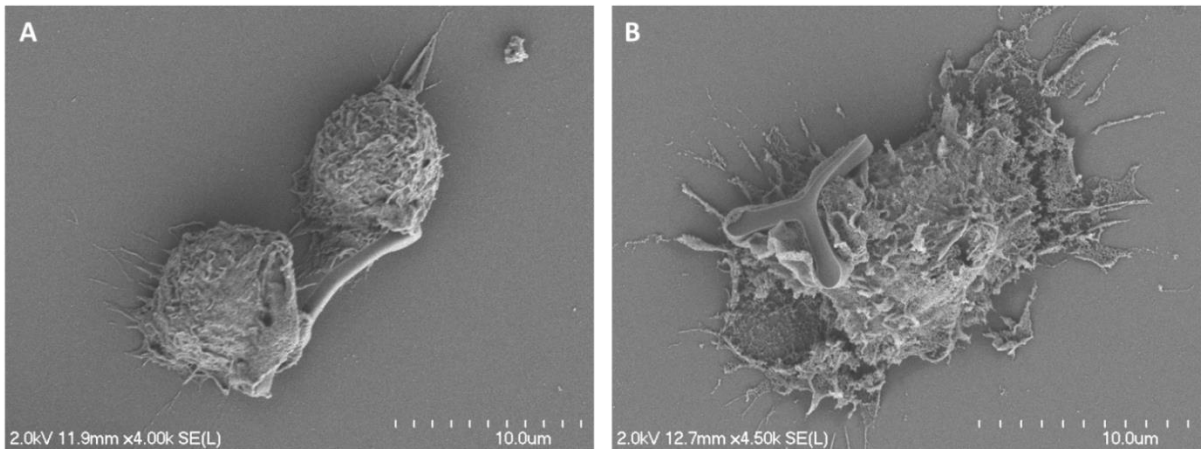

Figure 2.8 Micrographs depicting the ability of macrophages to deform highly cross-linked PEG particles. (A) V-boomerangs being stretched into a more linear particle by two cells. (B) Helicopter shape being drawn towards the cell membrane.

2.5 Conclusion

We wanted to investigate both the macro- and micro- implications of particle shape in targeting or de-targeting macrophage uptake. Using PRINT technology, particles with similar aerodynamic diameters but very different geometries were fabricated. From the flow cytometry data we show that macrophage internalization can be reduced over two-fold by increasing the volume of the particle through manipulation of particle shapes. Since particles with similar MMAD's deposit in the same area of the lung, the ability to tailor particles to avoid macrophage uptake for specific therapies should increase the efficiency of pulmonary drug delivery, and may improve the safety and therapeutic index of a given drug therapy. In order to more fully understand shape dynamics on macrophage uptake we looked at the influence of individual geometric features. Previous studies on shape have shown that local particle contact angle influences the initiation of phagocytosis. We found that while internalization kinetics were correlated to Ω, local contact angles greater than 45° did not necessarily prevent the initiation of phagocytosis. The inclusion of angles or asymmetry in

the particles was shown to have an influence on macrophage uptake. These studies demonstrate the capacity of PRINT to develop a toolbox of particle shapes that can be used to better understand the cellular mechanisms responsible for these observations.

Because the PRINT fabrication method allows for particle compositions of pure drug and other biodegradable components [115], different therapeutics can be incorporated into these geometries and shape-dependent efficacy can be further investigated. We hope that by applying the knowledge from fundamental biological studies of macrophage phagocytosis to pulmonary delivery applications we can design more efficient drug carriers to the lung.

CHAPTER 3

ANALYSIS OF THE MURINE IMMUNE RESPONSE TO PULMONARY DELIVERY OF PRECISELY FABRICATED NANO- AND MICROSCALE PARTICLES[1]

3.1 Overview

The pulmonary route of administration for inhaled therapeutics has been actively explored due to its non-invasive nature, the ease of access to the lung, and its large absorptive surface area. However, the physiological effects of particulate delivery to the lung have not yet been fully defined for materials commonly utilized in inhaled particle compositions. In this work, Particle Replication in Non-wetting Templates (PRINT) was used to fabricate particles on the nano- and micro-scale with precisely defined parameters in particle shape, size, and matrix. These calibration quality particles were then instilled into the lungs of mice to investigate the murine innate immune response as a function of different particle parameters. Both poly(lactic-co-glycolic acid) (PLGA) and polyethylene glycol (PEG) particles did not induce the release of pro-inflammatory cytokines or inflammasome activation *in vitro* and *in vivo*. All particle sizes tested (80x320 nm, 1 μm, 1.5 μm, and 6 μm in diameter) were shown to remain in the lung out to seven days without triggering host immunity which is promising for use of these particles in sustained and localized pulmonary drug delivery.

[1] Adapted from: Roberts RA, Shen T, Allen IC, Hasan W, DeSimone JM, et al. (2013**) Analysis of the Murine Immune Response to Pulmonary Delivery of Precisely Fabricated Nano- and Microscale Particles.** PLoS ONE 8(4): e62115. doi:10.1371/journal.pone.0062115

3.2 Introduction

The development of nano- and micro-particles as therapeutic vehicles for the treatment of disease has demonstrated the potent ability of these carriers to influence physiological responses. From genetic modulation by delivery of small interfering RNA to enhanced chemotherapeutic responses to even multi-functional imaging diagnostics, the use of particle formulations has had a transformative effect on pharmaceutical approaches towards disease therapies [127-129]. Another emerging aspect of therapeutic materials delivery is that of immunoengineering in which modulation of the intrinsic defense systems in the body may instruct specific immunological responses to influence the pathological outcomes of disease states [130]. Studies on programming antibody responses, enhancing humoral responses with nanoparticle vaccines, and increasing antibody responses to particle-delivered antigens have shown great promise in being able to direct immunological outcomes [131-133]. These advances are opening up the field not only to improved vaccines, but also to autoimmune disease, organ transplantation, diabetes, and cancer immunotherapies [134-136].

In order to fully realize the potential of particulate drug carriers for localized and sustained release systems in the lung, safety as well as efficacy must be investigated. A particle designed to circumvent lung clearance mechanisms may enhance local drug delivery and improve efficacy; yet, if it also initiates inflammatory or other host immune responses its safety profile would undermine its intended function and use as a therapeutic intervention. Particles developed for immunotherapy, or the treatment of a disease by engendering an appropriate immune response may be more efficacious with design parameters that can

activate the appropriate immune response or tailor the degree of the adaptive immune response.

Not much is yet known on how specific particle parameters may influence the host immune response, thus, it is appropriate to investigate the potential particle design characteristics that may activate these responses. Particle Replication in Non-wetting Templates (PRINT) is a top-down nanofabrication technique that utilizes soft-lithography to produce calibration quality, monodisperse nano- and micro-particles with precise control over particle size, shape, composition, modulus, and surface chemistry [94-97]. Thus, specific particle parameters can be probed to investigate their roles in influencing biological responses upon administration. In this work, *in vitro* and *in vivo* assays were used to investigate the murine inflammatory response to PLGA- and PEG-based particles. We find that PRINT nano- and micro-particles do not prompt systemic or localized inflammatory responses. This demonstrates that rational design strategies of therapeutic modalities can help develop an essential fundamental understanding of the biological effects of these particulate carriers without the concern of anti-vector effects.

3.3 Materials and Methods

Particle Materials

Poly(ethylene glycol) diacrylate (Mn 700) ($PEG_{700}DA$), 2-aminoetheyl methacrylate hydrochloride (AEM), Diphenyl (2,4,6-trimethylbenzoyl)phosphine oxide (TPO), and poly lactic co-glycolic acid (PLGA; 85:15 lactic acid/glycolic acid, MW= 55 000 g/mol) were purchased from Sigma-Aldrich. Tetraethylene glycol monoacrylate (HP_4A) was synthesized in-house as previously described [137]. Thermo Scientific Dylight 650 maleimide, PTFE

syringe filters (13mm membrane, 0.220 μm pore size), dimethylformamide (DMF), triethanolamine (TEA), pyridine, sterile water, borate buffer (pH 8.6), Dulbecco's phosphate buffered saline (DPBS) (pH 7.4), 1X phosphate buffered saline (PBS) (pH 7.4), acetic anhydride and methanol were obtained from Fisher Scientific. Conventional filters (2 μm) were purchased from Agilent. Polyvinyl alcohol (Mw 2000) (PVOH) was purchased from Acros Organics. Liquidia Technologies provided all PRINT molds used in these studies (80 nm x 320 nm, 1μm cylinder, 1.5μm and 6μm donuts).

PRINT PLGA Particle Fabrication

The fabrication process for PLGA PRINT particles has been described previously [114, 138]. Briefly, pre-particle solutions of PLGA were prepared in a 4:16:1 solvent mixture of DMSO:DMF:water and cast onto a poly(ethylene terephthalate) (PET) sheet and a Mayer rod was used to draw a thin polymer film. A PRINT mold with the desired features (80x320 nm or 1 μm cylinder shapes) was placed on top of the pre-particle polymer film and run through a heated laminator to allow filling of the mold. These particles were then cooled below the polymer glass transition temperature then transferred from the mold onto a harvest layer of poly(vinyl alcohol) (PVOH) by passing the filled mold/PVOH sheets through a heated laminator. Particles were collected from the harvest layer via bead harvesting using water to dissolve away the PVOH resulting in free particles.

PRINT Hydrogel Fabrication

PRINT hydrogel fabrication used a preparticle solution of 67.5 wt.% HP_4A, 20 wt.% AEM (functional monomer), 10 wt.% $PEG_{700}DA$ (crosslinker), 1 wt.% TPO (photoinitiator),

and 1.5 wt.% Dylight 650 maleimide. This solution was dissolved in methanol at 3.5 wt% solids and cast onto a PET sheet with a Mayer rod. The appropriate mold was then placed in contact with the pre-particle film and filled by running through a heated laminator in which the mold and PET sheet were split as the sheets emerged from the nip. The filled mold was then cured with ultra-violet radiation (395 nm) and a PVOH harvesting layer was used to transfer the particles out of the mold. Water was used to dissolved away the PVOH and collect the free particles.

The micron-sized (1.5 μm and 6 μm) particles were fabricated using a dropcast method. The preparticle solution was spread directly onto the mold and a PET sheet was laminated on top of the mold by running through a heated laminator. The PET sheet was removed and the mold was UV with a UV LED lamp for 30 seconds. Particles were transferred out of the mold using a Luvitec® (BASF SE) harvest sheet and particles were again collected with water.

Particle Characterization

Particle concentrations were determined using thermogravimetric analysis (TGA) (TA Instruments Q5000). Scanning electron microscopy was used to visualize the harvested particles (Hitachi S-4700 scanning electron microscope).

In vitro Confocal Analysis of Hydrogel Particle Uptake

MH-S murine alveolar macrophages were plated in complete DMEM at 20,000 cells per well in 8-well chamber slides (LabTek) 48 hours prior to treatment with particles. Particles were resuspended in DMEM at 20 μg/mL and 300 μL of particle solution were

added to each well. Particles were incubated with cells at 37°C for 4 hours. Cells were then washed twice with PBS and cells fixed with 4% Paraformaldehyde (PFA) solution and later stained with Alexa Fluor 488 Phalloidin (Invitrogen) and DAPI (Vectashield, Vector Labs). Fluorescent imaging of stained cells was performed on a Zeiss 710 laser scanning confocal imaging system (Zeiss).

In vitro Inflammation Assays

Bone marrow macrophages (BMMs) were isolated as described previously [139] from the femurs of C57Bl/6 and BALB/c mice. Cells were cultured for six days in DMEM with 10% FBS, L-Glutamine, pen/strep, and 20% L929 media. Adherent cells were plated at 200,000 cells per well in a 96-well plate 24 hours prior to particle treatment. Control cells were primed with LPS (50 ng/mL) 24 hours prior to treatment to provide signal 1 for inflammasome activation. Particles were then dosed to the cells and supernatant were collected 24 hours post-dose. ELISAs of IL-1β, TNF-α, and IL-6 were used to analyze cytokine response. Lactate dehydrogenase release was used to measure cytotoxicity.

Assessment of Airway Inflammation

C57Bl/6 mice (10-12 wk old) were anesthetized by isofluorane inhalation and particles were instilled orotracheally with 50 µg particles/50 µL PBS (n=5). Instillation of PBS (50 µL) or LPS (20 µg/50µL PBS) were given as negative and positive controls, respectively. Mice were euthanized two or seven days after installation. Blood was collected by cardiac puncture, and the serum was separated by centrifugation and utilized for ELISA analysis of inflammatory cytokines. Bronchoalveolar lavage fluid (BALF) was also collected

and both the cells and supernatants were kept for further analysis. BALF cellularity was assessed using a hemocytometer and cellular composition was analyzed by cytospin of BALF aliquots onto slides and staining with Diff-Quik for differential cell counts. After BALF collection, lungs were harvested and stored in 10% buffered formalin.

Histopathological Analysis

After H&E staining of 5 μm sections of fixed lungs, inflammation was determined by scoring as described previously [140, 141]. Briefly, histology images were evaluated on inflammatory parameters (mononuclear cell infiltration, polymorphonuclear cell infiltration, airway epithelial cell hyperplasia/injury, extravasation, perivascular cuffing, and estimated percentage of lung with inflammation) and given a score between 0 (absent) to 3 (severe).

Particle Uptake in BALF

Cells from the BALF were seeded onto 8-well chamber slides and fixed with 2% paraformaldehyde. Cells were stained for actin (Phalloidin 488) and nuclei (DAPI). Particle (Dylight 650) uptake was then analyzed by counting the number of cells with particles in five distinct fields of view.

Statistical Analysis

GraphPad Prism 5 software was used to identify statistical significance. Student's two-tailed t-test was used for single data point comparisons while Analysis of Variance (ANOVA) was used for multiple comparisons. A p-value less than 0.05 was considered statistically significant.

3.4 Results and Discussion

3.4.1 PRINT enables the fabrication of monodisperse and homogenous particles

Utilizing PRINT technology to fabricate monodisperse particles of precisely defined matrix, shape, and size allowed us to address which particle parameters may influence inflammatory immune responses in mice. Literature has described how size and shape may affect biological processes and outcomes such as cellular uptake of particles or vaccine delivery [76, 142]. Thus, particles spanning from 80x320 nm to 6 μm in diameter were generated to investigate sizes that were biologically relevant. The measured size and zeta potential of these particles are shown in **Figure 3.1A and C.** The polydispersity index (PDI) is a reflection of the heterogeneity in a particle population, and the PDIs shown indicate a nearly monodisperse population. The micron-sized particles were not analyzed for size by DLS due to their propensity for settling very quickly. SEM images were used to determine the size of the micron-sized particles as well as further visualize the monodisperse character of the particle population as a whole (**Figure 3.1 B, D**). All particle surface charges were also measured to be negative. Particle uptake by MH-S alveolar macrophages was performed on the hydrogel particles to validate particle uptake in a pulmonary immune cell population (**Figure 3.1 E**).

A

PLGA Particle Type	Size (nm)	PDI	Charge (mV)
80x320nm	226	0.03	-4.21
1µm cylinder	1465	NA	-18

B

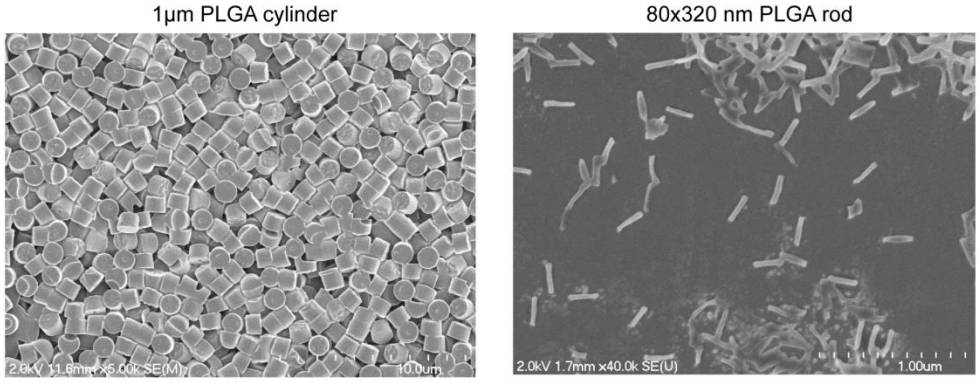

C

Hydrogel Particle Type	Composition (solids, wt%)					Size (nm)	PDI	Charge (mV)
	PEG_{700}-DA	HP_4A	Dye	TPO (PI)	AEM			
6 µm Donut	20	78	1	1	-	-	-	-6.87
1.5 µm Donut	20	78	1	1	-	-	-	-8.96
80x320 nm (acetylated)	10	68	1	1	20	236.1	0.06	-41.5

D

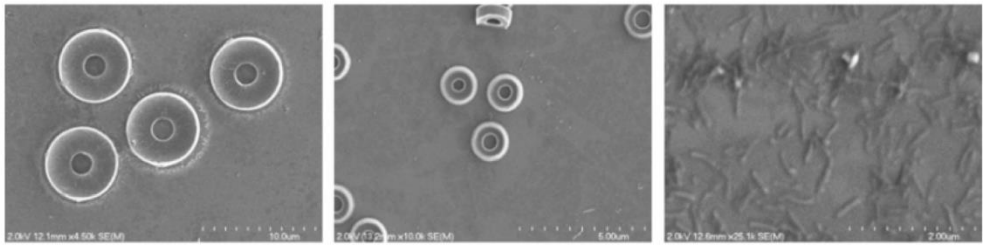

E

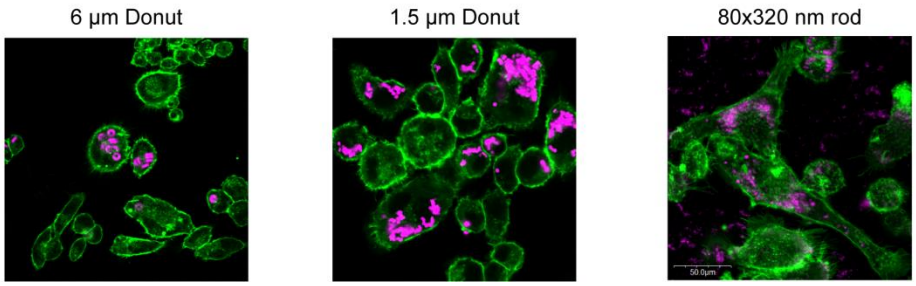

Figure 3.1 PRINT Particle Characterization
A) Dynamic light scattering (DLS) and zeta potential measurements of PLGA particles used in studies. Particle charge decreases with increasing size. B) Scanning electron microscope (SEM) images of PLGA particles. C) PEG particle composition and characterization. D) SEM of PEG particles. E) Confocal images of hydrogel particle uptake in MH-S alveolar macrophage cells after 4 hours of treatment. Scale bar is 50µm. Figure and caption reproduced from Roberts (2012) [143].

3.4.2 PLGA particles do not induce inflammation by bone-marrow-derived macrophages

While the efficacy and diagnostic power of nanoparticles has been comprehensively explored, the immune response to these nanomaterials has not yet been fully characterized. The innate immune system is responsible for initiating a swift response after identification of foreign material in the body. This response is characterized by the release of cytokines and other soluble protein messengers that recruit additional immune cells to the area to help with defense and host repair [144]. Environmental toxicologists have studied the role of particulates in inducing inflammation in the lung, often for industrial and air pollutants [145, 146]. Much of the literature indicates that there is not yet clear correlation between the particle's physical properties and the resulting inflammatory response, however, it has been shown that certain particle compositions such as titanium dioxide and silica dioxide trigger inflammation while zinc oxide nanoparticles do not [147, 148]. These results indicate the sensitive immunological influence of the size, shape, and matrix of the particle.

PLGA and PEG particles were dosed to bone marrow-derived macrophages from C57Bl/6 mice *in vitro* to assess the immune response of these particles. Pro-inflammatory cytokines TNF-α, IL-6, and IL-1β were analyzed by ELISA from the cell supernatant. At both the 5 and 24 hour time points, no detectable levels of any of the tested cytokines were seen (**Figure 3.2**). Lipopolysaccharide (LPS) was used as a positive control for the release of inflammatory cytokines.

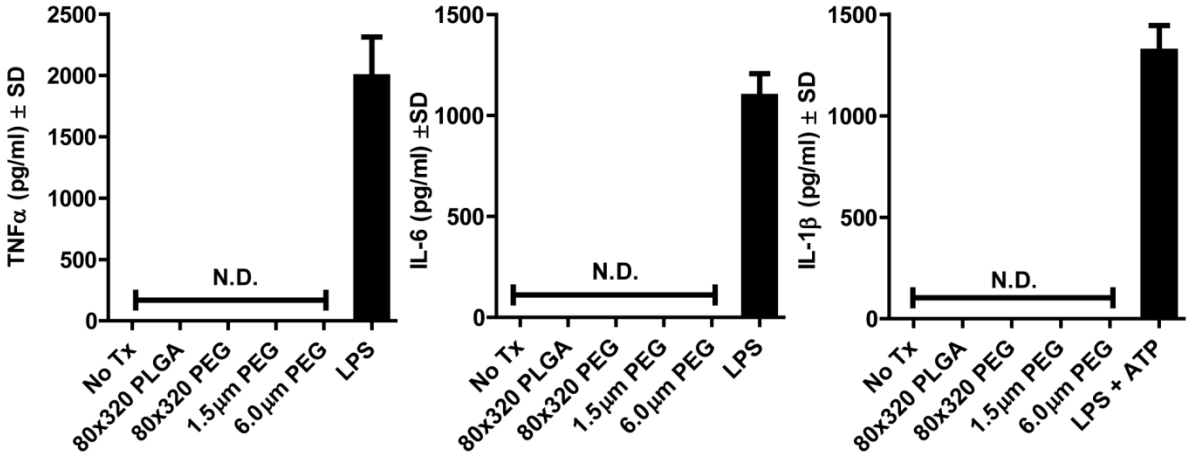

Figure 3.2 PRINT particles do not cause inflammation in bone marrow-derived macrophages from BALB/c or C57BL/6 mice
Overnight stimulation with a panel of PRINT PLGA and hydrogel particles (PEG) at 100μg/mL does not cause TNF-α, IL-6, or IL-1β release from bone marrow-derived macrophages from C57BL/6 mice as measured by ELISA. Figure and caption adapted from Roberts (2012) [143].

3.4.3 PLGA particles do not induce lung inflammation

The lung was chosen to probe the inflammatory influence of the PRINT particles because of its clearly defined markers of inflammation and its therapeutic relevance for diseases such as asthma, allergies, COPD, and TB [149, 150]. In addition, the lung has been characterized as a "hub" where lymphocytes undergo gene modulation to direct them to a specific location in the body [151]. With both local drug delivery and immunomodulation a goal of particulate delivery to the lung, testing the physiological effects in this organ of interest would allow for a better understanding of the role of specific particle parameters on the inflammatory pathway.

Although PLGA is approved by the F.D.A., there is disagreement in literature on the inflammatory potential of PLGA *in vivo*, with both positive and negative outcomes being reported [152-155]. In this study, we found that instilled PLGA particles into the lung do not

induce lung inflammation. BALF cellularity was the same for both the PBS and PLGA treated mice, indicating no additional cell recruitment (**Figure 3.3 A**). As expected, LPS-treated mice resulted in increased cellularity, and, in particular, an increase in the monocyte and neutrophil populations. In particle-treated mice, no significant recruitment of specific immune cells was shown (**Figure 3.3 B)**. Analysis of lung histopathology of the main bronchi of the left lobe was used as another method to determine lung inflammation (**Figure 3.3 C,D**). No cell infiltration was seen in the particle-treated mice while the LPS-treated mice showed a significant recruitment of leukocytes in the lung. BALF assessments of cytokine levels also showed that there was no significant release of IL-1β (**Figure 3.3 E**) or IL-6 (**Figure 3.3 F**). Serum measurements for these cytokines and TNF-α were also undetectable for particle-treated mice (data not shown).

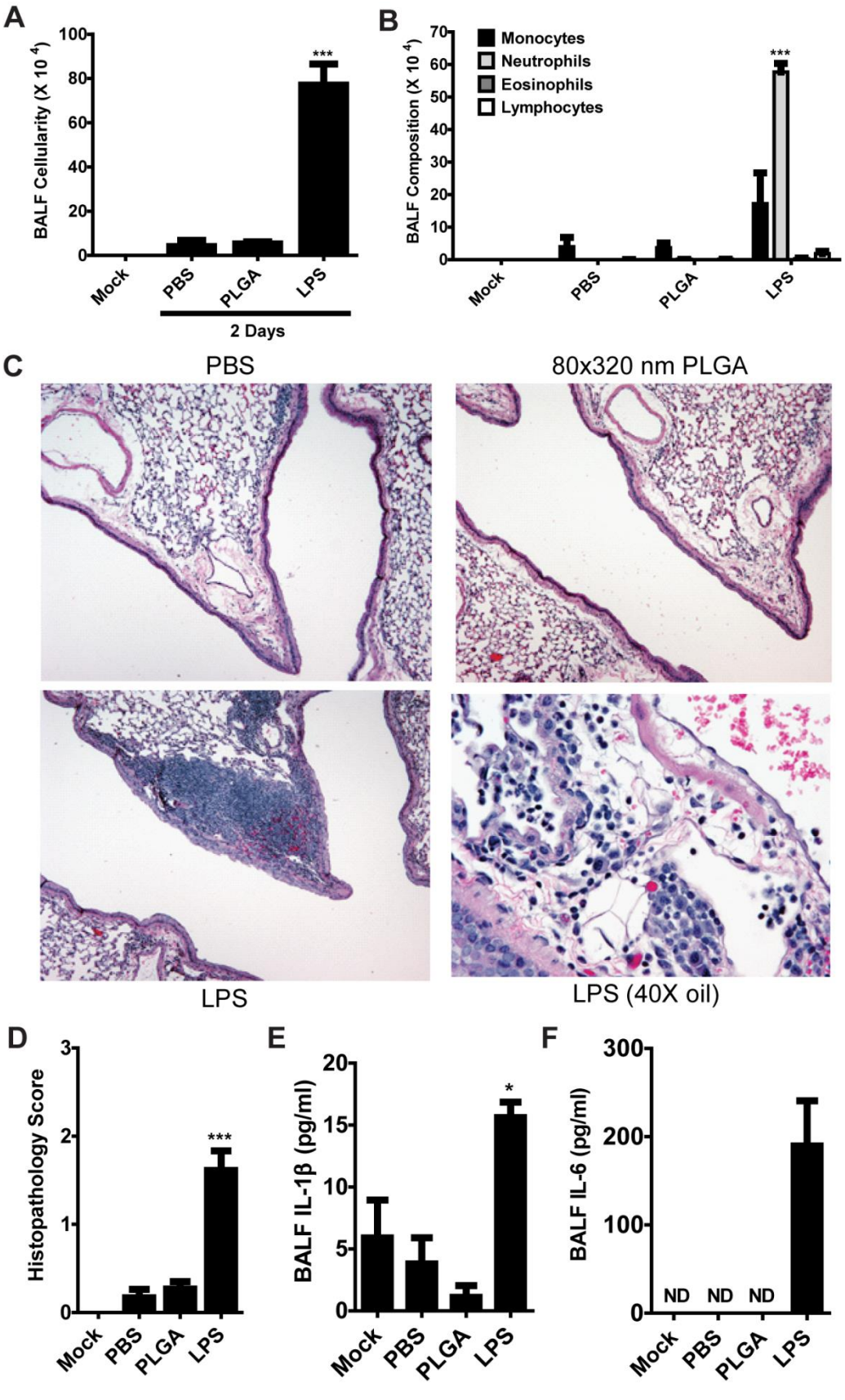
A
BALF Cellularity (X 10 4)
100
80
60
40
20
0
***
Mock
PBS
PLGA
LPS
2 Days
B
BALF Composition (X 10 4)
70
60
50
40
30
20
10
0
Monocytes
Neutrophils
Eosinophils
Lymphocytes
***
Mock
PBS
PLGA
LPS
C
PBS
80x320 nm PLGA
LPS
LPS (40X oil)
D
Histopathology Score
3
2
1
0
***
Mock
PBS
PLGA
LPS
E
BALF IL-1β (pg/ml)
20
15
10
5
0
*
Mock
PBS
PLGA
LPS
F
BALF IL-6 (pg/ml)
300
200
100
0
ND
ND
ND
Mock
PBS
PLGA
LPS

Figure 3.3 80x320 nm PLGA particles do not cause lung inflammation in mice.
Mice were challenged with either 50μg of 80x320nm PLGA particles or 20μg LPS i.t. and airway inflammation was assessed 48 hours post-challenge. A) Total cellularity of bronchoalveolar lavage fluid (BALF) in treated C57BL/6 mice is no different after 48 hours than PBS-treated mice and is significantly less than the inflammatory cell recruitment seen in LPS-treated mice. B) PLGA particle treatment does not induce any appreciable immune cell recruitment to the lungs of mice, as opposed to the heightened levels of monocytes and neutrophils seen in the lungs of LPS-treated mice. C) Histopathology revealed no significant differences in lung architecture between PBS- and 80x320nm PLGA particle-treated mice. This is in stark contrast to the airway occlusion and significant innate immune cell recruitment seen in LPS-treated mice. D) Histopathology scoring confirmed that no significant differences were seen between the lungs of PBS and PLGA particle treated mice. E-F) The increased lung levels of pro-inflammatory IL-1β and IL-6 seen in LPS-treated mice is not found in PLGA-treated mice. PBS, n=3; 80x320nm PLGA particle-treated, n=5; LPS-treated, n=3. ND = Not Detected. * = $p< 0.05$, *** = $p<0.001$. Experiments were performed using 3-5 mice per group. Data shown are representative of at least two independent experiments. Figure and caption reproduced from Roberts (2012) [143].

3.4.4 PEG particles remain in the lung for 7 days without causing lung inflammation

Particles dosed to the lung were labeled with a fluorescent dye to facilitate confocal analysis of particle uptake in BALF cells. The hydrogel particles fabricated had particles sizes of 80x320 nm, 1.5 μm and 6 μm diameters as shown in **Figure 3.1**. Using the same methodology as with the PLGA particles, the PEG particles also showed no increase in cell recruitment in the BALF at two and seven days post dose (**Figure 3.4 A-D**). Lung histopathology also showed no increases in cell infiltration (**Figure 3.4 E, F**).

Interestingly, the 6 μm particles could be seen in the H&E stained lungs of multiple mice at both two and seven days post-challenge without showing overt signs of inflammation (**Figure 3.5 A, B**). Because of the lack of immune cell recruitment and tissue disruption around the particles, this may suggest that these particles are immunologically inert and can remain in the alveolar space for out to seven days. Since the smaller particles (80x320 nm and 1.5 μm) were too small to visualize on the histology samples, BALF cells were imaged

to analyze particle uptake. BALF cells contained particles of all sizes at both two and seven days post-instillation (**Figure 3.5 C,D,F,G**) with fewer cells taking up the larger 6 μm particles (**Figure 3.5 E**). This may be due to the fact that particles were instilled by mass, thus, a larger number of the smaller particles will be dosed compared to the larger particles. Particle size and its effect on macrophage phagocytosis may also play a role in this decrease in uptake. BALF and serum samples were also tested for IL-1β, IL-6, and TNF-α cytokines and no detectable levels were seen at both the two and seven day time points (data not shown). This data again suggests that these particles are immunologically inert and can remain in the lung for at least seven days.

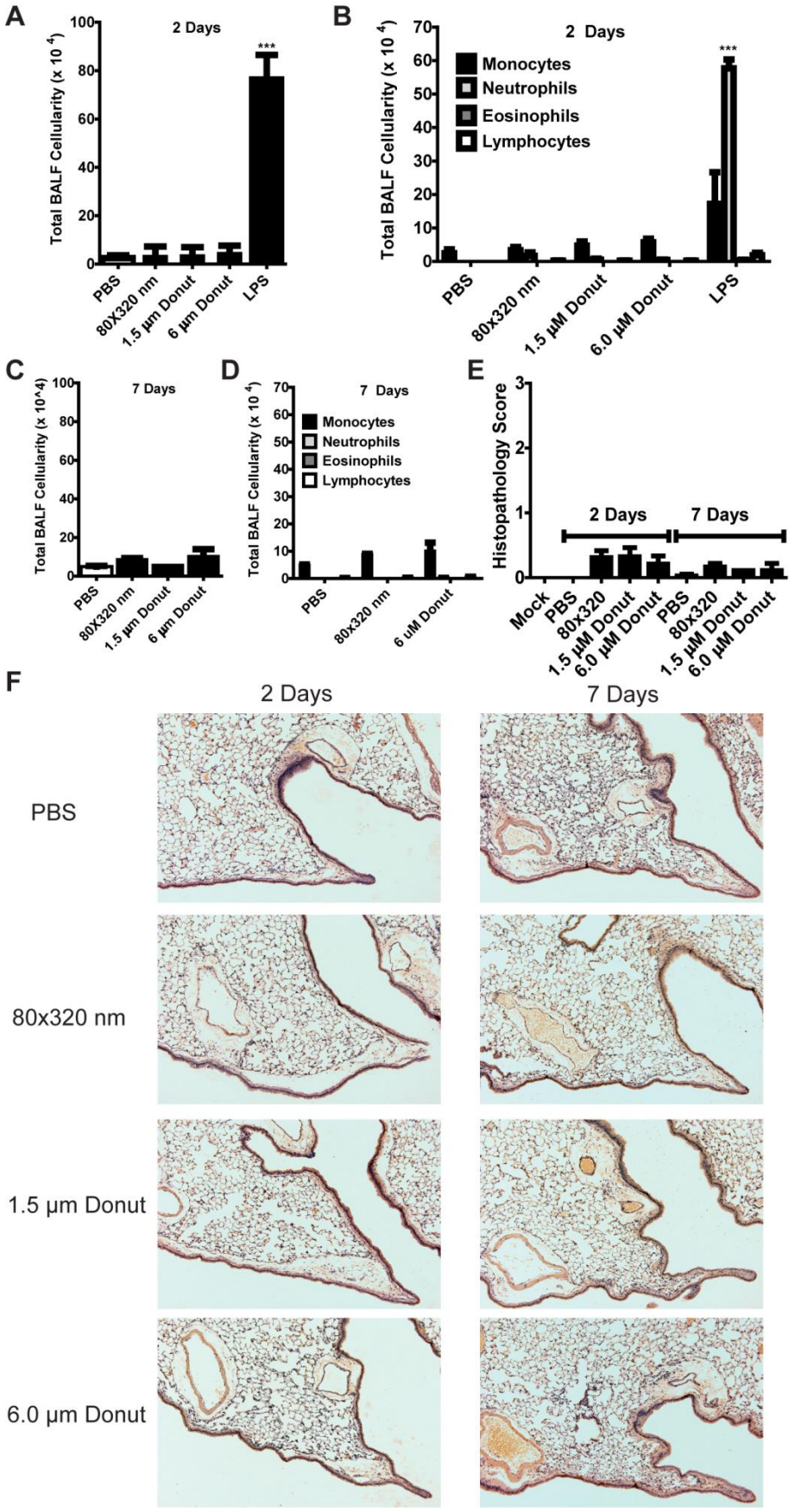
A
2 Days
Total BALF Cellularity (x 10 4)
***
PBS
80X320 nm
1.5 µm Donut
6 µm Donut
LPS
B
2 Days
Monocytes
Neutrophils
Eosinophils
Lymphocytes
Total BALF Cellularity (x 10 4)
***
PBS
80x320 nm
1.5 µM Donut
6.0 µM Donut
LPS
C
7 Days
Total BALF Cellularity (x 10^4)
PBS
80X320 nm
1.5 µm Donut
6 µm Donut
D
7 Days
Monocytes
Neutrophils
Eosinophils
Lymphocytes
Total BALF Cellularity (x 10 4)
PBS
80x320 nm
6 uM Donut
E
Histopathology Score
2 Days
7 Days
Mock
PBS
80x320
1.5 µM Donut
6.0 µM Donut
PBS
80x320
1.5 µM Donut
6.0 µM Donut
F
2 Days
7 Days
PBS
80x320 nm
1.5 µm Donut
6.0 µm Donut

Figure 3.4 Hydrogel particles do not cause lung inflammation in mice.
Mice were challenged with 50μg of hydrogel particles (80x320nm, 1.5μm, or 6.0 μm donuts) i.t. and airway inflammation was assessed 48 hours and 7 days post-challenge. A) BALF analysis indicated no increased cellularity 48 hours after hydrogel particle treatment, whereas a significant cellular influx was seen in LPS-treated controls. B) At 48 hours, BALF cellular composition does not show any significant trend for immune cell recruitment in hydrogel particle-treated mice. C-D) BALF cellularity and composition was not significantly augmented seven days after hydrogel particle treatment. E) Histopathology analysis revealed no significant differences in lung architecture between PBS- and hydrogel particle-treated mice at either 2 or 7 days post-treatment. F) Histopathology scoring confirmed that no significant differences were seen between the lungs of PBS and hydrogel particle treated mice at any time points. ***=$p<0.001$. Experiments were performed using 2-5 mice per group. Data shown are representative of at least two independent experiments. Figure and caption reproduced from Roberts (2012) [143].

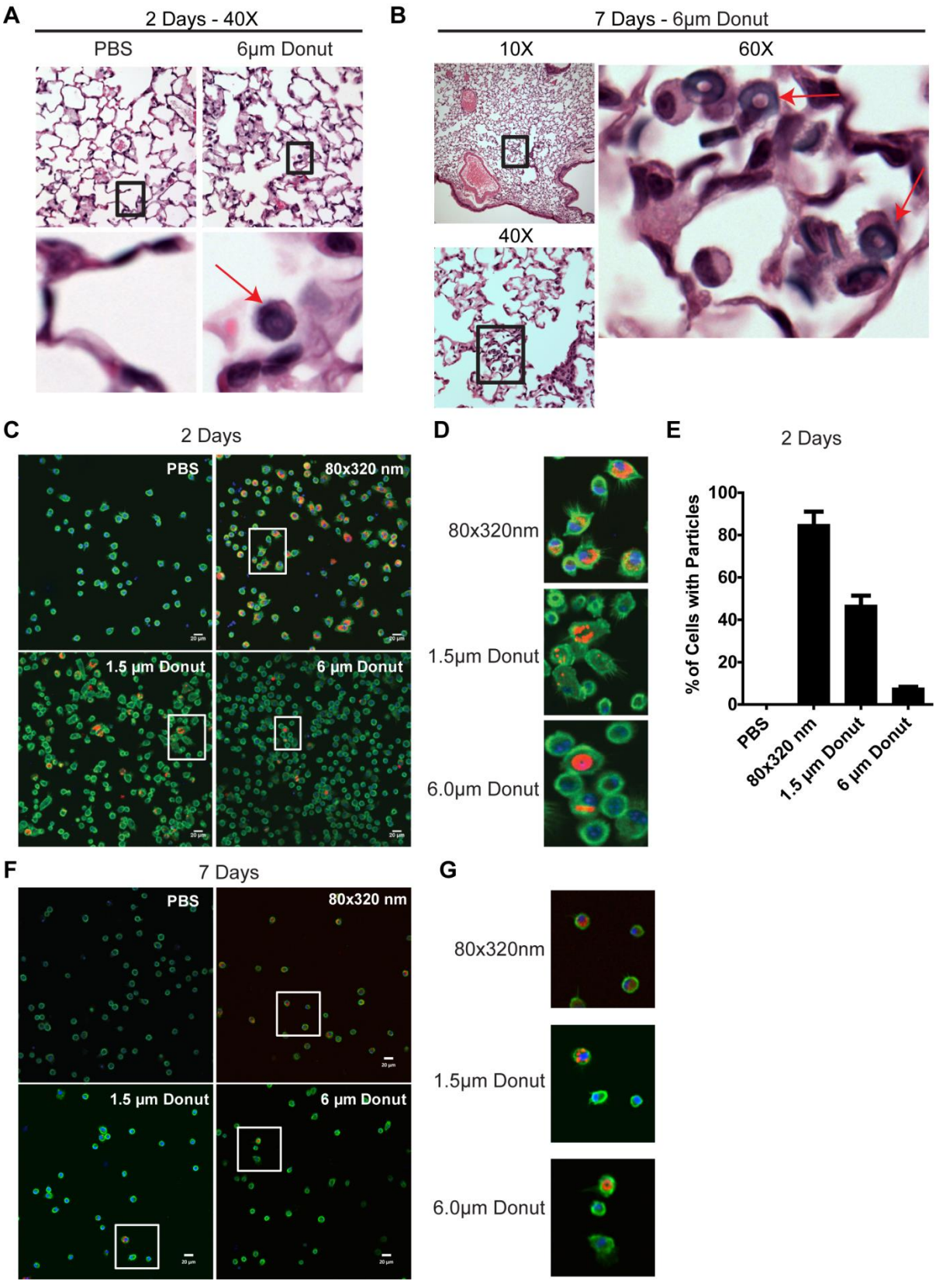
A
2 Days - 40X
PBS
6µm Donut
B
7 Days - 6µm Donut
10X
60X
40X
C
2 Days
PBS
80x320 nm
1.5 µm Donut
6 µm Donut
D
80x320nm
1.5µm Donut
6.0µm Donut
E
2 Days
% of Cells with Particles
100
80
60
40
20
0
PBS
80x320 nm
1.5 µm Donut
6 µm Donut
F
7 Days
PBS
80x320 nm
1.5 µm Donut
6 µm Donut
G
80x320nm
1.5µm Donut
6.0µm Donut

Figure 3.5 Hydrogel particles remain in the lungs for multiple days without overt signs of inflammation.
A) 6μm hydrogel particles (denoted by red arrows) are visible in the alveolar spaces 2 days after intratracheal installation. Lower insets are a magnified view of black bounding box. PBS treated mice are shown as control. B) Multiple 6μm hydrogel particles (denoted by black bounding box and red arrows) are visible in the alveolar spaces 7 days after intratracheal installation. C) Two days after treatment with hydrogel particles, BALF cells were stained and visualized for particle uptake via epifluorescence microscopy. Particles (Dylight 650, red); nuclei (DAPI, blue); F-actin (Phalloidin 488, green). D) Magnified views of BALF cells taking up hydrogel particles as denoted by white bounding boxes in Figure C. E) Quantification of particle uptake indicates smaller particles are more readily taken up in BALF cells than larger particles. F) All types of hydrogel particles can still be seen in BALF cells seven days after treatment, though there is a marked decrease in the number of particles present as compared to the 2 day time point. G) Magnified views of BALF cells taking up hydrogel particles 7 days after treatment as denoted by white bounding boxes in Figure C. Scale bar is 20μm. Data shown are representative of at least two independent experiments. Figure and caption reproduced from Roberts (2012) [143].

3.5 Conclusions

Utilizing PRINT technology to generate particles of defined matrices, shapes, and sizes allowed the exploration of how different particle parameters may influence the immune response in the lung. The resulting data indicates that both PLGA and PEG particles do not cause the release of inflammatory cytokines *in vitro* and *in vivo*, and that size also does not affect its immunological response. That the PEG hydrogel particles were also seen in the lung out to seven days without signs of overt inflammation may indicate that they may be promising drug depot systems for sustained-release therapeutics.

CHAPTER 4

DISTRIBUTION AND CELLULAR UPTAKE OF PEGYLATED POLYMERIC PARTICLES IN THE LUNG

4.1 Overview

Bridging the gaps between particle engineering, environmental health sciences, biology, and medicine will enable us to develop more efficient drug delivery vehicles by increasing our fundamental knowledge and understanding of the physiological outcomes of particulate delivery to the lung. Utilizing Particle Replication in Non-wetting Template (PRINT) technology to fabricate particles on both the nano- and micro-scale with precisely defined shapes and compositions allows the exploration of the effects and importance of certain design parameters for local lung delivery of drug carriers. In this study, polymeric hydrogel PRINT particles ranging from 80 nm to 6 μm in diameter were fabricated and modified with a surface layer of polyethylene glycol (PEG) and instilled into the lungs of mice. The size and surface modification of these particles can significantly affect uptake and retention by certain cell populations in the lung, thus allowing for potential sustained and cell-specific targeted delivery of therapeutics. In addition, these particles were shown to reside in the lung out to twenty-eight days without inducing a significant inflammatory cytokine response. These results indicate that this platform is a promising and flexible system for testing and developing particles of specific design parameters towards more efficient drug carriers to the lung.

4.2 Introduction

The study of particles in the lung spans several different fields of research. Research in environmental health science studies the effects of environmental particulates, such as diesel exhaust particles and TiO_2 particles, on lung injury, inflammatory responses and cellular clearance mechanisms in the lung. [3-8] In pharmaceutical particle engineering, the technology of formulating and characterizing aerodynamically relevant particles for drug delivery to the lung is an area of high interest in both administration (e.g. dry powder inhalers and nebulizers) and therapeutic efficacy.[9-11] In medicine and physiology, the pharmacodynamics and pharmacokinetic effects of the drug molecule itself as well as how the disease states affects particle deposition and drug release are investigated.[1, 12] Integrating the methodology and knowledge from these various particle research areas will allow for a better understanding of specific design parameters important for the development of more safe and efficient drug delivery vehicles to the lung.

Particle Replication in Non-Wetting Templates (PRINT) technology is itself a product of the synergistic merger between research in the microelectronics industry, polymer chemistry, and pharmaceutical sciences. It is a top-down lithography-based particle fabrication process that allows for the precise control over many particle characteristics such as size, shape, composition, porosity, modulus, and surface functionality. Utilizing the plug-and-play characteristics of PRINT, applications in red blood cell mimics [99, 100], chemotherapeutic delivery [101, 102], and microneedle drug delivery [103] have been explored. For pulmonary applications, the ability to generate monodisperse populations of particles of a variety of geometries, matrices, and surface properties can be used to explore particle deposition properties based on particle shape [156], enhancement of drug delivery

from dry powder inhalers (DPIs) [90], and the physiological responses of particulate delivery to the lung. [143]

Much remains to be explored of the *in vivo* cellular fate and inflammatory response to micro- and nano-particles composed of relatively inert polymers, such as poly(ethylene) glycol (PEG), often used for in drug delivery applications. In addition, there is a significant unmet need in the delivery of respiratory drugs to target or de-target cells in the lung depending on the desired site of action of various therapeutics. Alveolar macrophages often present a significant barrier to efficient pulmonary drug delivery applications because of i) their sequestration and undesirable clearance of certain deposited drug particles in the lung whose site of action involves non-macrophage targets, like aerosolized therapeutics targeted to the alveoli and epithelial cells [57, 157] or ii) by their protection and harboring of disease targets, such as infectious bacteria like tuberculosis, which makes it difficult to treat effectively. [61] Because particles with geometric diameters of 1-5 microns have been shown to be preferentially taken up by AMs [58, 59], large, porous particles [58] and swellable microparticles [60] were developed to deposit in the alveolar airspace and successfully avoid macrophage uptake due to their large (> 5 μm) geometric size. PEGylation of particles has been shown to reduce uptake by macrophages in systemic circulation, [158, 159] and coating of particles with the phospholipid 1,2-dipalmitoylphosphatidylcholine (DPPC) was shown to reduce uptake in alveolar macrophages [160]. Physicochemical particle properties targeting macrophages have also been explored for enhancing host defense and regulating immune responses [161]. Dendritic cell uptake of particles containing an antigen may be advantageous for vaccine applications or immunomodulation therapies [162, 163]. Thus, the ability to screen particles by altering

one variable at a time should provide insights into the underlying fundamental mechanisms of particle uptake and clearance in the lung, which may progress towards an efficient delivery vehicle for sustained therapeutics in the lung.

In this study, non-spherical polymeric hydrogel PRINT particles ranging from 80 nm to 6 μm in diameter were fabricated and surface modified with PEG. These particles were then instilled into the lungs of mice and particle uptake and residence time in the lung was determined by flow cytometry and confocal microscopy. In addition, the induction of inflammatory cytokines and recruitment of inflammatory cells to the lung upon particle delivery to the lung was investigated. We show that dendritic cells in the lung and the BALF have distinct particle uptake preferences from that of macrophages, thus shedding light on the potential to target specific cellular subtypes in the lung by both surface chemistry and shape and size. PEGylated particles were shown to reside in the lung out to twenty-eight days post-dose demonstrating the potential for their use as delivery vehicles for sustained release therapeutics.

4.3 Materials and Methods

Fabrication of PEGylated Hydrogel PRINT Particles

Particles were composed of 10% PEG700DA (cross-linker) (Sigma), 67% hydroxyl-tetraethylene glycol monoacrylate (HP4A, monomer), 20% 2-aminoethyl methacrylate hydrochloride (AEM), 2% fluorescent dye (Dylight 650 Maleimide, Thermo Fisher), and 1% 2,4,6-Trimethylbenzoyl-diphenyl-phosphineoxide (TPO, photoinitiator) (Sigma) by weight. This pre-particle solution was filled into a Fluorocur mold of the intended geometric shape and cross-linked in a UV curing chamber (λ=365 nm). Particles were then transferred from

the filled mold onto a polyvinyl alcohol (PVOH) harvest layer. Water was used to dissolve away the harvesting layer and free particles were collected. PEG5k-succinimidyl carboxymethyl ester (PEG5k-SCM) was reacted with the amine functional handles resulting in a layer of PEG on the particle surface.[65] Both PEGylated and unPEGylated particles were then succinylated to quench any remaining free amine groups.

Particle Characterization

Geometric particle dimensions were measured by SEM analysis. Particle zeta potential was measured using a Zetasizer Nano ZS (Malvern Instruments, Ltd.). Particle aerodynamic diameter was measured using an Anderson Cascade Impactor (ACI) as described previously [156].

Fluorescent Microscopy of In vitro Macrophage Uptake

MH-S, a mouse alveolar macrophage cell line, (ATCC) was used for particle uptake experiments. Cells were plated at 4 x 10^4 cells/well in 8-well chamber slides (LabTek) 48 hours before particle addition. Cells were dosed with 25 µg particles in media consisting of high glucose Dulbecco's Modified Eagle Medium (DMEM) (Gibco) and 10% fetal bovine serum (FBS). Particles were incubated on the cells for 4 hours at 37°C with 5% CO_2. After incubation, cells were washed with Dulbecco's Phosphate Buffer Saline (PBS) solution and fixed with 4% paraformaldehyde (PFA) solution. Staining of actin (Alexa Fluor 555, Invitrogen) and DAPI (Vectashield, Vector Labs) of fixed cells was then performed. Fluorescent imaging of stained cells was performed on a Zeiss 710 laser scanning confocal microscope (Zeiss).

In vivo Lung Instillation

To assess PRINT particle uptake in the lungs of mice, 8-10 week old female C57Bl/6 mice (Jackson Laboratories) were anesthetized with isofluorane and 50 µL particle solution was orotracheally administered. Particles were dosed at 50 µg per mouse in PBS solution. Administration of 50 µL PBS or 20 µg/50 µL lipopolysaccharide (LPS) served as negative and positive controls, respectively. At timepoints of one, seven, and twenty-eight days post-particle dose, mice were euthanized and bronchoalveolar lavage fluid (BALF) was collected and the whole lung was excised. O.C.T. (Tissue-Tek)-filled lungs of one to two mice per timepoint for each particle treatment was also collected and frozen for fluorescent lung tissue staining.

Flow Cytometry Analysis

Cells collected from BALF and single cell suspensions collected form homogenized whole lung were stained with a panel of fluorescent antibodies for flow cytometric analysis of particle uptake and cell populations. The following antibodies were used for staining (BioLegend): CD45-PacBlue, CD11c-PE, MHCII-PE-Cy7, F4/80-BV605, Ly6-G-AF700. Cells were fixed with 4% PFA in PBS after staining and kept at 4°C until analysis. Flow cytometry data was collected on the LSRII flow cytometer (BD Biosciences) and analyzed using FlowJo software.

Cytokine Analysis

ELISA kits for IL-6 (BD Biosciences) and MIP-2 (R & D Systems) were used to measure cytokine release in BALF supernatant.

Fluorescent Lung Tissue Staining

Frozen lung was sliced into 7 µm thick sections, fixed with acetone, and fluorescently stained for phalloidin (Alexa Fluor 555 Phalloidin, Molecular Probes), CD11c (AF888 anti-mouse CD11c, BioLegend), and cell nuclei (DAPI, Thermo Scientific). Images were obtained on the Zeiss 710 confocal microscope.

4.4 Results

4.4.1 Fabrication and Characterization of PEGylated Hydrogel PRINT Particles

Three different particle shapes, 80x320 nm, 1.5 µm donuts, and 6 µm donuts composed of PEG_{700}-DA and with amine-functional handles were fabricated using the PRINT method. SEM images show the monodispersity of the fabricated hydrogel particles (**Figure 4.1**). Methoxy-PEG5k-SCM was then conjugated to these particles (designated 80x320P, 1.5P, 6P) to provide a stealthing PEG layer on the surface. Any remaining free amine groups were quenched with succinic acid. Particles that were not PEGylated, (designated 80x320U, 1.5U, 6U), were also quenched with succinic acid so that all particle groups would have a comparable negative surface charge. The particles were then characterized by surface area, volume, aerodynamic diameter and surface charge (**Table 4.1**).

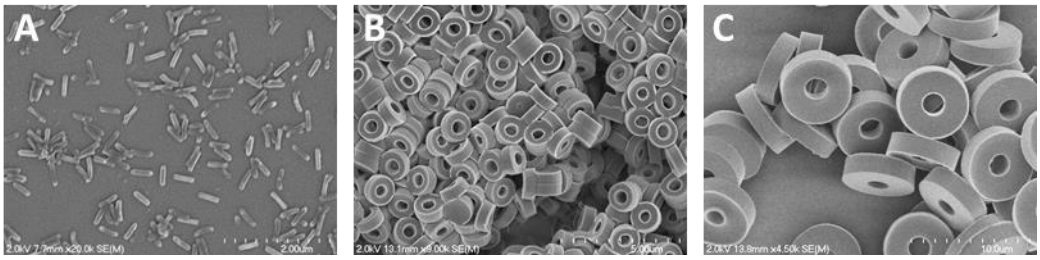

Figure 4.1 SEM images of PRINT hydrogel particles
(A) 80x320 nm, (B) 1.5 µm donut, (C) 6 µm donut

Table 4.1 Particle characterization of surface are (SA), volume (Vol), aerodynamic diameter and charge.

	SA (μm^2)	Vol (μm^3)	Aerodynamic Dia. (μm)	Zeta Potential (mV)	
Particle				**UnPEGylated**	**PEGylated**
80x320 nm	0.097	.0018	---	-34.7	-28.5
1.5 μm Donut	5.655	0.79	1.11	-25.3	-32.3
6 μm Donut	88.593	40.68	3.26	-5.6	-31.3

4.4.2 PEGylation of particles significantly reduces uptake by macrophages in vitro

To confirm the surface modification of the particles with a PEG layer, particles with and without PEG surface modification were incubated *in vitro* with MH-S mouse alveolar macrophages at a dose of 25 μg / 40k cells. Cells were fixed and stained for fluorescent confocal microscopy 4 hours after particle dose. As seen in the confocal images (**Figure 4.2**), PEGylation significantly reduced particle association in macrophages for all particle sizes tested. As expected, the macrophages most readily internalized the unPEGylated 1.5 μm donuts compared to the other two particle sizes as particles with geometric diameters of 1-5 microns have been shown to be preferentially taken up by alveolar macrophages.

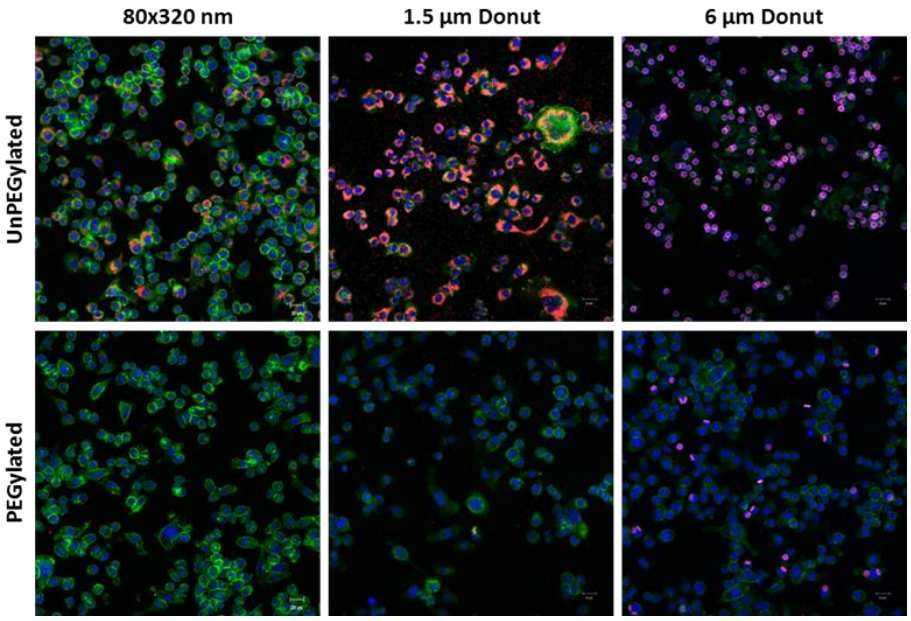

Figure 4.2 Particles dosed to MH-S cells at 25 µg/40 k cells and imaged 4 hours post-dose. Particles (red), Nuclei (blue), Actin (green)

4.4.3 Particle effects on cell populations and cytokine response in the lung

Relative cell populations of macrophages (Mϕ), dendritic cells (DCs), and granulocytes in the whole lung and bronchoalveolar lavage fluid (BALF) were analyzed by flow cytometry to determine the effect of particle administration on cell recruitment in the lung (**Figure 4.3**). Macrophages constituted the major cell type in the BALF, ranging between 85-99% of the total (**Figure 4.3A**). DC percentages of total cells ranged from 1-5% (**Figure 4.3B**). Granulocyte populations were negligible (**Figure 4.3C**) in the saline and particle-treated mice. The macrophage population was observed to change based on the size and surface modification of the particle dosed. One day after particle instillation, it was observed that in the 80x320 nm and 1.5 µm donut treated mice, the unPEGylated particles had a mean macrophage population that was 5% and 10% lower, respectively, than their PEGylated counterparts while there was no statistical difference between the 6 µm donuts of

different surface modifications. This trend continues out to day seven for the 80x320 nm sized particles. The LPS-treated mice had a significant influx of granulocytes in the BALF at 24 hours post-dose such that the relative number of macrophages was decreased by 2-fold.

Interestingly, although the percentage of DC's in the BALF was low; there was a surface modification effect on the DC population at 24 hours post-dose that compliments the macrophage population trends. More specifically, the percentage of DC's was 2.5 and 3.8 fold lower in the mice treated with the PEGylated particles verses the unPEGylated particles of the 80x320 nm and 1.5 μm donut shapes, respectively. This difference only occurs at the day one timepoint, as no other significant differences in the DC cell populations between particle-treated mice occurs in the BALF collected on days seven and twenty-eight. However, there was a significant decrease in DC populations in the saline control mice compared to the particle-treated mice. Only the 80x320P and 1.5P particles had similar DC levels (~ 1%) as the saline treated mice, while the 80x320U, 1.5U, 6U, and 6P particles had about a 4-fold increase in the DC population. This observation suggests that both surface modification and particle size may play a role in the appearance of DCs in the BALF.

In the whole lung, macrophages, dendritic cells, and granulocytes typically make up less than 20% of the cell population as endothelial, epithelial, and interstitial cells comprise a greater majority of lung cells (**Figure 4.3 D-F**). In these experiments, the macrophage, DC, and granulocyte populations ranged from 5-20%, 5-15%, and 1-6% of the total whole lung cell population, respectively. Interestingly, the surface modification effect seen on the DCs in the BALF is not replicated in the whole lung. After 24 hours the particle-dosed mice had 50% fewer macrophages in the lung than the saline-dosed mice which may indicate macrophage recruitment to the airspace to assist in particle clearance. Similar to the BALF,

LPS-treated mice had a significant influx of granulocytes in the lung and the relative number of macrophages in the lung tissue was decreased by 8-fold. Slight increases in the granulocyte population in both BALF and lung was observed with the 6 µm particles at one day post-dose, but reverted back to saline levels at later time points. No other statistical difference between cell populations of the particle-treated mice was observed at one, seven, or twenty-eight days in the whole lung.

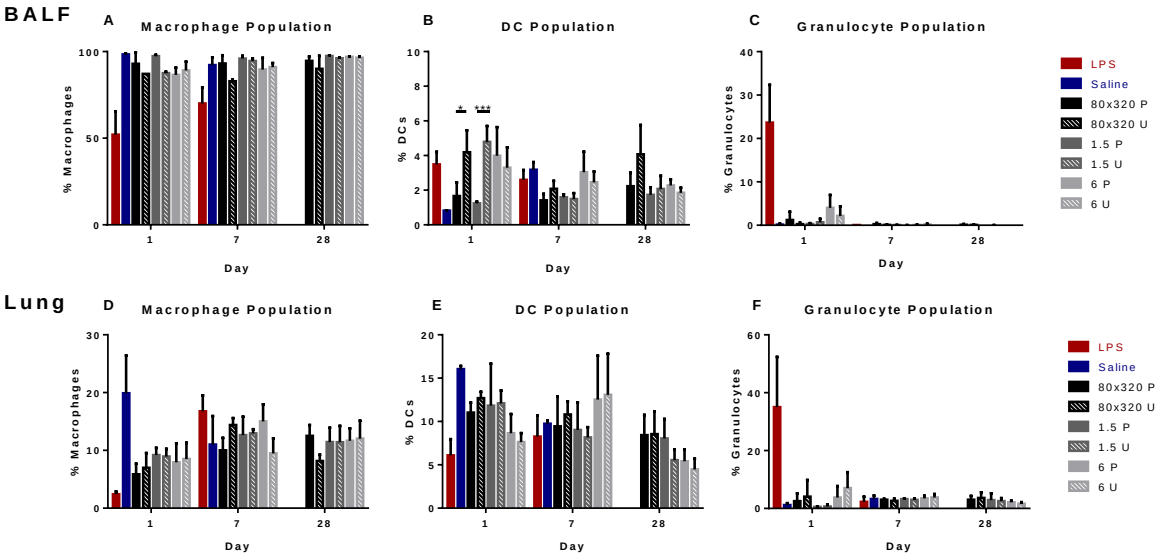

Figure 4.3 Relative populations of macrophages, dendritic cells (DC) and granulocytes BALF(A-C) and whole lung (D-F) as determined by flow cytometry analysis. Saline and LPS cell populations analyzed only at 1 and 7 days post-dose. (* $p < 0.05$, *** $p < 0.0001$)

Lung architecture and cell infiltration was also analyzed by lung histology (**Figure 4.4**). Cell infiltration was noticeable only in the unPEGylated 6 µm donuts one day post dose. All other particles doses at one, seven, and twenty-eight days showed no change in lung architecture or infiltration of granulocytes to the lung.

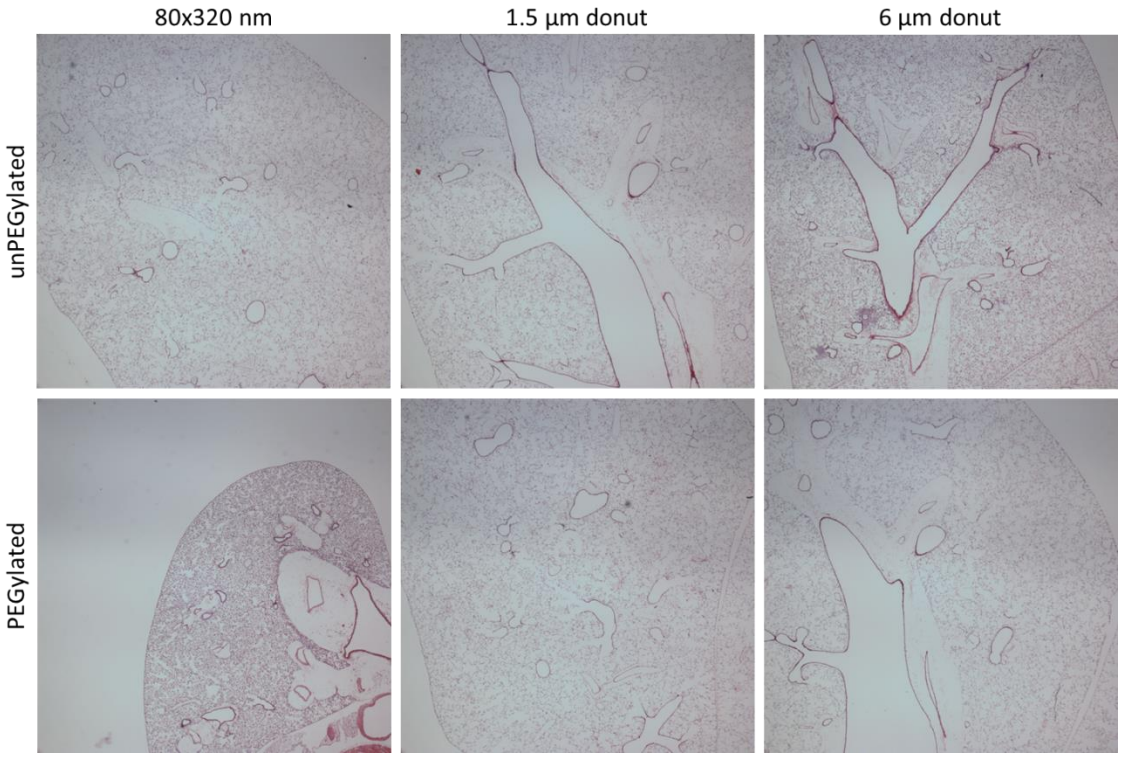

Figure 4.4 H&E stained lung tissue 24 hours after particle dose. *(2x magnification)*

Previous studies from Chapter 3 have shown that PRINT PEG hydrogel particles do not induce an inflammatory response of TNF-α, IL-1β,and IL-6 production in the lung out to 14 days. [143] In this work, IL-6 and MIP-2, a mouse macrophage inflammatory protein that may play a key role in neutrophil recruitment, was analyzed in BALF collected at one, seven, and twenty-eight days after particle administration. By ELISA, detectable levels of IL-6 and MIP-2 were only seen one day post particle instillation (**Figure 4.5**). This cytokine data is indicative of the immune cell recruitment seen in the flow cytometry analysis of the cell populations in the BALF: both the 80x320U and the 6U dosed mice had slightly elevated granulocyte levels at day one compared to saline. Interestingly, histopathology on these samples shows no significant neutrophil recruitment to the lungs.

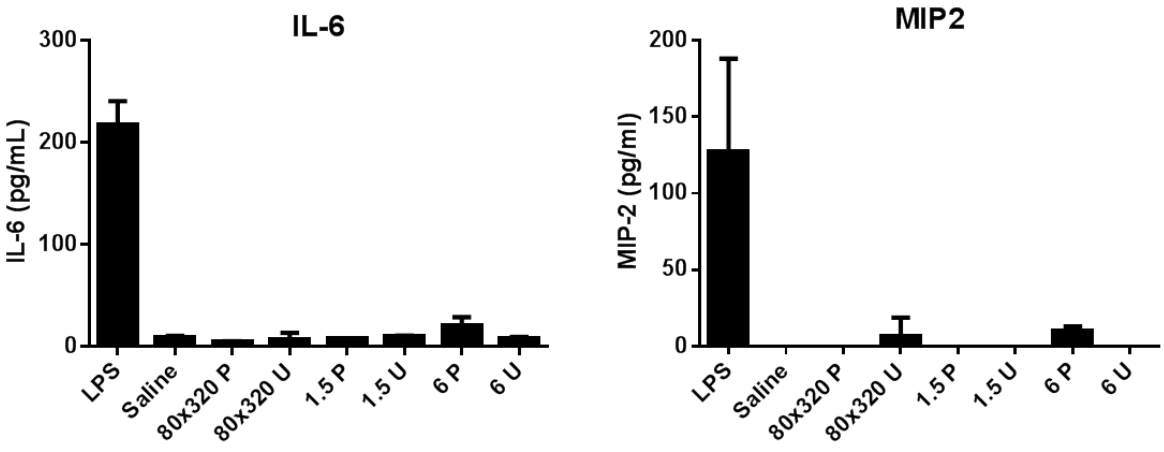

Figure 4.5 IL-6 and MIP-2 cytokine levels measured from BALF 24 hours post-instillation.

4.4.4 Surface modification of particles affects particle retention time and cellular uptake in the lung

To determine particle size and surface modification effects on particle retention time and cellular uptake in the lung, flow cytometry was run on collected BALF and whole lung cells. Different cell populations were determined by gating based on CD45, Ly6G, F4/80, CD11c, and MHCII surface markers. The particles contained Dylight 650 dye, thus allowing uptake in specific cell populations to be determined by flow cytometry analysis as well. The percentage of particle positive cells within a population was determined for BALF macrophages (**Figure 4.6 A**), lung macrophages (**Figure 4.6 D**), and lung DC's (**Figure 4.6 G**). The median fluorescence intensity (MFI), a measure of the volume of particles taken up by each particle positive cell, was also graphed (**Figure 4.6 B, E, and H**). In addition, the total fluorescence was calculated by multiplying the number of positive particle cells by the MFI in order to give an overall view of the total volume of particles internalized (**Figures 4.6 C, F, and I**).

Unlike what was seen *in vitro*, macrophages in the BALF were non-discriminating of surface modification for the smaller 1.5 µm donuts and 80x320 nm particles at one day post instillation with over 80% of macrophages having taken up particles. Yet, at day 28, the PEGylated 80x320 nm particles were present in 60% of BALF macrophages versus only 20% for their unPEGylated counterparts indicating a surface modification response to particle uptake and/or clearance. With the larger 6 µm donuts, the macrophages had preferential uptake of the unPEGylated particles at one and seven days post-dose with no uptake seen at day 28. Because particles were dosed by mass and not by number, the reduced percentage of particle positive cells for the 6 µm donut instilled mice may be due to a reduced surface area coverage of the particles in the lung. In addition, the significantly larger volume of the 6 µm donut may also play a role in reduced uptake by macrophages.

The MFI data better normalizes the volume of particles taken up by each particle positive cell. In BALF macrophages (**Figure 4.6 B**), the median fluorescence intensity of the cells that were associated with the 6 µm donuts was 2-3 times greater than that of the other shapes at one day post-dose, indicating a larger mass of particles per cell. After one day, there was a 1.6-fold reduction in MFI of the 80x320P particle positive macrophages compared to that of the 80x320U and a 3-fold reduction in MFI of the 1.5 P particles compared to the 1.5 U particles after 1 day. This indicates that a greater number of unPEGylated particles were initially taken up by macrophages, thus, surface modification may affect the propensity and degree of particle uptake *in vivo*. At day twenty-eight, the MFI levels of all particles were extremely low, yet, as mentioned previously, over 60% of macrophages in the BALF were particle positive for PEGylated 80x320 nm particles. This may indicate that macrophage clearance and/or turnover rates can be affected by surface

modification as well, with the addition of a PEG layer being able to prolong particle residence time in the lung.

The total fluorescence data for BALF macrophages (**Figure 4.6 C**), shows a clear pattern in the effects of surface modification on particle uptake. At 24 hours post-dose, there is a 1.5, 3.4, and 3.7 fold difference between surface modified and unmodified 80x320 nm, 1.5 µm donut, and 6 µm donut particles, respectively, indicating that PEGylation of particles can significantly reduce uptake by macrophages in the lung of both nanoparticles and microparticles, with perhaps a stronger influence on microparticles. Interestingly, at day seven, the total fluorescence of the 80x320P particles remains at similar levels to those at day one which suggests slower clearance of macrophages with these particles and/or continued uptake of free particles residing in the alveolar space. This hypothesis is supported by the fact that the 80x320U particles have a 3.2 fold reduction in total fluorescence between days one and seven implying clearance of particle loaded macrophages from the BALF and/or fewer free particles for further uptake by alveolar macrophages.

In macrophages from the lung tissue (**Figure 4.6 D**), the trends in percent particle positive cells are identical to that of the BALF macrophages. Surface modification again does not play a role in the number of particle positive cells one day after instillation with 80x320 nm and 1.5 µm donut particles. However, unlike in the BALF, the 1.5 µm donut particles had 20% less particle positive cells than the 80x320 nm particles. This indicates a higher exposure of the 80x320 nm particles to lung-residing macrophages compared to the other two particle sizes. Interestingly, the percentage of 80x320 nm positive cells increases from day one to day seven suggesting that there may be free particles residing in the alveolar space which are not immediately internalized by cells in the lung. The unPEGylated 6 µm donuts

have over a 5-fold increase in particle positive cells versus the unPEGylated particles at both one and seven days post-instillation. In both the BALF and the lung, surface modification on larger micron-sized (6 µm) particles has a greater effect on uptake at early time points than modifications on smaller (80x320 nm and 1.5 µm) particles.

The MFI data for the lung macrophage population (**Figure 4.6 E**) is quite different from that of the BALF. While the fluorescence intensity of the 80x320 nm particles and 1.5 µm donuts at day one are similar in intensity to that of the BALF, the 6P and 6U particles in the lung tissue had a 25% and 98% reduction in MFI, respectively. This indicates that macrophages in the BALF are associated with a greater number of 6 µm particles compared to macrophages in the lung tissue, and that the unPEGylated particles are more quickly cleared from the lung. In furthering the evidence of 80x320P particles having the ability to be retained in the lung both free and in macrophages, the MFI value of these particles increases 2-fold from day one to day seven. One would expect that if only the macrophage clearance rate was reduced, that the MFI levels would have a slower rate of decay, but would not increase over time. Because the percent particle positive cells and the MFI increase over time this indicates that additional particles may be continually taken up by macrophages in the lung, and are retained within the lung tissue, rather than being cleared to the BALF. At twenty-eight days post-instillation, all particle MFIs are significantly reduced and no difference is seen between particle types.

While the total fluorescence data from macrophages in the BALF indicated a preference for unPEGylated particles at one day post-dose, the total fluorescence data from macrophages in the lung (**Figure 4.6 F**) shows no effect of surface modification on the total volume of particles internalized. For the longer seven and twenty-eight day time points, the

trends hold from the MFI data, indicating an increase in particle uptake of 80x320 P particles from day one to day seven and then a clearance of particle-loaded macrophages by day twenty-eight.

Unlike the macrophages in both the BALF and the lung, DC's in the lung showed a preference for unPEGylated particles one day post-dose (**Figure 4.6 G**). Particle uptake of unPEGylated particles increased by 2.0, 4.2, and 1.6-fold in 80x320 nm, 1.5 µm, and 6 µm particles, respectively compared to their PEGylated counterparts. At days seven and twenty-eight, surface modification effects are no longer seen. Interestingly, although there was a higher percentage of particle positive cells with the 80x320 U particles, the MFI data indicates that DCs in the lung have a much higher preference for 1.5 µm donuts, and in particular, the unPEGylated 1.5 µm donuts (**Figure 4.6 H**). One caveat for the MFI analysis is demonstrated with the 6 µm donut particles at days seven and twenty-eight. Because MFI analyzes the median fluorescence intensity of only particle positive cells, and because of the extremely low percentage of particle positive DCs containing 6 µm donuts (all less than 0.2%), the MFI may not be truly representative of the population and inferences of the data may not be relevant. The vertical axis of the total fluorescence graph of lung DCs (**Figure 4.6 I**) is an order of magnitude lower than that of the BALF and lung macrophages, but it follows the trend of the MFI data, indicating a strong preference for unPEGylated 1.5 µm particles at one day post-dose. At day seven, the total fluorescence equalizes among the 80x320 nm and 1.5 µm particles which suggests that there may be a homeostatic effect in regulating the volume of particles within DCs in the lung.

These results indicate that there are significant differences in particle uptake and clearance among difference resident lung cell populations. In addition, surface modification, and in this case, PEGylation, of both nano- and micron-sized particles affects particle uptake and retention in the lung. PEGylated 80x320 nm particle association with BALF and lung macrophages is seen out to twenty-eight days, suggesting a slower clearance rate of these cells and/or continued uptake of free particles in the alveolar region.

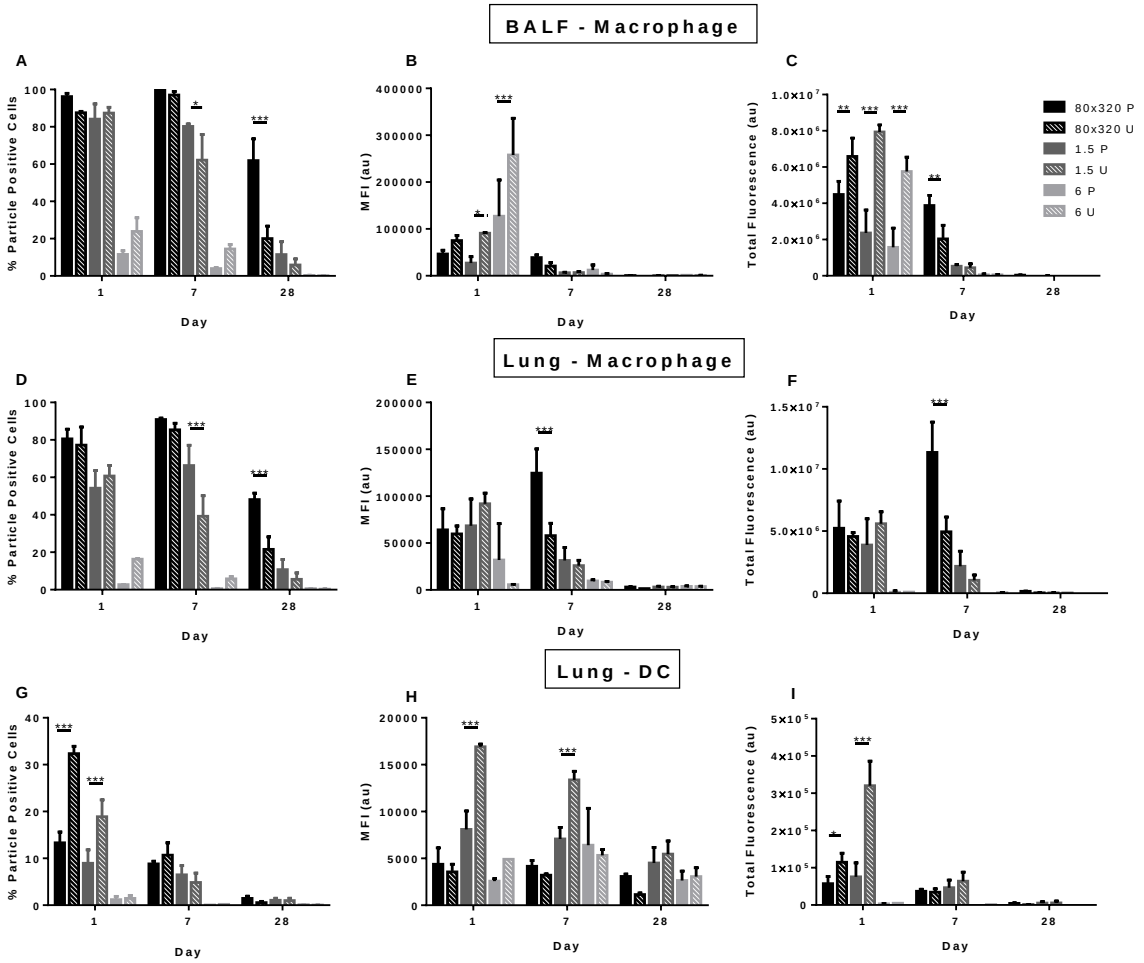

Figure 4.6 Flow cytometry analysis of particle uptake, median fluorescence intensity of particle positive cells, and total fluorescence.
BALF macrophage (**A-C**), lung macrophage (**D-F**), and lung DCs (**G-I**) at 1, 7 and 28 days post-instillation. (* $p < 0.05$, ** $p < 0.001$, *** $p < 0.0001$)

4.4.5 Particle Distribution in the Lung Tissue

To observe the distribution of the particles within the lung tissue, sections of frozen lung tissue were stained for actin, cell nuclei, and CD11c followed by analysis via fluorescent microscopy (**Figure 4.7**). As expected, more 80x320 nm particles were observed in the lung tissue due to the number dosed as compared to the micron-sized particles. Interestingly, the PEGylated 80x320nm particles were shown to have a more homogeneous deposition throughout the lung tissue. Because of this higher distribution in the lung epithelium, the retention time of these particles may be extended, supporting the flow cytometry data which shows that PEGylated 80x320 nm particles can remain in the lung out to twenty-eight days. The unPEGylated 80x320 nm particles were shown to be less evenly distributed in the lung and were often seen in larger aggregates than the unPEGylated particles. More free PEGylated 1.5 μm particles were also observed compared to their unPEGylated counterparts. There were no differences in particle distribution in the lung with the 6 μm particles.

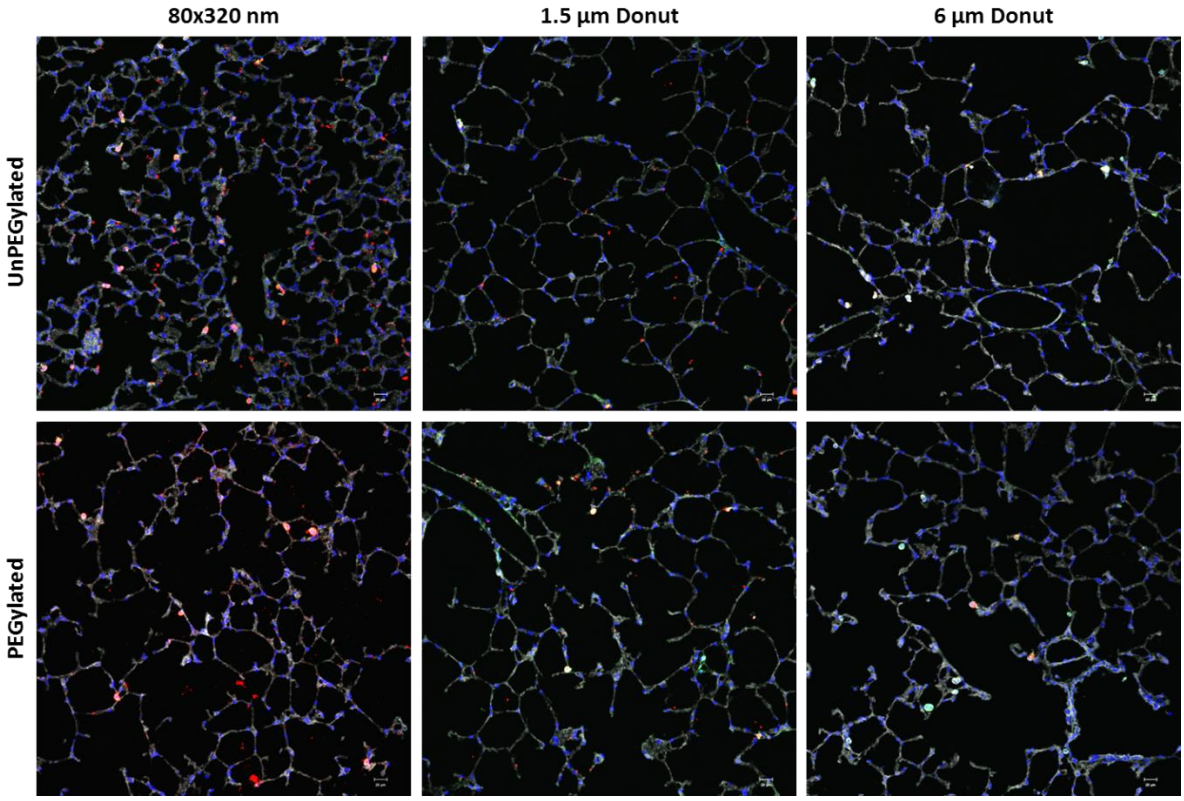

Figure 4.7 Particle distribution in the lung 1 day post-instillation.
Particles (red), Actin (gray), Nuclei (blue), CD11c (green).

4.5 Discussion

The ease of access, large absorptive surface area, and reduced enzymatic activity of the lung make it an attractive target for both local and systemic drug delivery, yet drug particles must circumvent the lung's highly efficient particle clearance mechanisms in order to successfully deliver their payload. In addition, the drug delivery vehicles must be inert, preferably not contributing to an adverse inflammatory response. While there are a multitude of studies in environmental toxicology analyzing the retention and inflammatory effects of polystyrene, pollutant and industrial (diesel exhaust, dust, carbon fiber) particle burdens in the lung, there are few studying the effect of polymeric drug carriers. In this study, we wanted to observe the effects of size and surface modification on polymeric particles on

particle retention and potential inflammatory consequences in the lung. The findings from these studies may help articulate important particle parameters towards designing more efficient pulmonary drug delivery vehicles. Here, we utilize PRINT technology to fabricate monodisperse, cross-linked hydrogel particles of nanometer and micrometer sizes that were further modified by adding an additional PEG layer to the particle surface.

For therapeutic applications targeting sentinel dendritic cells, our findings show that lung DCs have a significant preference for unPEGylated 1.5 μm particles. Although there are a higher percentage of particle positive DCs in the lung with the 80x320U particles, the total volume of internalized particles is over 3-fold greater for the 1.5U particles. From a more physiological view, we show that the DC population that migrates out to the airway surface can potentially be modulated by the surface modification of the particle; unPEGylated 80x320 nm and 1.5 μm particles were shown to double the DC population in the BALF one day post-dose.

Interestingly, although the *in vitro* macrophage uptake studies showed that PEGylated particles of all three particle sizes tested had a significant decrease in number of cells with particle positive cells compared to their unPEGylated counterparts, only the 6 μm donut particles followed this trend in BALF and lung macrophages with a 2-fold and 5-fold decrease in particle positive cells, respectively. This indicates that PEGylated 6 μm donuts may be promising drug carriers as well for disease targets where de-targeting macrophage uptake is preferred. Taking into account total fluorescence, or overall amount of particles internalized, there was indeed a difference due to surface modification of all particle sizes in the BALF indicating the ability to reduce mass of particles taken up by immune cells in the lung via surface PEGylation.

Our results show that these particles can reside in the lung out to twenty-eight days without causing an inflammatory response. In particular, the 80x320 nm and 1.5 μm particles are seen in BALF and lung cells out to a month which may make them a prime candidate for sustained release of drug for diseases targeting macrophages in the lung, such as tuberculosis. Additionally, the PEGylated 80x320 nm actually show an increase in uptake from day one to day seven, indicating that there are likely free particles residing in the alveolar airspace and/or epithelial tissue. This is supported by fluorescent microscopy of the lung tissue which shows the particles significantly distributed throughout the epithelial cells of the lung. Thus, this may also make these particles ideal for gene delivery to treat cystic fibrosis and local delivery of therapeutics to airway cells to treat chronic obstructive pulmonary disease (COPD).

4.6 Conclusions

This study on PRINT particle distribution and retention in the lung indicates this platform as a promising and flexible system for testing and developing sustained drug release systems in the lung. Not only are these particles non-inflammatory, but they can also be retained in the lung for at least a month, with potential to serve as drug depots. Surface modification of these particles can also significantly affect uptake by certain cell populations in the lung, thus allowing for cell-specific targeted delivery of therapeutics. We hope that by applying the knowledge from these fundamental biological studies of particle interactions in the lung to pulmonary delivery applications we can design more efficient drug carriers.

4.7 Supplemental

Particle shape has been shown to induce different cytokine responses in several different studies. Hutter *et al.* demonstrated that sphere, rod, and "urchin"-shaped gold nanoparticles dosed to microglial cells would release different levels of cytokines [72]. Other studies have shown a size-influenced cytokine release where 0.49, 4.3, and 7.2 μm polyethylene particles were demonstrated to increase production of IL-6, IL-1β, and TNF-α [164]. Elongated ultra-high molecular weight polyethylene (UHMWPE) particles were documented to cause more severe local inflammatory responses than globular particles [165]. The studies involving polyethylene particles are often in response to particulate wear debris from implanted prosthetics. For lung relevance, elongated particles of mica and asbestos were shown to be more potent stimulators of cytokines [166, 167]. However, there are no published studies investigating shape effects on *in vivo* cytokine responses of polymer-based micron-sized particles in the lung.

In this study, PRINT fabrication was used to generate PEG particles of different shapes, sizes, and surface chemistries (lollipops, 80x320 nm, 1.5 μm donuts, and 6 μm donuts; all sizes have groups that are PEGylated (P) and unPEGylated (U)). Due to the micro-molding technique utilized by PRINT, a monodisperse population of particles was able to be generated (**Figure 1**). PEGylated and unPEGylated lollipop shaped particles were instilled into the lungs of mice using the same particle composition and protocol as described in Chapter 4. BALF supernatant was collected for cytokine analysis and lungs were also frozen and stained for histology. A shape-based effect on cytokine release was seen in the BALF where only the lollipop-shaped particles were seen to induce cytokine production.

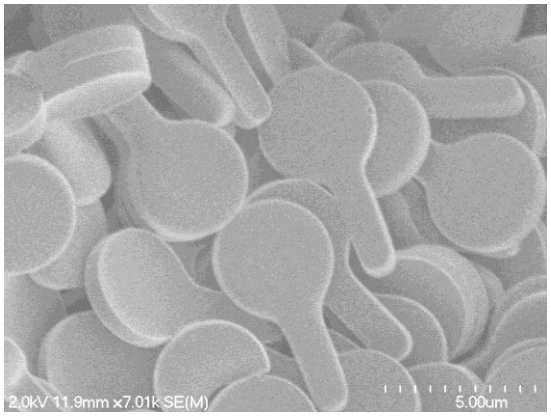

Figure 4.8 Lollipop-shaped particles generated with PRINT

An 8-plex mouse cytokine array (Invivogen) was used to assess the immune profile of the BALF after particle dosing. IL-6, IL-1β, TNF-α, CCL2, CCL3, CCL4, CCL5, and CXCL2 cytokines were measured in the BALF. A summary of the function of each cytokine is listed in the **Table 4.2**. Cytokine concentrations of instilled particles at 24 hours post-dose are shown in **Figure 2**. Surprisingly, only the lollipop particles induced any significant cytokine response. More interestingly, there was observed to be a surface-modification response to the induction of CCL2 where the unPEGylated particles resulted in over a 4-fold increase in CCL2 concentration compared to PEGylated lollipop particles.

Table 4.2 Summary of Cytokine Functions

Name	Induced by	Cell Source	Cell Target
IL-6	Infection, tissue damage	Macrophages, monocytes, B cells, DCs	B cells, T helper cells, NK cells, Epithelial cells
IL-1β	Infection, tissue damage	Macrophages	Lymphocytes
TNF-α	Infection, gram-neg bacteria	Macrophages, T-cells	Neutrophils, Macrophages
CCL2 (MCP-1)	Infection, tissue damage	Macrophages, monocytes, DCs	Monocytes, memory T cells, DCs
CCL3 (MIP-1α)	Bacterial endotoxins	Macrophages	Leukocytes
CCL4 (MIP-1β)	Bacterial endotoxins	Macrophages	Leukocytes
CCL5 (RANTES)	Viral infection of epithelial cells	T cells, Lymphocytes, Epithelial cells	T cells, Monocytes, Eosinophils
CXCL2 (MIP-2)	Infection, inflammation	Macrophages, monocytes	Leukocytes

It has been shown previously that PEG-coated gold nanorods have decreased IL-6 and TNF-α release compared to particles coated with poly(sodium 4-styrenesulfonate) (PSS), a negatively charged polyelectrolyte, or coated with poly (diallyldimethylammonium chloride) (PDAC), a positively charged polyelectrolyte [168]. This decreased cytokine production may be due to fewer PEGylated particles internalized by cells in the BALF, however, both PEGylated and unPEGylated lollipop particles generated high concentrations of CCL4 which is a primary recruiter of leukocytes. This data may demonstrate that certain particle parameters may have a greater influence in the release of specific cytokines.

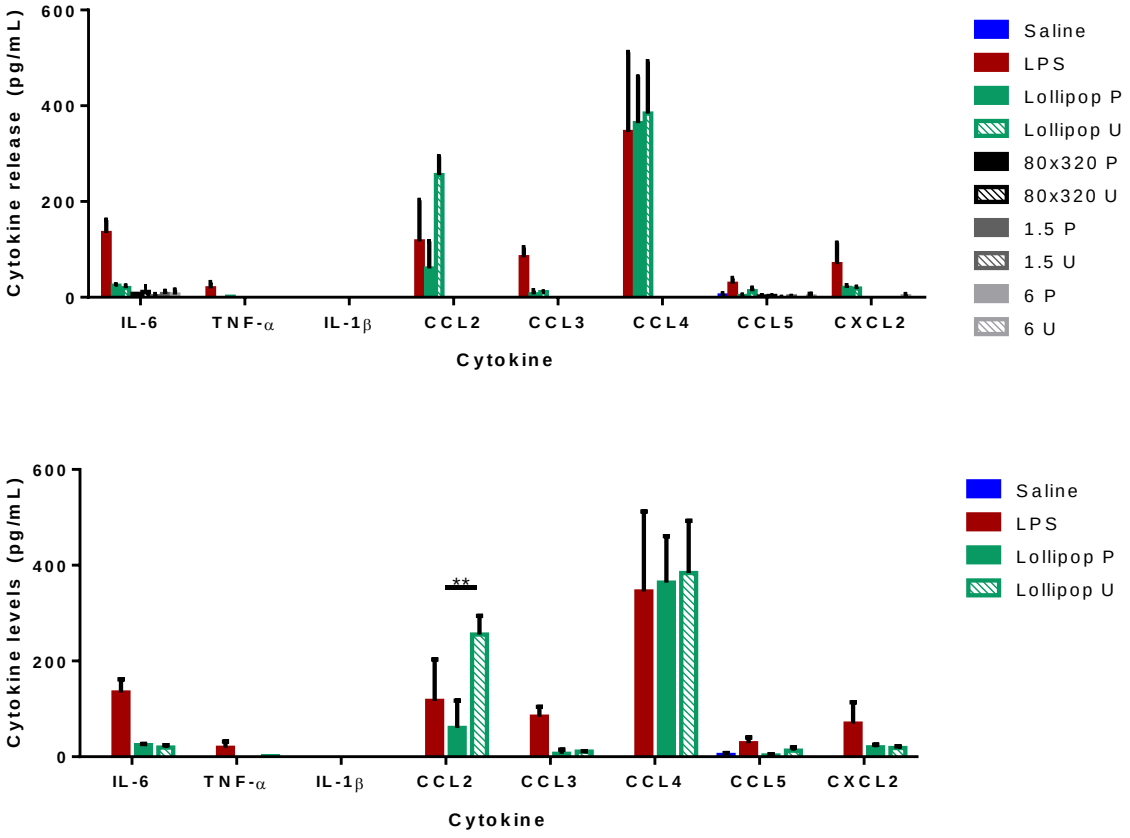

Figure 4.9 Cytokine concentrations 24 hours after particle instillation in the BALF
The top figure includes the cytokine analysis of all particles tested. The bottom figure displays only the cytokine concentrations of the saline and LPS controls and the lollipop particles. (** $p < 0.001$)

The increased release of cytokines was also verified by flow cytometry which showed enhanced neutrophil recruitment into the BALF **(Figure 3**). Neutrophils were gated based on Ly6G expression in the flow cytometry analysis and the population in the LPS positive control is circled in red. This neutrophil population is also seen in the lollipop-treated mice, but not in the mice instilled with 80x320 nm or 6 µm donut particles.

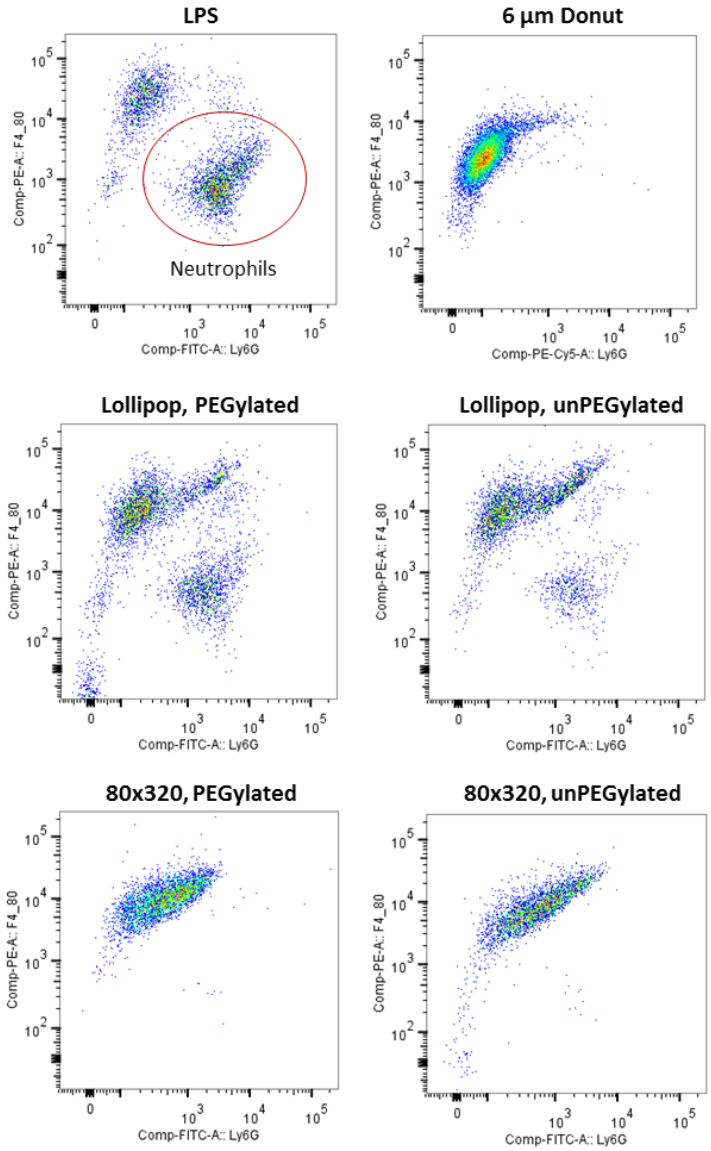

Figure 4.10 Flow cytometry analysis of neutrophil population in the BALF

Fluorescent confocal microscopy of lung tissue additionally validated these observations. Areas of increased cell infiltration are seen in the particles dosed with unPEGylated lollipops 24 hours post dose **(Figure 4**).

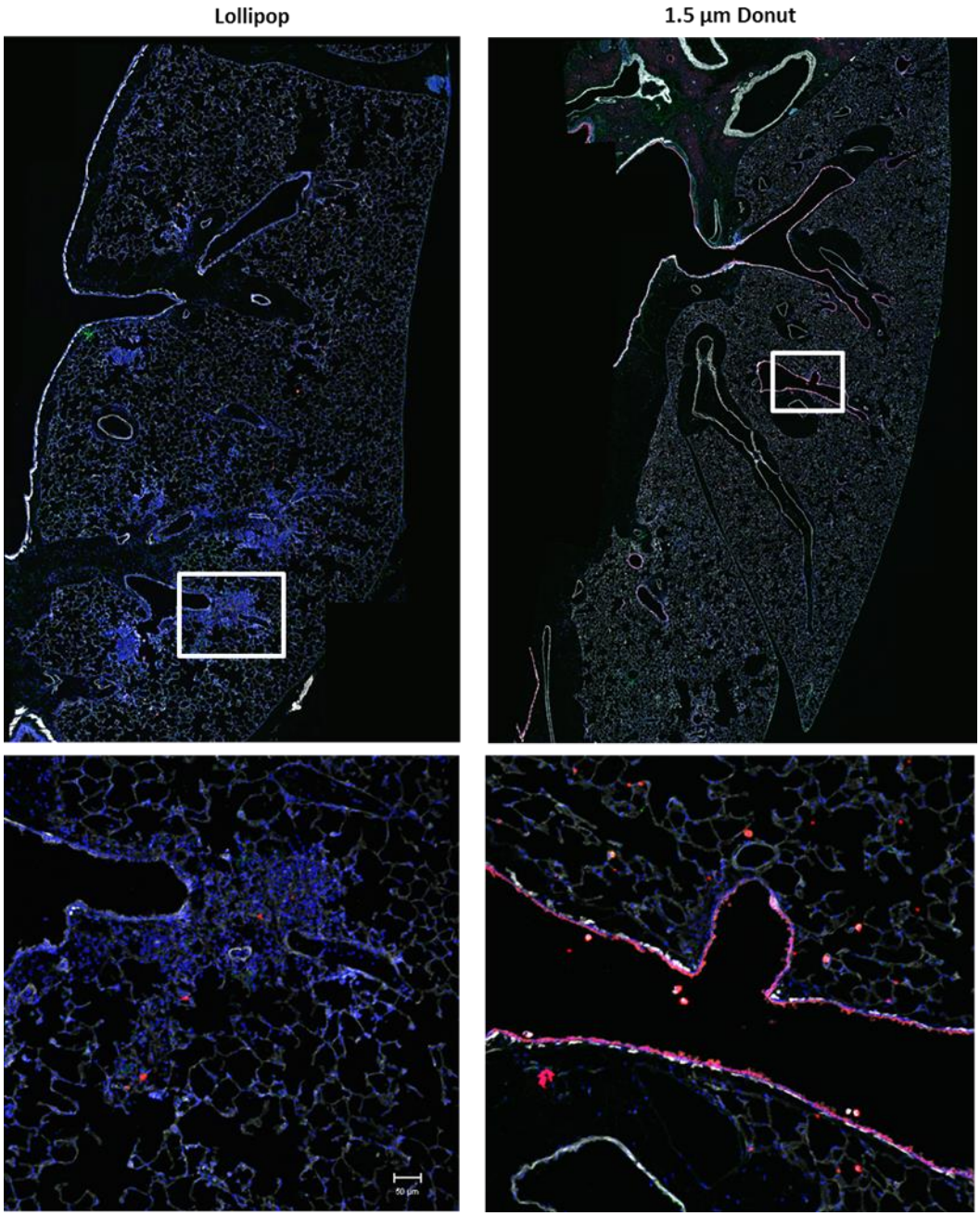

Figure 4.11 Fluorescent microscopy of lung tissue.
Cell nuclei (blue), Particles (red), Actin (Gray).

Previous litereature has shown increased cytokine production after intratracheal instillation of crocidolite asbestos and refractory ceramic fibres 2-10 μm in length [169, 170]. Studies on the effect of fiber length on lung pathogenicity demonstrated that longer amosite asbestos induced inflammation while shorter amosite fibers presented virtually no inflammation [171, 172]. The majority of research investigating particle length and lung inflammation has focused on exposure of mineral-based asbestos found in industrial settings. Milling is often used to shorten long fibers for these studies and often results in a significantly heterogeneous population of fiber lengths.

In this work, polymer-based, monodisperse particles were utilized to assay the effect of particle geometry on lung inflammation. Polymer-based drug carriers are actively being explored for therapeutic applications, but their inflammatory potential in the lung has not yet been fully realized. Using PRINT technology, monodisperse particle populations can be generated to eliminate the added variability of differing particle sizes thus allowing one to better attribute geometry-based effects of specific particle dimensions. While PRINT PEG particles of rod shape (80x320 nm) and donut shapes (1.5 μm and 6 μm) have previously been shown to be non-inflammatory when dosed in the lung [143], the cytokine release profiles of the lollipop-shaped particles indicate that there is a shape-based response. In addition, PEGylation of these lollipop particles was also shown to affect the magnitude of cytokine release, indicating a surface-modification response. While many applications of drug delivery to the lung will prefer inert carriers, therapies targeting the manipulation of the immune system may benefit from further understanding of particle characteristics which can influence the immune response. The lung has also been shown to be a “hub” for the programming of immune cells directing them to different areas of the body [151]. Thus,

these studies have shown the ability to shape the immune response in the lung based on changing specific particle parameters. Future studies may further demonstrate the ability to precisely tune the immune response based on programmable particle features.

CHAPTER 5

SUMMARY AND FUTURE DIRECTIONS

5.1 Summary

The overall scope of this work was to utilize the PRINT fabrication process to generate a set of particles with precisely tuned particle parameters such that the influence of these individual parameters on biological systems could be systematically investigated. The lung was chosen as the primary target of interest due to its clinical relevance and the need to develop drug carriers that can overcome its highly efficient clearance mechanisms. The quick immune response to foreign invaders and its influence of the body's adaptive immunity also made the lung an interesting system to explore potential immunomodulatory effects of different particle parameters.

Taking advantage of PRINT technology's ability to generate particles of non-spherical geometries, several unique micron-sized polymer-based shapes were designed and fabricated. These shapes had physical geometries varying from 1 μm to 11 μm in diameter and volumes ranging from 1 μm^3 to 40 μm^3. Yet, all these shapes had aerodynamic diameters between 1 μm and 5 μm, making them ideal for deep lung deposition. When dosed *in vitro* to alveolar macrophages, a significant difference in uptake was seen among particle shapes with cells less likely to internalize shapes with larger volumes. The ability to

tailor macrophage uptake offers the opportunity to develop cell-specific drug carriers. Therapies that would benefit from increased macrophage internalization of antibiotic drugs such as tuberculosis could be dosed with a particle shape more likely to be internalized. For drugs that would need to avoid rapid macrophage sequestration or clearance from the lung, shapes that can de-target macrophages such as the 6 μm donuts would be ideal.

In addition, it was also observed that macrophages had a preference for initiating phagocytosis at the more narrow ends of the particle shapes tested. This was demonstrated with the lollipop shaped particles in which over 70% of particles still undergoing phagocytosis were internalized with the "stick" end first. This result corresponds to other work which has described the ability of macrophages to recognize shape and may point to an evolutionary process of awareness from the body's constant exposure to bacteria, many of which are rod-shaped.

To lend more clinical and field relevance to these initial studies, collaboration with an immunology laboratory was initiated to observe the residence time of these particles in the lung and to explore the influence particles may have on the innate and adaptive immune system. The goal of this study was to investigate which particle parameters may trigger inflammation in the lung and which parameters may render a particle more immunologically inert. These particles were composed of the FDA approved polymer, PLGA, or a biocompatible polymer, PEG, and ranged in size from 80x320 nm to 6 μm in diameter. *In vitro* testing of these particles with murine bone marrow-derived macrophages showed that both PLGA and PEG particles of all sizes did not induce inflammatory cytokine release. Instillation of these particles into the lungs of mice was conducted to observe the potential inflammatory effects of these particles in a more complex biological system and to explore

the effect of size and shape on *in vivo* particle uptake. In correlation with the *in vitro* results, both PLGA and PEG particles of all sizes did not induce cytokine release as measured in the BALF and serum. As expected, smaller particles were taken up more significantly by cells in the BALF, but all particle sizes were still seen out to seven days in the lung. It was also observed that the 6 μm PEG particles could remain in the lung tissue for two weeks without causing overt signs of inflammation. This work has shown that PRINT PLGA and PEG particles have a good safety profile conducive towards their use as drug delivery vehicles in the lung. Thus, future applications can utilize these immunologically inert particles for sustained drug delivery in the lung.

A more comprehensive study on the cellular fate and inflammatory response of nano- and micro-particles in the lung was undertaken to further investigate the use of PRINT particles as potential pulmonary drug delivery vehicles. In addition to particle size and shape, particle surface chemistry was explored to analyze the effects PEGylation may have on particle residence time and macrophage uptake *in vivo*. Again, PEG particles of 80x320 nm, 1.5 μm and 6 μm diameters were fabricated and an additional PEG5k was covalently attached to form a stealthing layer on the surface of the particles.

Dendritic cells were observed to have a propensity for taking up unPEGylated 1.5 μm donut-shaped particles which may make these particles ideal for therapies targeting DCs such as vaccines or immunoengineering applications. PEGylation effects on overall percentage of macrophage uptake were most noticeable in the 6 μm donut-shaped particles in both the BALF and lung data sets in which there was a 2-5 fold decrease in particle positive cells with administration of PEGylated particles compared to an unPEGylated control. However, taking into account total fluorescence, or overall amount of particles internalized, there was

indeed a difference due to surface modification of all particle sizes in the BALF indicating the ability to reduce mass of particles taken up by surface PEGylation. Most interestingly, there was shown to be an increase in internalization of PEGylated 80x320 nm over time indicating that free particles are localized in the airway even out to seven days. A significant number of macrophages were still particle positive with the PEGylated 80x320 nm particles even out to twenty-eight days after administration. Analysis of IL-6 and MIP-2, two inflammatory cytokines, in the BALF indicated that there was no significant cytokine release from the PEGylated and unPEGylated micron-sized donut and the nanometer-sized rod-shaped particles tested. Thus, these tests confirm the immunologically inert characteristics of these particles and give rise to their potential as sustained-release drug carriers in the lung.

Interestingly, the lollipop-shaped polymeric particles were shown to induce cytokine production which supports previous literature that longer fibrous particles are more likely to induce inflammatory responses in the lung.

5.2 Future Directions

Utilizing PRINT as a toolbox to further fundamental understanding of cellular processes would be an area of great interest. Natural pathogens and particulates are optimized for specific functions *in vivo* and embody many desired traits for drug delivery vehicles. Current synthetic drug carriers have not yet been able to successfully replicate the efficiency of these innate properties of natural particulates. However, more advanced technology and creative approaches towards bio-mimetic carriers have inspired and greatly advanced the field of drug delivery.

Bacteria- and virus- based mimetics often take advantage of the particulate nature and size of the pathogen. Synthetic particulate vaccines utilize the findings that antigen presenting cells (APCs) internalizing particle-associated proteins leads to 1,000-fold more efficient antigen processing and presentation to CD8+ T cells than internalization of the soluble form of the protein [173, 174]. The co-presentation and delivery of particulate-associated danger signals and antigens to APCs have been shown to trigger the host response [175, 176]. Viruses smaller than 100 nm in size have been shown to more efficiently traffic to lymph nodes and promote increased immune responses and many synthetic polymeric antigen-carrying particles have exploited this feature to increase vaccine efficiency [177, 178]. Others have mimicked the surface properties of viruses which allow for increased diffusion of the particle through mucus for better intracellular delivery of cargo [54]. PRINT particles mimicking these natural characteristics of size and activation of antigen presentation have been explored and yielded promising results towards more efficient vaccines.

Along these lines, the work in Chapter 4 of this thesis has shown preferential uptake of unPEGylated 80x320 nm and 1.5 μm particles by dendritic cells in the lung. As these particles have also been shown to be immunologically inert, unintended inflammatory responses in vivo upon particle dose are avoided. When dosed at equal mass (50 μg) into the lung, 80x320 U particles resulted in a greater number of particle-associated dendritic cells while the 1.5 U particles resulted in a greater MFI in DCs indicating that a greater mass of 1.5 U particles are taken up by DCs. It would be interesting to add a surface-conjugated antigen and examine the immune response of antigen processing by number of cells with

associated antigen or by mass of the antigen internalized. This study could tease out particle parameters that may be more ideal for vaccine applications.

The PEGylated 80x320 nm particles in the same study were observed to reside in close to half of total lung macrophages even twenty-eight days after instillation. This lends itself to potential applications for the treatment of tuberculosis. Nebulized poly(DL-lactide-co-glycolide) particles (186-290 nm in size) loaded with antitubercular drugs have demonstrated therapeutic concentrations in the lung of guinea pigs out to eleven days and no tubercle bacilli were detected after five doses while oral doses taken daily for forty-six days were required for the same therapeutic benefit [179]. This demonstrates the utility of a sustained-release platform that can reduce the dosing regime and potentially increase patient compliance for the treatment of TB. Loading these PRINT particles with anti-TB drugs such as isoniazid, rifampin, pyrazinamide or a combination of first-line treatments and triggering release by pH-sensitive cross-linkers or particle swelling would allow for the targeted delivery of these drugs to bacteria-harboring macrophages in the lung. Current TB treatments utilize oral drugs with undesirable side effects, thus, a localized treatment directly to the lung would be ideal for increasing the therapeutic dose at the site of action as well as reducing systemic toxicities. With the potential to sustain therapeutic concentrations for out to a month or longer would greatly reduce number of doses required and simplify the dosing schedule for TB patients. While 80x320 nm sized particles may not be efficiently deposited in the alveolar region, incorporation of these nano-sized particles into larger micron-sized carriers is a possibility. Future work building off of these results may incorporate the use of mothership particles in which the 80x320 nm particles are embedded in a larger, more aerodynamically ideal particle for targeted lung delivery (**Figure 5.1**).

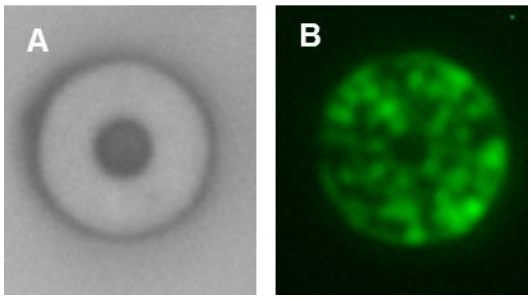

Figure 5.1 Mothership Particles. A) Bright field image of a 6 μm PLGA particle with 80x320 nm PEG particles embedded within. B) Fluorescence image of the same particle in which the 80x320 nm particles have an incorporated fluorescein dye (green).

Physical characteristics of bacteria have also been shown to affect macrophage responses. *Lactobacillus* bacteria strains with rigid cell walls resistant to intracellular digestion were observed to induce macrophage production of IL-12 [180]. Increased substrate rigidity has been demonstrated to affect innate functions of macrophages such as the uptake of particles [124, 181]. More rigid nanoparticles were also shown to be more significantly phagocytosed by RAW 264.7 murine macrophage cells [182]. The aforementioned studies were performed *in vitro* with cultured cell lines. With the *in vivo* instillation and particle uptake analysis protocols optimized from past experimental studies in the DeSimone group, it would be interesting to explore the *in vivo* response of lung cells to a series of particles that ranged from low to high modulus. The ability of PRINT to generate particles of the same geometry but with different modulus has been shown previously with red blood cell mimics [99, 100]. Can we further de-target macrophages with highly swellable and/or less rigid particles? In addition to investigating the effect of particle modulus on particle uptake, looking into the effects of lung disease states on macrophage uptake would also be interesting. Pneumonia is often associated with significant increases in lung tissue rigidity [183, 184]. Bacterial pathogen associated molecular patterns (PAMPs) and cytokines have also been shown to influence tissue rigidity [185, 186]. Does the disease

state affect the modulus range at which macrophages will more significantly take up particles? Because pneumonia is a bacteria-based disease, will macrophages be more activated to ingest particles of a greater modulus range to ensure containment of the pathogen? These studies will not only enhance our understanding of influencing characteristics on innate macrophage functions, but will also allow us to tailor more optimal design parameters of drug delivery carriers for specific diseases of the lung.

Environmental toxicologists have extensively explored the role of environmental particulate burdens in the lung and their effects on lung injury. Studies on particles of TiO_2 have shown that ultrafine particles (< 50 nm) elicit a greater inflammatory response in the lung compared to larger particles due to increased particle localization in the interstitium and greater surface area interactions with macrophages [187]. Overloading of the rat alveolar macrophages with dust particles on the order of 60 μm^3/AM initiated reduction of particle clearance from the deep lung [188, 189]. Overloaded macrophages displayed impairment in chemotactic responses (cell motility) and particle clearance functions [190, 191]. Few studies have investigated the effect of repeated dosing of polymeric drug carriers. As emerging matrices for inhaled drug delivery, there is a need to assess their toxcicological effects in the lung. Although the fabricated hydrogel PRINT particles (80x320 nm, 1.5 μm donuts, and 6 μm donuts) have been shown to be inert upon installation in the lung, issues such as impairment of lung clearance or alveolar macrophage uptake of pathogens post particle dose remain to be explored. Proposed experiments to investigate these responses would be to analyze particle uptake and cytokine responses in mice instilled with multiple doses of polymeric particles with similar protocols described in Chapter 4. Each particle dose would incorporate a different colored dye, thus allowing for the analysis of particle

uptake based on dose number. In addition, a bacterial challenge can be included to measure pathogen clearance effects of particle loaded macrophages. These studies would help guide dosing regimens of these polymeric drug carriers to enhance therapeutic efficacy without compromising the innate immune response.

Additional studies comparing the cytokine properties of particles dosed through the pulmonary route verses other routes of administration would perhaps provide insights on the influences of the biological environment on the cytokine response. This information would be particularly important for inhaled drug particles that may enter the systemic circulation. A biodistribution study of inhaled PRINT particles and their drug cargo would also be interesting to analyze local verse systemic delivery of particles and drugs.

Generating a more systematic series of shapes to explore the kinetics of macrophage phagocytosis and the resulting physiological response would enhance our knowledge on the influence of particle geometry. Experiments in this thesis used shapes that had distinct geometries, but no unifying control parameter (aside from the different diameter donut shapes). Fabricating particles with differing geometric shapes, but with the same volume would allow for a more controlled comparison of particle geometry. In particular, it would be interesting to look at the "ball-and-stick" family of shapes to investigate how particle angles or number of arms may affect macrophage particle uptake and cytokine response. Can we further de-target macrophages purely based on geometry? Are there certain geometries that induce frustrated phagocytosis or increased cytokine release? From Section 4.7, it was shown that lollipop particles induced the release of cytokines in the BALF significantly more than other particle shapes. Expounding on the research from Chapter 2, what are the cellular mechanisms underlying this phenomenon of shape-induced cytokine

release? Is it a frustrated phagocytosis effect? Does orientation of particle internalization affect these macrophages?

In summary, this work has demonstrated the modularity of the PRINT process to fabricate particles with specifically tuned parameters. Because of this, individual particle characteristics such as size, shape, and surface chemistry could be systematically tested in complex biological systems. Thus, optimal particle parameters for specific therapeutic applications can be applied for more efficient disease treatments. The findings from this research can be used in the development of sustained-release drug delivery in the lung, specific cell-based therapies, and immunomodulatory applications.

REFERENCES

1. Patton, J.S. and P.R. Byron, *Inhaling medicines: delivering drugs to the body through the lungs.* Nat Rev Drug Discov, 2007. **6**(1): p. 67-74.

2. Azarmi, S., W.H. Roa, and R. Löbenberg, *Targeted delivery of nanoparticles for the treatment of lung diseases.* Advanced Drug Delivery Reviews, 2008. **60**(8): p. 863-875.

3. Takano, H., et al., *Diesel exhaust particles enhance antigen-induced airway inflammation and local cytokine expression in mice.* Am J Respir Crit Care Med, 1997. **156**(1): p. 36-42.

4. Salvi, S., et al., *Acute inflammatory responses in the airways and peripheral blood after short-term exposure to diesel exhaust in healthy human volunteers.* Am J Respir Crit Care Med, 1999. **159**(3): p. 702-9.

5. Geiser, M., et al., *Ultrafine Particles Cross Cellular Membranes by Nonphagocytic Mechanisms in Lungs and in Cultured Cells.* Environmental Health Perspectives, 2005. **113**(11): p. 1555-1560.

6. Oberdorster, G., J. Ferin, and B.E. Lehnert, *Correlation between particle size, in vivo particle persistence, and lung injury.* Environ Health Perspect, 1994. **102 Suppl 5**: p. 173-9.

7. Oberdörster, G., E. Oberdörster, and J. Oberdörster, *Nanotoxicology: An Emerging Discipline Evolving from Studies of Ultrafine Particles.* Environmental Health Perspectives, 2005. **113**(7): p. 823-839.

8. Lippmann, M., D.B. Yeates, and R.E. Albert, *Deposition, retention, and clearance of inhaled particles.* Br J Ind Med, 1980. **37**(4): p. 337-62.

9. Chow, A.H., et al., *Particle engineering for pulmonary drug delivery.* Pharm Res, 2007. **24**(3): p. 411-37.

10. Fu, J., et al., *New polymeric carriers for controlled drug delivery following inhalation or injection.* Biomaterials, 2002. **23**(22): p. 4425-33.

11. Vehring, R., *Pharmaceutical particle engineering via spray drying.* Pharm Res, 2008. **25**(5): p. 999-1022.

12. Bennett, W.D., et al., *Effect of inhaled dust mite allergen on regional particle deposition and mucociliary clearance in allergic asthmatics.* Clin Exp Allergy, 2011. **41**(12): p. 1719-28.

13. Global Tuberculosis Programme. and World Health Organization, *Global tuberculosis report*. 2012, World Health Organisation: Geneva, Switzerland. p. volumes.

14. MacKenzie, T., et al., *Longevity of patients with cystic fibrosis in 2000 to 2010 and beyond: survival analysis of the cystic fibrosis foundation patient registry.* Ann Intern Med, 2014. **161**(4): p. 233-41.

15. Centers for Disease Control and Prevention., *Asthma Facts - CDC's National Asthma Control Program Grantees*. 2013, Atlanta, GA: Centers for Disease Control and Prevention.

16. Global Initiative for Chronic Obstructive Lung Disease., *Global strategy for the diagnosis, management, and prevention of chronic obstructive pulmonary disease / Global Initiative for Chronic Obstructive Lung Disease*. Revised 2011. ed. 2011, Bethesda, MD: Global Initiative for Chronic Obstructive Lung Disease. ix, 78 pages.

17. Salvi, S.S. and P.J. Barnes, *Chronic obstructive pulmonary disease in non-smokers.* Lancet, 2009. **374**(9691): p. 733-43.

18. National Heart, L., and Blood Institute.,, *Morbidity and mortality chartbook on cardiovascular, lung and blood diseases.* 2009, Bethesda, Maryland: US Department of Health and Human Services, Public Health Service, National Institutes of Health.

19. Loddenkemper, R., *European Lung White Book. The first comprehensive survey on respiratory health in Europe*. 2003. p. vi-+ 182 .

20. Knapp, S., et al., *Alveolar Macrophages Have a Protective Antiinflammatory Role during Murine Pneumococcal Pneumonia.* American Journal of Respiratory and Critical Care Medicine, 2003. **167**(2): p. 171-179.

21. Ferlay J, S.I., Ervik M, Dikshit R, Eser S, Mathers C, Rebelo M, Parkin DM, Forman D, Bray, F. *GLOBOCAN 2012 v1.0, Cancer Incidence and Mortality Worldwide: IARC CancerBase No. 11 [Internet]*. 2013; Available from: http://globocan.iarc.fr.

22. *Surveillance, Epidemiology, and End Results (SEER) Program (www.seer.cancer.gov) Research Data (1973-2011).* 2014, National Cancer Institute, DCCPS, Surveillance Research Program, Surveillance Systems Branch.

23. Azarmi, S., et al., *Formulation and cytotoxicity of doxorubicin nanoparticles carried by dry powder aerosol particles.* Int J Pharm, 2006. **319**(1-2): p. 155-61.

24. Zarogoulidis, P., et al., *Inhaled chemotherapy in lung cancer: future concept of nanomedicine.* Int J Nanomedicine, 2012. **7**: p. 1551-72.

25. Tatsumura, T., et al., *[New chemotherapeutic method for the treatment of tracheal and bronchial cancers--nebulization chemotherapy]*. Gan No Rinsho, 1983. **29**(7): p. 765-70.

26. Hershey, A.E., et al., *Inhalation chemotherapy for macroscopic primary or metastatic lung tumors: proof of principle using dogs with spontaneously occurring tumors as a model.* Clin Cancer Res, 1999. **5**(9): p. 2653-9.

27. Sharma, S., et al., *Development of inhalational agents for oncologic use.* J Clin Oncol, 2001. **19**(6): p. 1839-47.

28. Kim, I., et al., *Doxorubicin-loaded highly porous large PLGA microparticles as a sustained- release inhalation system for the treatment of metastatic lung cancer.* Biomaterials, 2012. **33**(22): p. 5574-83.

29. Dye, C., et al., *Consensus statement. Global burden of tuberculosis: estimated incidence, prevalence, and mortality by country. WHO Global Surveillance and Monitoring Project.* JAMA, 1999. **282**(7): p. 677-86.

30. Adams, D.O., *The granulomatous inflammatory response. A review.* Am J Pathol, 1976. **84**(1): p. 164-92.

31. Ramakrishnan, L., *Revisiting the role of the granuloma in tuberculosis.* Nat Rev Immunol, 2012. **12**(5): p. 352-66.

32. Sakamoto, K., *The pathology of Mycobacterium tuberculosis infection.* Vet Pathol, 2012. **49**(3): p. 423-39.

33. Dartois, V., *The path of anti-tuberculosis drugs: from blood to lesions to mycobacterial cells.* Nat Rev Micro, 2014. **12**(3): p. 159-167.

34. Garcia-Contreras, L., et al., *Inhaled large porous particles of capreomycin for treatment of tuberculosis in a guinea pig model.* Antimicrob Agents Chemother, 2007. **51**(8): p. 2830-6.

35. Garcia-Contreras, L., et al., *Immunization by a bacterial aerosol.* Proc Natl Acad Sci U S A, 2008. **105**(12): p. 4656-60.

36. Alton, E.W., et al., *Non-invasive liposome-mediated gene delivery can correct the ion transport defect in cystic fibrosis mutant mice.* Nat Genet, 1993. **5**(2): p. 135-42.

37. Suk, J.S., et al., *N-acetylcysteine enhances cystic fibrosis sputum penetration and airway gene transfer by highly compacted DNA nanoparticles.* Mol Ther, 2011. **19**(11): p. 1981-9.

38. Usmani, O.S., M.F. Biddiscombe, and P.J. Barnes, *Regional lung deposition and bronchodilator response as a function of beta2-agonist particle size.* Am J Respir Crit Care Med, 2005. **172**(12): p. 1497-504.

39. Kleinstreuer, C., Z. Zhang, and J.F. Donohue, *Targeted drug-aerosol delivery in the human respiratory system.* Annu Rev Biomed Eng, 2008. **10**: p. 195-220.

40. Weibel, E.R., *Morphometry of the human lung*. 1963, New York,: Academic Press. xi, 151 p.

41. Smyth, H.D.C. and A.J. Hickey, *Controlled pulmonary drug delivery*. Advances in delivery science and technology. 2011, New York: Springer. xiii, 557 p.

42. Stone, K.C., et al., *Allometric relationships of cell numbers and size in the mammalian lung.* Am J Respir Cell Mol Biol, 1992. **6**(2): p. 235-43.

43. Craig, A., et al., *Neutrophil Recruitment to the Lungs during Bacterial Pneumonia.* Infection and Immunity, 2009. **77**(2): p. 568-575.

44. Lambrecht, B., et al., *Lung Dendritic Cells and Pulmonary Defence Mechanisms to Bacteria*, in *Mucosal Immunology of Acute Bacterial Pneumonia*, A. Prince, Editor. 2013, Springer New York. p. 49-66.

45. Oakland, M., P.L. Sinn, and P.B. McCray Jr, *Advances in Cell and Gene-based Therapies for Cystic Fibrosis Lung Disease.* Mol Ther, 2012. **20**(6): p. 1108-1115.

46. El-Sherbiny, I., et al., *Overcoming Lung Clearance Mechanisms for Controlled Release Drug Delivery*, in *Controlled Pulmonary Drug Delivery*, H.D.C. Smyth and A.J. Hickey, Editors. 2011, Springer New York. p. 101-126.

47. Thornton, D.J. and J.K. Sheehan, *From Mucins to Mucus.* Proceedings of the American Thoracic Society, 2004. **1**(1): p. 54-61.

48. Wells, U. and P. Richardson, *Mucus Hypersecretion and Its Role in the Airway Obstruction of Asthma and Chronic Obstructive Pulmonary Disease*, in *Airway Mucus: Basic Mechanisms and Clinical Perspectives*, D. Rogers and M. Lethem, Editors. 1997, Birkhäuser Basel. p. 275-300.

49. Smith, J.J., et al., *Cystic Fibrosis Airway Epithelia Fail to Kill Bacteria Because of Abnormal Airway Surface Fluid.* Cell, 1996. **85**(2): p. 229-236.

50. Musante, C.J., et al., *Factors affecting the deposition of inhaled porous drug particles.* Journal of Pharmaceutical Sciences, 2002. **91**(7): p. 1590-1600.

51. Suarez, S. and A.J. Hickey, *Drug properties affecting aerosol behavior.* Respir Care, 2000. **45**(6): p. 652-66.

52. Yamamoto, H., et al., *Surface-modified PLGA nanosphere with chitosan improved pulmonary delivery of calcitonin by mucoadhesion and opening of the intercellular tight junctions.* Journal of Controlled Release, 2005. **102**(2): p. 373-381.

53. Takeuchi, H., H. Yamamoto, and Y. Kawashima, *Mucoadhesive nanoparticulate systems for peptide drug delivery.* Advanced Drug Delivery Reviews, 2001. **47**(1): p. 39-54.

54. Lai, S.K., et al., *Rapid transport of large polymeric nanoparticles in fresh undiluted human mucus.* Proc Natl Acad Sci U S A, 2007. **104**(5): p. 1482-7.

55. Yang, M., et al., *Biodegradable nanoparticles composed entirely of safe materials that rapidly penetrate human mucus.* Angew Chem Int Ed Engl, 2011. **50**(11): p. 2597-600.

56. Lombry, C., et al., *Alveolar macrophages are a primary barrier to pulmonary absorption of macromolecules.* American journal of physiology. Lung cellular and molecular physiology, 2004. **286**(5): p. L1002-8.

57. Lehnert, B.E., *Pulmonary and thoracic macrophage subpopulations and clearance of particles from the lung.* Environ Health Perspect, 1992. **97**: p. 17-46.

58. Edwards, D.A., et al., *Large porous particles for pulmonary drug delivery.* Science, 1997. **276**(5320): p. 1868-71.

59. Tabata, Y. and Y. Ikada, *Effect of the size and surface charge of polymer microspheres on their phagocytosis by macrophage.* Biomaterials, 1988. **9**(4): p. 356-362.

60. El-Sherbiny, I.M., S. McGill, and H.D. Smyth, *Swellable microparticles as carriers for sustained pulmonary drug delivery.* J Pharm Sci, 2010. **99**(5): p. 2343-56.

61. Sharma, R., et al., *Inhalable microparticles containing drug combinations to target alveolar macrophages for treatment of pulmonary tuberculosis.* Pharm Res, 2001. **18**(10): p. 1405-10.

62. Leemans, J.C., et al., *Depletion of alveolar macrophages exerts protective effects in pulmonary tuberculosis in mice.* Journal of immunology (Baltimore, Md. : 1950), 2001. **166**(7): p. 4604-11.

63. Harris, J.M. and R.B. Chess, *Effect of pegylation on pharmaceuticals.* Nat Rev Drug Discov, 2003. **2**(3): p. 214-221.

64. Walkey, C.D., et al., *Nanoparticle Size and Surface Chemistry Determine Serum Protein Adsorption and Macrophage Uptake.* Journal of the American Chemical Society, 2011. **134**(4): p. 2139-2147.

65. Perry, J.L., et al., *PEGylated PRINT nanoparticles: the impact of PEG density on protein binding, macrophage association, biodistribution, and pharmacokinetics.* Nano Lett, 2012. **12**(10): p. 5304-10.

66. Bazile, D., et al., *Stealth Me.PEG-PLA nanoparticles avoid uptake by the mononuclear phagocytes system.* Journal of Pharmaceutical Sciences, 1995. **84**(4): p. 493-498.

67. Nakano, K., Y. Bando, and Y. Tozuka, *Cellular interaction of PEGylated PLGA nanospheres with macrophage J774 cells using flow cytometry*. 亚洲药物制剂科学, 2007. **2**: p. 220-226.

68. Evora, C., et al., *Relating the phagocytosis of microparticles by alveolar macrophages to surface chemistry: the effect of 1,2-dipalmitoylphosphatidylcholine*. Journal of Controlled Release, 1998. **51**(2–3): p. 143-152.

69. Surendrakumar, K., et al., *Sustained release of insulin from sodium hyaluronate based dry powder formulations after pulmonary delivery to beagle dogs.* Journal of Controlled Release, 2003. **91**(3): p. 385-394.

70. Champion, J.A. and S. Mitragotri, *Role of target geometry in phagocytosis.* Proceedings of the National Academy of Sciences of the United States of America, 2006. **103**(13): p. 4930-4934.

71. Champion, J.A. and S. Mitragotri, *Role of target geometry in phagocytosis.* Proc Natl Acad Sci U S A, 2006. **103**(13): p. 4930-4.

72. Hutter, E., et al., *Microglial Response to Gold Nanoparticles.* ACS Nano, 2010. **4**(5): p. 2595-2606.

73. Albanese, A., E.A. Sykes, and W.C.W. Chan, *Rough around the Edges: The Inflammatory Response of Microglial Cells to Spiky Nanoparticles.* ACS Nano, 2010. **4**(5): p. 2490-2493.

74. Chithrani, B.D., A.A. Ghazani, and W.C.W. Chan, *Determining the Size and Shape Dependence of Gold Nanoparticle Uptake into Mammalian Cells.* Nano Letters, 2006. **6**(4): p. 662-668.

75. Arnida, et al., *Geometry and surface characteristics of gold nanoparticles influence their biodistribution and uptake by macrophages.* European Journal of Pharmaceutics and Biopharmaceutics, 2011. **77**(3): p. 417-423.

76. Gratton, S.E., et al., *The effect of particle design on cellular internalization pathways.* Proc Natl Acad Sci U S A, 2008. **105**(33): p. 11613-8.

77. Sanders, M., *Pulmonary Drug Delivery: An Historical Overview*. Controlled Pulmonary Drug Delivery, 2011: p. 51-73.

78. Hickey, A.J., *Pharmaceutical inhalation aerosol technology*. 2nd ed. Drugs and the pharmaceutical sciences. 2004, New York: M. Dekker. xv, 603 p.

79. Cheng, Y.S., et al., *Behavior of Compact Nonspherical Particles in the TSI Aerodynamic Particle Sizer Model APS33B: Ultra-Stokesian Drag Forces.* Aerosol Science and Technology, 1993. **19**(3): p. 255-267.

80. Son, Y.-J., J. Mitchell, and J. McConville, *In Vitro Performance Testing for Pulmonary Drug Delivery*, in *Controlled Pulmonary Drug Delivery*, H.D.C. Smyth and A.J. Hickey, Editors. 2011, Springer New York. p. 383-415.

81. Lam, C.-W., et al., *Pulmonary toxicity of single-wall carbon nanotubes in mice 7 and 90 days after intratracheal instillation.* Toxicological Sciences, 2004. **77**(1): p. 126-134.

82. Warheit, D.B., et al., *Comparative pulmonary toxicity assessment of single-wall carbon nanotubes in rats.* Toxicological sciences, 2004. **77**(1): p. 117-125.

83. Lipka, J., et al., *Biodistribution of PEG-modified gold nanoparticles following intratracheal instillation and intravenous injection.* Biomaterials, 2010. **31**(25): p. 6574-6581.

84. Gill, K.K., S. Nazzal, and A. Kaddoumi, *Paclitaxel loaded PEG5000–DSPE micelles as pulmonary delivery platform: Formulation characterization, tissue distribution, plasma pharmacokinetics, and toxicological evaluation.* European Journal of Pharmaceutics and Biopharmaceutics, 2011. **79**(2): p. 276-284.

85. Schreier, H., R.J. Gonzalez-Rothi, and A.A. Stecenko, *Pulmonary delivery of liposomes.* Journal of Controlled Release, 1993. **24**(1–3): p. 209-223.

86. Conley, J., et al., *Aerosol delivery of liposome-encapsulated ciprofloxacin: aerosol characterization and efficacy against Francisella tularensis infection in mice.* Antimicrobial agents and chemotherapy, 1997. **41**(6): p. 1288-1292.

87. Kumar, M., et al., *Cationic silica nanoparticles as gene carriers: synthesis, characterization and transfection efficiency in vitro and in vivo.* Journal of nanoscience and nanotechnology, 2004. **4**(7): p. 876-881.

88. Kleemann, E., et al., *Nano-carriers for DNA delivery to the lung based upon a TAT-derived peptide covalently coupled to PEG–PEI.* Journal of Controlled Release, 2005. **109**(1): p. 299-316.

89. Rasenack, N. and B.W. Müller, *Micron-size drug particles: common and novel micronization techniques.* Pharmaceutical development and technology, 2004. **9**(1): p. 1-13.

90. Garcia, A., et al., *Microfabricated engineered particle systems for respiratory drug delivery and other pharmaceutical applications.* J Drug Deliv, 2012. **2012**: p. 941243.

91. Shoyele, S.A. and S. Cawthorne, *Particle engineering techniques for inhaled biopharmaceuticals.* Advanced Drug Delivery Reviews, 2006. **58**(9–10): p. 1009-1029.

92. Senatore, D., et al., *Microencapsulation of Epoxidized Linseed Oil Liquid Cross-Linker in Poly(N-vinyl-pyrrolidone): Optimization by a Design-of-Experiments Approach.* Industrial & Engineering Chemistry Research, 2010. **49**(8): p. 3642-3653.

93. Zijlstra, G.S., et al., *The role of particle engineering in relation to formulation and de-agglomeration principle in the development of a dry powder formulation for inhalation of cetrorelix.* European Journal of Pharmaceutical Sciences, 2004. **23**(2): p. 139-149.

94. Jeong, W., M.E. Napier, and J.M. DeSimone, *Challenging nature's monopoly on the creation of well-defined nanoparticles.* Nanomedicine (Lond), 2010. **5**(4): p. 633-9.

95. Perry, J.L., et al., *PRINT: a novel platform toward shape and size specific nanoparticle theranostics.* Acc Chem Res, 2011. **44**(10): p. 990-8.

96. Canelas, D.A., K.P. Herlihy, and J.M. DeSimone, *Top-down particle fabrication: control of size and shape for diagnostic imaging and drug delivery.* Wiley Interdiscip Rev Nanomed Nanobiotechnol, 2009. **1**(4): p. 391-404.

97. Rolland, J.P., et al., *Direct fabrication and harvesting of monodisperse, shape-specific nanobiomaterials.* J Am Chem Soc, 2005. **127**(28): p. 10096-100.

98. Rothrock, G.D., et al. *High-performance imprint lithography and novel metrology methods using multifunctional perfluoropolyethers*. 2006.

99. Chen, K., et al., *Low modulus biomimetic microgel particles with high loading of hemoglobin.* Biomacromolecules, 2012. **13**(9): p. 2748-59.

100. Merkel, T.J., et al., *Using mechanobiological mimicry of red blood cells to extend circulation times of hydrogel microparticles.* Proc Natl Acad Sci U S A, 2011. **108**(2): p. 586-91.

101. Chu, K.S., et al., *Particle replication in nonwetting templates nanoparticles with tumor selective alkyl silyl ether docetaxel prodrug reduces toxicity.* Nano Lett, 2014. **14**(3): p. 1472-6.

102. Chu, K.S., et al., *Plasma, tumor and tissue pharmacokinetics of Docetaxel delivered via nanoparticles of different sizes and shapes in mice bearing SKOV-3 human ovarian carcinoma xenograft.* Nanomedicine, 2013. **9**(5): p. 686-93.

103. Moga, K.A., et al., *Rapidly-dissolvable microneedle patches via a highly scalable and reproducible soft lithography approach.* Adv Mater, 2013. **25**(36): p. 5060-6.

104. Rolland, J.P., et al., *Direct Fabrication and Harvesting of Monodisperse, Shape-Specific Nanobiomaterials.* Journal of the American Chemical Society, 2005. **127**(28): p. 10096-10100.

105. Euliss, L.E., et al., *Imparting size, shape, and composition control of materials for nanomedicine.* Chemical Society Reviews, 2006. **35**(11): p. 1095-1095.

106. Chan, H.K., et al., *Spray dried powders and powder blends of recombinant human deoxyribonuclease (rhDNase) for aerosol delivery.* Pharm Res, 1997. **14**(4): p. 431-7.

107. O'Hara, P. and A.J. Hickey, *Respirable PLGA microspheres containing rifampicin for the treatment of tuberculosis: manufacture and characterization.* Pharm Res, 2000. **17**(8): p. 955-61.

108. Olschewski, H., et al., *Inhaled iloprost for severe pulmonary hypertension.* N Engl J Med, 2002. **347**(5): p. 322-9.

109. Oberdörster, G., *Lung Clearance of Inhaled Insoluble and Soluble Particles.* Journal of Aerosol Medicine, 1988. **1**(4): p. 289-330.

110. Edsbacker, S., et al., *Do airway clearance mechanisms influence the local and systemic effects of inhaled corticosteroids?* Pulm Pharmacol Ther, 2008. **21**(2): p. 247-58.

111. Geng, Y.A.N., et al., *Shape effects of filaments versus spherical particles in flow and drug delivery.* Nature nanotechnology, 2007. **2**(4): p. 249-255.

112. Gratton, S.E.A., et al., *The effect of particle design on cellular internalization pathways.* Proceedings of the National Academy of Sciences, 2008. **105**(33): p. 11613-11618.

113. Sharma, G., et al., *Polymer particle shape independently influences binding and internalization by macrophages.* Journal of Controlled Release, 2010. **147**(3): p. 408-412.

114. Enlow, E.M., et al., *Potent engineered PLGA nanoparticles by virtue of exceptionally high chemotherapeutic loadings.* Nano Lett, 2011. **11**(2): p. 808-13.

115. Garcia, A., et al., *Microfabricated engineered aerosols for respiratory drug delivery.* Journal of Drug Delivery, in press.

116. Fattorossi, A., et al., *New, simple flow cytometry technique to discriminate between internalized and membrane-bound particles in phagocytosis.* Cytometry, 1989. **10**(3): p. 320-5.

117. Gantner, B.N., R.M. Simmons, and D.M. Underhill, *Dectin-1 mediates macrophage recognition of Candida albicans yeast but not filaments.* EMBO J, 2005. **24**(6): p. 1277-86.

118. Champion, J.A. and S. Mitragotri, *Shape Induced Inhibition of Phagocytosis of Polymer Particles.* Pharmaceutical research, 2009. **26**(1): p. 244-249.

119. May, R.C. and L.M. Machesky, *Phagocytosis and the actin cytoskeleton.* J Cell Sci, 2001. **114**(Pt 6): p. 1061-77.

120. Allen, L.A. and A. Aderem, *Molecular definition of distinct cytoskeletal structures involved in complement- and Fc receptor-mediated phagocytosis in macrophages.* J Exp Med, 1996. **184**(2): p. 627-37.

121. Aderem, A. and D.M. Underhill, *Mechanisms of Phagocytosis in Macrophages.* Annual Review of Immunology, 1999. **17**(1): p. 593-623.

122. Swanson, J.A., *Shaping cups into phagosomes and macropinosomes.* Nat Rev Mol Cell Biol, 2008. **9**(8): p. 639-49.

123. Clarke, M., et al., *Curvature recognition and force generation in phagocytosis.* BMC Biol, 2010. **8**: p. 154.

124. Beningo, K.A. and Y.L. Wang, *Fc-receptor-mediated phagocytosis is regulated by mechanical properties of the target.* J Cell Sci, 2002. **115**(Pt 4): p. 849-56.

125. Geng, Y., et al., *Shape effects of filaments versus spherical particles in flow and drug delivery.* Nat Nanotechnol, 2007. **2**(4): p. 249-55.

126. Champion, J.A. and S. Mitragotri, *Shape induced inhibition of phagocytosis of polymer particles.* Pharm Res, 2009. **26**(1): p. 244-9.

127. Leuschner, F., et al., *Therapeutic siRNA silencing in inflammatory monocytes in mice.* Nat Biotechnol, 2011. **29**(11): p. 1005-10.

128. Dhar, S., et al., *Targeted delivery of a cisplatin prodrug for safer and more effective prostate cancer therapy in vivo.* Proc Natl Acad Sci U S A, 2011. **108**(5): p. 1850-5.

129. Kircher, M.F., et al., *A brain tumor molecular imaging strategy using a new triple-modality MRI-photoacoustic-Raman nanoparticle.* Nat Med, 2012. **18**(5): p. 829-34.

130. Hubbell, J.A., S.N. Thomas, and M.A. Swartz, *Materials engineering for immunomodulation.* Nature, 2009. **462**(7272): p. 449-60.

131. Kasturi, S.P., et al., *Programming the magnitude and persistence of antibody responses with innate immunity.* Nature, 2011. **470**(7335): p. 543-U136.

132. Moon, J.J., et al., *Enhancing humoral responses to a malaria antigen with nanoparticle vaccines that expand T-fh cells and promote germinal center induction.* Proceedings of the National Academy of Sciences of the United States of America, 2012. **109**(4): p. 1080-1085.

133. Bershteyn, A., et al., *Robust IgG responses to nanograms of antigen using a biomimetic lipid-coated particle vaccine.* Journal of Controlled Release, 2012. **157**(3): p. 354-365.

134. Ali, O., et al., *Biomaterial-Based Vaccine Induces Regression of Established Intracranial Glioma in Rats.* Pharmaceutical Research, 2011. **28**(5): p. 1074-1080.

135. Fife, B.T., et al., *Insulin-induced remission in new-onset NOD mice is maintained by the PD-1–PD-L1 pathway.* The Journal of Experimental Medicine, 2006. **203**(12): p. 2737-2747.

136. Notohamiprodjo, M., et al., *Generation of GPI-linked CCL5 based chemokine receptor antagonists for the suppression of acute vascular damage during allograft transplantation.* Protein Engineering Design and Selection, 2006. **19**(1): p. 27-35.

137. Guzmán, J., et al., *Synthesis and polymerization of acrylic monomers with hydrophilic long side groups. Oxygen transport through water swollen membranes prepared from these polymers.* Polymer, 1997. **38**(20): p. 5227-5232.

138. Hasan, W., et al., *Delivery of multiple siRNAs using lipid-coated PLGA nanoparticles for treatment of prostate cancer.* Nano Lett, 2012. **12**(1): p. 287-92.

139. Zhang, X., R. Goncalves, and D.M. Mosser, *The Isolation and Characterization of Murine Macrophages*, in *Current Protocols in Immunology*. 2001, John Wiley & Sons, Inc.

140. Allen, I.C., et al., *The NLRP3 inflammasome mediates in vivo innate immunity to influenza A virus through recognition of viral RNA.* Immunity, 2009. **30**(4): p. 556-65.

141. Willingham, S.B., et al., *NLRP3 (NALP3, Cryopyrin) facilitates in vivo caspase-1 activation, necrosis, and HMGB1 release via inflammasome-dependent and -independent pathways.* J Immunol, 2009. **183**(3): p. 2008-15.

142. Bachmann, M.F. and G.T. Jennings, *Vaccine delivery: a matter of size, geometry, kinetics and molecular patterns.* Nat Rev Immunol, 2010. **10**(11): p. 787-96.

143. Roberts, R.A., et al., *Analysis of the murine immune response to pulmonary delivery of precisely fabricated nano- and microscale particles.* PLoS One, 2013. **8**(4): p. e62115.

144. Pulendran, B. and R. Ahmed, *Immunological mechanisms of vaccination.* Nature Immunology, 2011. **131**(6): p. 509-517.

145. Sayes, C., K. Reed, and D. Warheit, *Nanoparticle Toxicology: Measurements of Pulmonary Hazard Effects Following Exposures to Nanoparticles*, in *Biomedical Nanotechnology*, S.J. Hurst, Editor. 2011, Humana Press. p. 313-324.

146. Oberdorster, G., et al., *Principles for characterizing the potential human health effects from exposure to nanomaterials: elements of a screening strategy.* Particle and Fibre Toxicology, 2005. **2**(1): p. 8.

147. Yazdi, A.S., et al., *Nanoparticles activate the NLR pyrin domain containing 3 (Nlrp3) inflammasome and cause pulmonary inflammation through release of IL-1alpha and IL-1beta.* Proc Natl Acad Sci U S A, 2010. **107**(45): p. 19449-54.

148. Limbach, L.K., et al., *Exposure of Engineered Nanoparticles to Human Lung Epithelial Cells: Influence of Chemical Composition and Catalytic Activity on Oxidative Stress.* Environmental Science & Technology, 2007. **41**(11): p. 4158-4163.

149. Barnes, P.J., *Immunology of asthma and chronic obstructive pulmonary disease.* Nat Rev Immunol, 2008. **8**(3): p. 183-92.

150. Roy, I. and N. Vij, *Nanodelivery in airway diseases: challenges and therapeutic applications.* Nanomedicine, 2010. **6**(2): p. 237-44.

151. Steinman, L., *Weighing in on autoimmune disease: 'Hub-and-spoke' T cell traffic in autoimmunity.* Nat Med, 2013. **19**(2): p. 139-41.

152. Sharp, F.A., et al., *Uptake of particulate vaccine adjuvants by dendritic cells activates the NALP3 inflammasome.* Proc Natl Acad Sci U S A, 2009. **106**(3): p. 870-5.

153. Demento, S.L., et al., *Inflammasome-activating nanoparticles as modular systems for optimizing vaccine efficacy.* Vaccine, 2009. **27**(23): p. 3013-21.

154. Dailey, L.A., et al., *Investigation of the proinflammatory potential of biodegradable nanoparticle drug delivery systems in the lung.* Toxicol Appl Pharmacol, 2006. **215**(1): p. 100-8.

155. Nicolete, R., D.F. dos Santos, and L.H. Faccioli, *The uptake of PLGA micro or nanoparticles by macrophages provokes distinct in vitro inflammatory response.* International Immunopharmacology, 2011. **11**(10): p. 1557-1563.

156. Fromen, C.A., et al., *Synthesis and characterization of monodisperse uniformly shaped respirable aerosols.* Aiche Journal, 2013. **59**(9): p. 3184-3194.

157. Lombry, C., et al., *Alveolar macrophages are a primary barrier to pulmonary absorption of macromolecules.* Am J Physiol Lung Cell Mol Physiol, 2004. **286**(5): p. L1002-8.

158. Li, S.D. and L. Huang, *Nanoparticles evading the reticuloendothelial system: role of the supported bilayer.* Biochim Biophys Acta, 2009. **1788**(10): p. 2259-66.

159. Owens, D.E., 3rd and N.A. Peppas, *Opsonization, biodistribution, and pharmacokinetics of polymeric nanoparticles.* Int J Pharm, 2006. **307**(1): p. 93-102.

160. Evora, C., et al., *Relating the phagocytosis of microparticles by alveolar macrophages to surface chemistry: the effect of 1,2-dipalmitoylphosphatidylcholine.* J Control Release, 1998. **51**(2-3): p. 143-52.

161. Ahsan, F., et al., *Targeting to macrophages: role of physicochemical properties of particulate carriers--liposomes and microspheres--on the phagocytosis by macrophages.* J Control Release, 2002. **79**(1-3): p. 29-40.

162. Moon, J.J., B. Huang, and D.J. Irvine, *Engineering nano- and microparticles to tune immunity.* Adv Mater, 2012. **24**(28): p. 3724-46.

163. Nembrini, C., et al., *Nanoparticle conjugation of antigen enhances cytotoxic T-cell responses in pulmonary vaccination.* Proc Natl Acad Sci U S A, 2011. **108**(44): p. E989-97.

164. Green, T.R., et al., *Polyethylene particles of a 'critical size' are necessary for the induction of cytokines by macrophages in vitro.* Biomaterials, 1998. **19**(24): p. 2297-2302.

165. Yang, S.-Y., et al., *Diverse cellular and apoptotic responses to variant shapes of UHMWPE particles in a murine model of inflammation.* Biomaterials, 2002. **23**(17): p. 3535-3543.

166. Holopainen, M., et al., *Effect of the shape of mica particles on the production of tumor necrosis factor alpha in mouse macrophages.* Scand J Work Environ Health, 2004. **30 Suppl 2**: p. 91-8.

167. Mossman, B.T. and A. Churg, *Mechanisms in the Pathogenesis of Asbestosis and Silicosis.* American Journal of Respiratory and Critical Care Medicine, 1998. **157**(5): p. 1666-1680.

168. Pissuwan, D., Y. Kumagai, and N.I. Smith, *Effect of Surface-Modified Gold Nanorods on the Inflammatory Cytokine Response in Macrophage Cells.* Particle & Particle Systems Characterization, 2013. **30**(5): p. 427-433.

169. Leikauf, G.D., et al., *Refractory ceramic fibers activate alveolar macrophage eicosanoid and cytokine release.* J Appl Physiol (1985), 1995. **78**(1): p. 164-71.

170. Driscoll, K.E., et al., *TNF alpha and increased chemokine expression in rat lung after particle exposure.* Toxicol Lett, 1995. **82-83**: p. 483-9.

171. Davis, J.M., et al., *The pathogenicity of long versus short fibre samples of amosite asbestos administered to rats by inhalation and intraperitoneal injection.* Br J Exp Pathol, 1986. **67**(3): p. 415-30.

172. Donaldson, K., et al., *Inflammation generating potential of long and short fibre amosite asbestos samples.* Br J Ind Med, 1989. **46**(4): p. 271-6.

173. Kovacsovics-Bankowski, M., et al., *Efficient major histocompatibility complex class I presentation of exogenous antigen upon phagocytosis by macrophages.* Proceedings of the National Academy of Sciences, 1993. **90**(11): p. 4942-4946.

174. e Sousa, C.R. and R.N. Germain, *Major histocompatibility complex class I presentation of peptides derived from soluble exogenous antigen by a subset of cells engaged in phagocytosis.* The Journal of experimental medicine, 1995. **182**(3): p. 841-851.

175. Blander, J.M. and R. Medzhitov, *Toll-dependent selection of microbial antigens for presentation by dendritic cells.* Nature, 2006. **440**(7085): p. 808-812.

176. Heit, A., et al., *Antigen co-encapsulated with adjuvants efficiently drive protective T cell immunity.* European journal of immunology, 2007. **37**(8): p. 2063-2074.

177. Junt, T., et al., *Subcapsular sinus macrophages in lymph nodes clear lymph-borne viruses and present them to antiviral B cells.* Nature, 2007. **450**(7166): p. 110-114.

178. Reddy, S.T., et al., *Exploiting lymphatic transport and complement activation in nanoparticle vaccines.* Nature biotechnology, 2007. **25**(10): p. 1159-1164.

179. Pandey, R., et al., *Poly (dl-lactide-co-glycolide) nanoparticle-based inhalable sustained drug delivery system for experimental tuberculosis.* Journal of Antimicrobial Chemotherapy, 2003. **52**(6): p. 981-986.

180. Shida, K., et al., *Induction of Interleukin-12 by Lactobacillus Strains Having a Rigid Cell Wall Resistant to Intracellular Digestion.* Journal of Dairy Science, 2006. **89**(9): p. 3306-3317.

181. Patel, N.R., et al., *Cell elasticity determines macrophage function.* PloS one, 2012. **7**(9): p. e41024.

182. Banquy, X., et al., *Effect of mechanical properties of hydrogel nanoparticles on macrophage cell uptake.* Soft Matter, 2009. **5**(20): p. 3984-3991.

183. Ingenito, E.P., L. Mark, and B. Davison, *Effects of acute lung injury on dynamic tissue properties.* Journal of Applied Physiology, 1994. **77**(6): p. 2689-2697.

184. Mink, S., R. Light, and L. Wood, *Effect of pneumococcal lobar pneumonia on canine lung mechanics.* J Appl Physiol, 1981. **50**(2): p. 283-291.

185. Allen, G. and J.H. Bates, *Dynamic mechanical consequences of deep inflation in mice depend on type and degree of lung injury.* Journal of applied physiology, 2004. **96**(1): p. 293-300.

186. Wheeler, A.P., G. Jesmok, and K.L. Brigham, *Tumor necrosis factor's effects on lung mechanics, gas exchange, and airway reactivity in sheep.* J Appl Physiol, 1990. **68**(6): p. 2542-2549.

187. Oberdörster, G., et al., *Role of the alveolar macrophage in lung injury: studies with ultrafine particles.* Environmental health perspectives, 1992. **97**: p. 193.

188. Morrow, P., *Possible mechanisms to explain dust overloading of the lungs.* Fundamental and applied toxicology, 1988. **10**(3): p. 369-384.

189. Morrow, P.E., *Dust overloading of the lungs: Update and appraisal.* Toxicology and Applied Pharmacology, 1992. **113**(1): p. 1-12.

190. Warheit, D.B. and M.A. Hartsky, *Role of alveolar macrophage chemotaxis and phagocytosis in pulmonary clearance responses to inhaled particles: comparisons among rodent species.* Microsc Res Tech, 1993. **26**(5): p. 412-22.

191. Warheit, D.B., et al., *Inhalation of High Concentrations of Low Toxicity Dusts in Rats Results in Impaired Pulmonary Clearance Mechanisms and Persistent Inflammation.* Toxicology and Applied Pharmacology, 1997. **145**(1): p. 10-22.